

THE CATHOLIC UNIVERSITY OF AMERICA

Chronic Alcohol Consumption Leads to Hepatic Lysine Hyperacetylation:  
Mechanisms and Consequences

A DISSERTATION

Submitted to the Faculty of the  
Department of Biology  
School of Arts and Sciences  
Of The Catholic University of America  
In Partial Fulfillment of the Requirements

For the Degree

Doctor of Philosophy

By

Blythe D. Shepard

Washington, D.C.

2011

## Chronic Alcohol Consumption Leads to Hepatic Lysine Hyperacetylation: Mechanisms and Consequences

Blythe D. Shepard, Ph.D.

Director: Pamela L. Tuma, Ph.D.

Although the clinical manifestations of alcoholic liver disease are well-described, little is known about the molecular basis for liver damage. We have been using hepatic WIF-B cells to examine ethanol-induced liver injury. These cells polarize in culture and maintain liver-specific activities including the ability to metabolize alcohol. Ethanol metabolism leads to the formation of highly reactive metabolites that covalently modify DNA, lipids and proteins. More recently, it is apparent that chronic ethanol consumption leads to increased post-translational protein modifications of the natural repertoire including acetylation. This reversible modification on lysine residues modulates multiple cellular processes. These studies were aimed at further characterizing ethanol-induced protein acetylation. Previously, we observed that ethanol induces microtubule hyperacetylation and stability and this requires ethanol metabolism. To determine the mechanism for increased microtubule acetylation, we examined the microtubule deacetylase, HDAC6. While ethanol does not alter its distribution or activity, HDAC6 protein levels are decreased 25%. Furthermore, ethanol impairs HDAC6-microtubule binding, likely due to ethanol-induced tubulin modifications. Therefore, lower HDAC6 levels combined with decreased microtubule binding leads to increased tubulin

acetylation. Ethanol consumption has been shown to impair clathrin-mediated internalization and addition of trichostatin A (TSA), an inhibitor of HDAC6 that leads to hyperacetylation, mimicked this defect. Using a morphological approach, it was determined that ethanol and TSA impairs clathrin internalization at a late stage of vesicle budding. We further determined that ethanol impairs dynamin-membrane binding and association with members of the clathrin machinery. Dynamin is the GTPase responsible for vesicle fission and decreased membrane association likely contributes to impaired internalization. A proteomics screen to identify novel ethanol-induced hyperacetylated proteins revealed that both actin and cortactin were hyperacetylated. Cortactin is thought to promote actin polymerization and mediate dynamin assembly on the necks of invaginated coated pits. Since cortactin acetylation disrupts its actin association, it is possible that ethanol-induced actin and cortactin hyperacetylation prevent proper dynamin recruitment and vesicle fission. Recently, a specific deacetylase activator, resveratrol, was shown to attenuate fatty liver in alcohol-exposed mice indicating that lysine acetylation plays a dominant role in regulating hepatic function and reducing acetylation is a promising novel therapeutic strategy.

This dissertation by Blythe D. Shepard fulfills the dissertation requirement for the doctoral degree in the Department of Biology approved by Pamela L. Tuma, Ph.D., as Director, and by Ann K. Corsi, Ph.D., and John E. Golin, Ph.D. as Readers

---

Pamela L. Tuma, Ph.D., Director

---

Ann K. Corsi, Ph.D., Reader

---

John E. Golin, Ph.D., Reader

## **DEDICATION**

To my loving family... Mom, Matt, Lily and Eeyore. Your unconditional love and encouragement has made this all possible. Thank you for believing in me and being there when I needed you most. I am proud to call you my family and best friends.

## TABLE OF CONTENTS

<b>List of Illustrations</b>	vi
<b>List of Tables</b>	viii
<b>Abbreviations</b>	ix
<b>Acknowledgements</b>	xiii
<b>Introduction</b>	
The liver	1
Alcoholic liver disease	4
WIF-B cells – A model of hepatotoxicity	7
Lysine acetylation	10
Ethanol-induced hepatic defects – A focus on the cytoskeleton	12
Ethanol-induced hepatic defects – A focus on protein trafficking	18
<b>Materials and Methods</b>	
Reagents and antibodies	23
Cell culture	24
Immunofluorescence microscopy and imaging	24
Total internal reflection fluorescence microscopy	25
Western blotting	26
HDAC activity	26
Solubility assay	27
Microtubule binding	27
Rat ethanol treatment	28
Liver fractionation and blotting	28
2D gel electrophoresis	29
Matrix-assisted laser desorption/ionization mass spectrometry	30
Immunoprecipitations from liver	31
Two-antibody sandwich enzyme-linked immunosorbent assay	32
Immunoprecipitations from WIF-B cells	32
K <sup>+</sup> depletion/repletion assays	33
Statistical analysis	33
<b>Part I: Alcohol-induced alterations in hepatic microtubule dynamics can be explained by impaired histone deacetylase 6 function</b>	34
HDAC6 is abundantly expressed and is a tubulin deacetylase in WIF-B cells	36
Ethanol decreases HDAC6 protein levels	37
HDAC6 is less tightly associated with microtubules in ethanol-treated cells	38
Ethanol-induced tubulin modifications likely prevent HDAC6-microtubule binding	41
Conclusions	46

<b>Part II: Chronic ethanol consumption induces global hepatic protein hyperacetylation</b>	48
Ethanol induces global hepatic protein hyperacetylation	50
Ethanol induces non-nuclear protein acetylation	54
Gpx-1 and actin hyperacetylation is confirmed	64
Conclusions	68
<b>Part III: Chronic ethanol administration impairs clathrin-mediated vesicle fission</b>	69
Components of the clathrin machinery accumulate at the plasma membrane in ethanol-treated cells	70
Protein hyperacetylation may contribute to the ethanol-induced defect in clathrin internalization	72
Internalization is blocked at the cell surface	72
Clathrin-mediated internalization is both delayed and impaired in ethanol-treated cells	75
Ethanol does not impair receptor recruitment into clathrin-coated pits	80
Ethanol impairs dynamin recruitment	82
Conclusions	87
<b>Discussion</b>	88
Lysine acetylation may be a regulator of hepatic protein function	89
Mechanisms of ethanol-induced hyperacetylation – ethanol metabolism	90
Consequences of ethanol-induced hyperacetylation – gene expression	92
Consequences of ethanol-induced hyperacetylation – mitochondrial dysfunction	94
Consequences of ethanol-induced hyperacetylation – oxidative stress	96
Consequences of ethanol-induced hyperacetylation – proteasome inhibition and aggresome formation	97
Ethanol impairs late-stage clathrin-vesicle internalization – Our working model	99
Consequences of ethanol-induced hyperacetylation – protein trafficking	101
Defects from the Golgi: Is there a similar mechanism?	105
Ethanol-induced hyperacetylation – a new therapeutic approach	107
<b>References</b>	110

## LIST OF ILLUSTRATIONS

	Page Number	
Figure 1	The structure of the liver	4
Figure 2	The first steps of chronic ethanol metabolism	7
Figure 3	WIF-B cells as a model for studying hepatotoxicity	8
Figure 4	Hepatic histone deacetylases and acetyltransferases that may play a role in nonnuclear protein acetylation	12
Figure 5	Ethanol alters cytoskeletal organization in hepatocytes	13
Figure 6	Alcohol-induced defects in hepatic trafficking	18
Figure 7	HDAC6 is an abundant microtubule deacetylase in WIF-B cells	37
Figure 8	HDAC6 protein levels decrease upon ethanol exposure	38
Figure 9	HDAC6 cytosolic distributions are not altered in ethanol or TSA-treated cells	39
Figure 10	HDAC6 is less stably associated with microtubules in ethanol and TSA-treated cells	40
Figure 11	HDAC6 microtubule binding is impaired in ethanol-treated cells	42
Figure 12	Cytosolic HDAC6 activity is increased in ethanol-treated WIF-B cells	43
Figure 13	Ethanol-induced tubulin modifications prevent HDAC6 binding	45
Figure 14	Chronic ethanol treatment induces global hepatic protein hyperacetylation	51
Figure 15	Chronic ethanol treatment induces acetylation of nuclear, cytosolic and membrane proteins	53

Figure 16	Numerous cytosolic proteins are hyperacetylated in livers from ethanol-fed rats	55
Figure 17	Ethanol induces cytosolic protein hyperacetylation	56
Figure 18	Numerous membrane proteins are hyperacetylated in livers from ethanol-fed rats	57
Figure 19	Ethanol induces total membrane hyperacetylation	58
Figure 20	Alcohol-induced hyperacetylation of glutathione peroxidase 1	65
Figure 21	Actin and cortactin are hyperacetylated in ethanol-treated liver cytosols	67
Figure 22	Components of the clathrin machinery accumulate at the plasma membrane in ethanol and TSA-treated WIF-B cells	71
Figure 23	Ethanol impairs clathrin-mediated internalization at the cell surface	74
Figure 24	Clathrin-mediated internalization is both delayed and impaired in ethanol and TSA-treated WIF-B cells	77
Figure 25	Ethanol impairs receptor internalization prior to vesicle fission	79
Figure 26	Receptor recruitment is not impaired by ethanol or TSA	81
Figure 27	Dynamin membrane recruitment is impaired in ethanol and TSA-treated cells	84
Figure 28	Co-immunoprecipitation confirms decreased dynamin-2 clathrin pit association in the presence of ethanol	86
Figure 29	Ethanol impairs late stage clathrin-vesicle internalization	100

## LIST OF TABLES

		Page Number
Table 1	Increased immunoreactivity is observed in a conserved set of proteins in livers from ethanol-fed rats	52
Table 2	Non-nuclear hyperacetylated proteins identified in livers from ethanol-fed rats	59
Table 3	Most alcohol-induced hyperacetylated proteins regulate liver metabolism	62

## ABBREVIATIONS

4MP	4-methylpyrazole
5'NT	5'nucleotidase
ABC	ATPase binding cassette
ABTS	2,2'-azino-di(3-ethyl-benzthiazoline-6-sulfonate)
AceCS2	acetyl CoA synthetase 2
AcK	acetylated lysine
ADH	alcohol dehydrogenase
ALDH	acetaldehyde dehydrogenase
AP2	adaptor protein 2
APN	aminopeptidase N
ASGP-R	asialoglycoprotein receptor
ATP	adenosine triphosphate
BAR	Bin/Amphiphysin/RVS
BC	bile canaliculus
BCA	bicinchroninic acid
BSA	bovine serum albumin
CBB	Coomassie brilliant blue
CHC	clathrin heavy chain
CYP2E1	cytochrome P450 2E1
DMEM	Dulbecco's modified Eagle medium
DNA	deoxyribose nucleic acid

DTT	dithiothreitol
EDTA	ethylene diaminetetraacetic acid
EE	early endosome
EGF	epidermal growth factor
EGTA	ethylene glycol tetraacetic acid
ELISA	enzyme-linked immunosorbent assay
ER	endoplasmic reticulum
EtOH	ethanol
F actin	filamentous actin
FBS	fetal bovine serum
G actin	globular (monomeric) acid
GED	GTPase effector domain
GPI	glycophosphatidylinositol
GPX-1	glutathione peroxidase-1
GST $\mu$ 2	glutathione s-transferase $\mu$ 2
GTP	guanosine triphosphate
HAT	histone acetyltransferase
HDAC	histone deacetylase
HNE	4-hydroxy-2-nonenal
HRP	horse radish peroxidase
HSP90	heat shock protein 90
IB	immunoblot

IFAP	intermediate filament associated protein
IL-6	interleukin 6
IL-10	interleukin 10
Lys	lysosome
MAA	malondialdehyde acetaldehyde
MALDI-MS	matrix-assisted laser desorption/ionization mass spectrometry
MDA	malondialdehyde
MOWSE	molecular weight search
NAD <sup>+</sup>	Nicotinamide adenine dinucleotide (oxidized)
NADH	Nicotinamide adenine dinucleotide (reduced)
NCBI	National Center for Biotechnology Information
NTA	nicotinamide
nz	nocodazole
PAGE	polyacrylamide gel electrophoresis
PBS	phosphate buffered saline
PBS-BT	PBS/BSA/Tween-20
PDGF	platelet-derived growth factor
PEM	Pipes/EGTA/MgSO <sub>4</sub>
PGC-1 $\alpha$	peroxisome proliferator-activated receptor $\gamma$ coactivator $\alpha$
PH	pleckstrin homology
PMSF	phenylmethanesulfonylfluoride
pIgA-R	polymeric IgA receptor

PIP <sub>2</sub>	phosphatidylinositol 4,5-bisphosphate
PRD	proline rich domain
PVDF	polyvinylidene fluoride
RE	recycline endosome
ROS	reactive oxygen species
SDS	sodium dodecyl sulfate
SEM	standard error of the mean
SH3	SRC homology 3
Sirt2	sirtuin 2
SNX9	sorting nexin 9
SOD	superoxide dismutase 1
SREBP	sterol response element binding protein
TBS	tris buffered saline
TGN	<i>trans</i> -Golgi network
TFA	trifluoroacetic acid
TF-R	transferrin receptor
TIRF	total internal reflection fluorescence
TJ	tight junction
TNF- $\alpha$	tumor necrosis factor $\alpha$
TRAIL	TNF-related apoptosis-inducing ligand
TSA	trichostatin A
TX-100	Triton X-100

## ACKNOWLEDGEMENTS

I am forever indebted to my advisor, Dr. Pamela Tuma. From the first day I entered her lab, she challenged me. Her unwavering patience and understanding combined with her humor and sharp witted remarks instilled in me the confidence to succeed.

I also extend my sincerest appreciation to the other members of my dissertation committee, Dr. John Golin and Dr. Ann Corsi. Their passion for research and teaching has inspired me and their advice and thought-provoking questions has greatly enhanced this dissertation.

I would also like to acknowledge the rest of the faculty in the Department of Biology, Dr. James Greene, Dr. Michael Mullins, Dr. Venigalla Rao, Dr. Nathalie Dautin, Ms. Marion Ficke, Dr. Barbara Howard, Dr. Karen Ross, Dr. Frank Portugal and Dr. Ekaterina Nestorovich. The collegiality of this department and their sincere interest in my scientific (and non-scientific) endeavors has provided me with the best education I could have ever asked for.

Much of the microscopy work presented in Part III of this dissertation was done at Johns Hopkins University School of Medicine. I would like to thank Dr. Ann Hubbard and the members of her lab, Dr. Lita Braiterman and Lydia Nyasae, for their welcoming and encouraging environment. I would also like to acknowledge members of the Microscope Facility, Dr. Scot Kuo and Barbara Smith, for their expertise and patience in training us on the microscopes and troubleshooting our many problems.

Special thanks to J.J. Kim and Wavell Pereira for their help with everything from our tube rotator and water baths to tracking down those missing appointment sheets. I will miss JJ's calls for "Dr. Shepard" from down the hall and the timely package arrival notifications!

The work presented in this dissertation directly reflects upon the wonderful lab environment that exists in the Tuma Lab. Many thanks to the current and former members of my "lab family" including Dr. Sai Prasad Ramnaryanan, Julie In, Dave Fernandez, Anneliese Striz, Julia Omotade and Ben Kalu. From lab meetings and conferences to "dry ice bombs" and "dress day" happy hours, I am truly grateful for all of our experiences we have shared together.

Lastly, I never would have made it through if it weren't for my one true obsession... Boston College football and basketball! Their successes (and failures) provided me with a much needed outlet from the lab and I am proud to call myself a Superfan. GO EAGLES!!

## INTRODUCTION

### **The Liver:**

The liver is the largest internal organ in the human body, comprising up to 5% of total body weight. Its organization and opportune anatomical placement reflects its unique roles. Located between the digestive tract and the rest of the body, the liver receives a dual blood supply from both the hepatic artery and portal vein. In addition to generating a highly vascularized organ, these blood vessels carry a large variety of xenobiotics including both nutrients and toxins directly to the liver. Thus, the main functions of this vital organ include the uptake, storage and processing of amino acids, carbohydrates, lipids and vitamins (Desmet, 2001). It also serves as the site for drug and toxin processing and secretion justifying its designation as the metabolic center of the body.

The functions of the liver are a result of a number of complex interactions between its many diverse cells. Functionally, the polygonal hepatocytes are the parenchymal cells in the liver (Fig. 1). These polarized epithelial cells constitute 70% of the liver and are flanked by at least two sinusoids. The cord-like arrangement of hepatocytes encloses a tubular structure known as the bile canaliculus. Hepatocytes have a highly complex polarity which separates the plasma membrane into three distinct and functionally important areas (Desmet, 2001; Schachter, 2001; Tuma and Hubbard, 2001)(Fig. 1). First, the sinusoidal domain, comprised of a vast number of irregular microvilli surrounds the blood sinusoids. This irregular surface is required for an efficient exchange of molecules with the bloodstream. As expected, this membrane is the

home to receptors for glycoproteins, hormones and many other metabolites found within the bloodstream. It is the primary site of endocytosis, both receptor-mediated clathrin internalization and fluid phase endocytosis (see below). The intercellular domain is the membrane region that is involved in hepatocyte-hepatocyte contact. Thus, it is the location of all adhesion and junctional complexes including the adherens junctions, tight junctions and gap junctions. Together with the sinusoidal domain, these membrane regions are often grouped together and termed the basolateral membrane (Desmet, 2001; Schachter, 2001; Tuma and Hubbard, 2001). Separated by tight junctions, the apical canalicular domain is the membrane surrounding the bile canaliculus. Differentiated from the basolateral membrane, the apical surface is enriched in lipids, cholesterol and sphingomyelin and is the primary site of organization for the cytoskeleton within the hepatocyte (see below). Due to its proximity to the bile canaliculus, the apical membrane functions in both bile export and secretion of processed toxins. It is the home to a variety of ATPase binding cassette (ABC) transporters that function in the unidirectional transport into the bile (Desmet, 2001; Schachter, 2001; Tuma and Hubbard, 2001; Ujhazy et al., 2001).

Since hepatocytes are surrounded by sinusoids and are thus in direct contact with the blood, the cells of the sinusoidal lining play important roles in both normal liver function and often contribute to liver perturbations under stressed conditions. Surrounding the sinusoids are endothelial cells whose main function is to serve as a sieve to filter particles that are exchanged between the sinusoid and the parenchymal cells. These endothelial cells are fenestrated, that is, they are full of holes or “windows”

allowing only those particles small enough to filter through the sinusoids. The diameter of these fenestrae is altered in the presence of both xenobiotics and endobiotics by constriction of the cytoskeleton (Braet et al., 2001; Desmet, 2001). Adhering to the surface of the fenestrated endothelial cells are the resident macrophages of the liver, the Kupffer cells. They function as a “waste receptacle” of sorts, engulfing blood-borne material that enters the liver and successfully removing 80-90% of foreign particles. Additionally, these cells are involved in maintaining homeostasis by removing senescent red blood cells. Activation of these cells by toxic agents results in the release of cytokines and other inflammatory mediators that serve to regulate hepatic injury (Desmet, 2001; Li and Friedman, 2001; Naito et al., 2004). On the other side of the sinusoidal endothelial cells are the hepatic stellate cells, which are found in the space of Disse (space between the sinusoid and hepatocytes). In the normal liver, these stellate cells are inactivated and serve as the main storage site for retinoids (vitamin A compounds). Upon liver injury, stellate cells become activated and differentiated. They lose their retinoid storage capacity and become proliferating fibroblasts whose main function is to secrete an array of cytokines, growth factors and other inflammatory mediators including interleukin-6 (IL-6), interleukin-10 (IL-10), epidermal growth factor (EGF) and platelet-derived growth factor (PDGF). These phenotypic changes also result in the accumulation of extracellular matrix due to collagen secretion that ultimately participates in the development of a fibrotic and cirrhotic liver (Desmet, 2001; Li and Friedman, 2001).

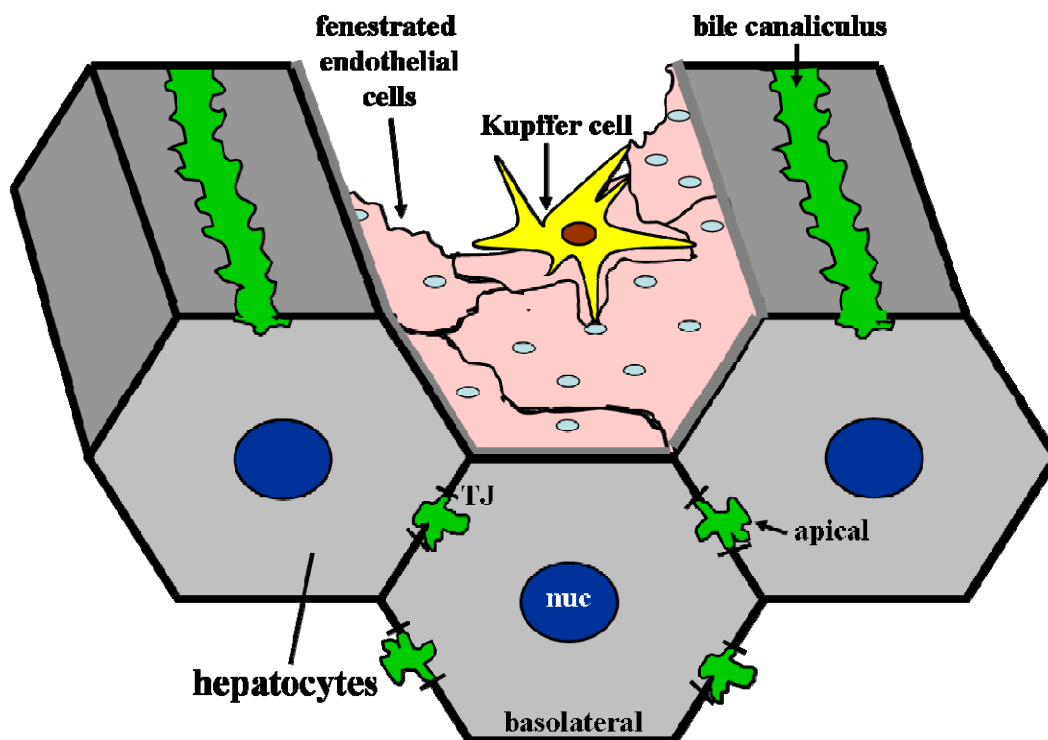


**Figure 1. The structure of the liver.** Polygonal hepatocytes (gray) are arranged in a cord-like manner and enclose a system of tubular bile canaliculi that feed secreted waste products into the bile. The apical membrane surrounds the bile canaliculus and is separated from the basolateral membrane by tight junctions (TJ). Hepatocytes are separated by the bloodstream by a single layer of fenestrated endothelial cells (pink). Kupffer cells are the resident macrophages of the liver that adhere to the endothelial cells, successfully removing 80-90% of foreign particles that enter the liver. (Figure adapted from Alberts et al., 2002)

### **Alcoholic Liver Disease:**

Included in the long list of xenobiotics that enter and are processed within the liver is ethanol, the potent chemical found in all alcoholic beverages. 2/3 of all Americans consume alcohol and chronic consumption can lead to liver damage. In fact, 44% of all liver disease related deaths were attributed to alcohol and it is the oldest form of liver disease known to man (O'Shea et al.). The progression of alcoholic liver disease is loosely grouped into three stages ranging from fatty liver to cirrhosis. The first stage,

steatosis or fatty liver, occurs in 90% of all individuals who drink (O'Shea et al.). This usually asymptomatic and completely reversible stage is described as an abnormal accumulation of fat within the hepatocytes. Approximately 1/3 of frequent drinkers progress to alcoholic hepatitis, the second stage of alcoholic liver disease. Like steatosis, this stage is generally asymptomatic and is characterized by an overall inflammation of the liver with an increase in neutrophil invasion (O'Shea et al.). While these first stages of liver damage are generally considered minor and reversible, the progression to fibrosis marks the beginning of end stage liver disease. Beginning in the perivenous area, fibrosis is the deposition of scar tissue and is often considered a model for wound healing (Bataller and Brenner, 2005; O'Shea et al.). During liver injury, hepatocytes regenerate and replace those cells undergoing apoptosis. However, if the injury persists, the result is a loss of proper regeneration and the activation of hepatic stellate cells. This leaves the liver with large deposits of extracellular matrix proteins including collagen and fibronectin. A cirrhotic liver is diagnosed when the scar tissue spreads throughout the liver and begins to severely impair normal liver function and blood flow (Bataller and Brenner, 2005; O'Shea et al.). It is during this final stage that the complications are noticeable and include jaundice, easy bruising and bleeding, portal hypertension, sensitivity to medications, and ascites fluid accumulating in the peritoneal cavity (Bataller and Brenner, 2005; O'Shea et al.). As linear as the progression of these stages may appear, very few alcoholics ever develop cirrhosis and identifying those with the potential to advance to this end stage has proven to be difficult.

Although the molecular mechanisms associated with alcoholic liver disease are

not well understood, much of the liver dysfunction is attributed to ethanol metabolism (Fig. 2). In the hepatocyte cytosol, alcohol dehydrogenase (ADH) converts ethanol to acetaldehyde, a highly reactive intermediate. Acetaldehyde is further metabolized in the mitochondria to acetate by acetaldehyde dehydrogenase (ALDH). Ethanol is also metabolized by the resident endoplasmic reticulum (ER) enzyme, cytochrome P450 2E1 (CYP2E1) (Tuma and Casey, 2003). CYP2E1-mediated ethanol metabolism not only leads to the formation of acetaldehyde, but also to the formation of oxygen and hydroxyethyl radicals. These radicals interact with lipids to generate reactive molecules such as malondialdehyde (MDA) and 4-hydroxy-2-nonenal (HNE). All of these aldehyde intermediates can readily and covalently modify proteins, DNA and lipids and are thought of as the key to the development of alcoholic liver disease (Brooks, 1997; Tuma and Casey, 2003; Tuma et al., 1987). Since these aldehydes coexist during ethanol metabolism, they can both modify proteins on their own or bind synergistically to form hybrid adducts known as MDA-Acetaldehyde (MAA) adducts (Brooks, 1997; Tuma and Casey, 2003; Tuma et al., 1987). In general, acetaldehyde and the oxygen radicals are thought to form stable adducts with the  $\epsilon$ -amino group of lysine residues though the exact chemical structure of stable adducts are unknown. So far, the list of modified proteins includes tubulin, actin, calmodulin, hemoglobin, hepatic enzymes and plasma proteins (Brooks, 1997; Tuma and Casey, 2003; Tuma et al., 1987). The hypothesis is that these cumulative covalent modifications disrupt the normal functioning of hepatic proteins leading to cell injury.

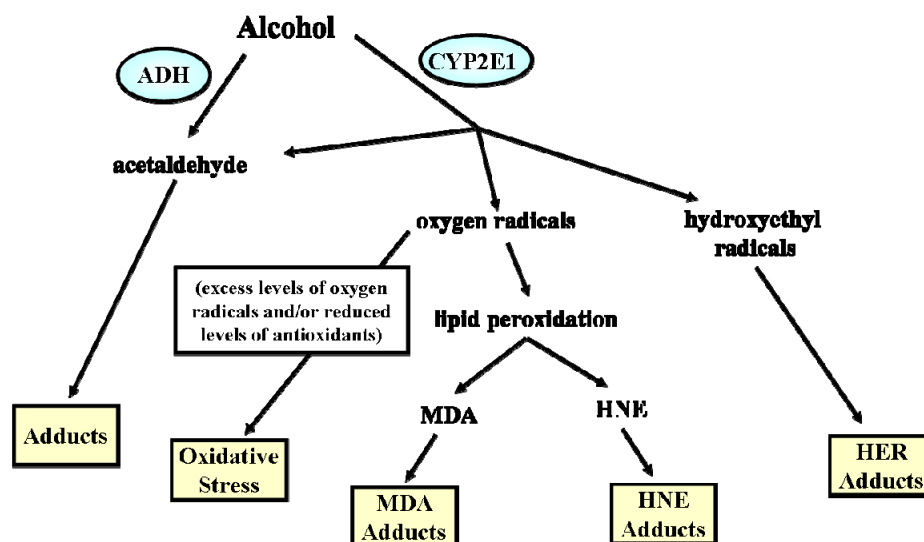


**Figure 2. The first steps of chronic ethanol metabolism.** Alcohol is first metabolized in the hepatocyte cytosol by alcohol dehydrogenase (ADH) and the ER-resident cytochrome p450 2E1 (CYP2E1) resulting in the formation of acetaldehyde. Acetaldehyde is further converted to acetate in the mitochondria by acetaldehyde dehydrogenase (not shown). Ethanol metabolism by both ADH and CYP2E1 can lead to the formation of highly reactive intermediates which can readily modify proteins, DNA and lipids that impair proper hepatic function. (Figure adapted from Tuma and Casey, 2003)

### WIF-B cells – A model for hepatotoxicity:

Meaningful research on ethanol-induced hepatotoxicity has been hampered by the lack of good *in vitro* models. So far, three models have been identified as promising candidates: isolated hepatocytes, HepG2 cells and WIF-B cells (Clemens et al., 1995; Schaffert et al., 2004). The first two models, however, have limitations. Isolated hepatocytes, while the most popular choice over the last 30 years, lose their liver-specific phenotype within hours of culture. Both cell surface polarity and expression of ADH are lost making only short-term experiments possible. Similarly, only 10% of HepG2 cells are polarized in culture and most of their liver specific functions are lost. In contrast, hepatic WIF-B cells have emerged as an excellent model for studying both hepatocyte

polarity and ethanol-induced hepatocyte injury (Fig. 3) (Ihrke et al., 1993; Schaffert et al., 2004)

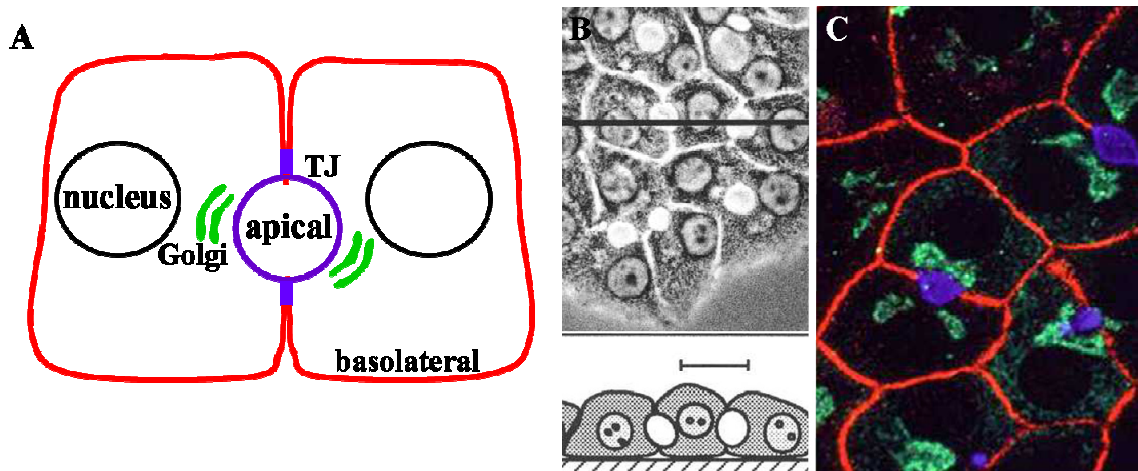


**Figure 3. WIF-B cells as a model for studying hepatotoxicity.** A, A schematic of two polarized WIF-B cells. As for hepatocytes, WIF-B cells have a distinct apical and basolateral membrane separated by tight junctions (TJ). B, The phase contrast of cultured WIF-B cells. The phase lucent structures are the functional equivalent of a bile canaliculus (BC) enclosed by the apical membrane. An imaginary cross-section of the monolayer taken along the line in the upper panel shows that the BCs are sequestered from both the substrate and medium. C, Triple labeling of WIF-B cells are shown. Notice the distinct staining for both the basolateral (red) and apical membrane (blue). The Golgi is labeled in green.

WIF-B cells are a hybrid cell line that were derived from fusing rat hepatoma cells (Fao) and human fibroblasts (WI38) and selecting for their ability to grow to a high density in culture. When cultured on plastic or glass coverslips, these cells enter a terminal differentiation program and after 7-9 days of growth, > 70% of the culture is polarized. WIF-B cells generate phase-lucent structures that are functionally equivalent to bile canaliculi despite not forming the traditional belt-like tubules (Ihrke et al., 1993)(Fig. 3). They maintain all the hallmarks of polarized hepatocytes *in situ* including the restriction of proteins and lipids to their respective membrane domains by tight

junctions (Ihrke et al., 1993; Shanks et al., 1994)(Fig 3). The hepatocyte-specific membrane trafficking patterns are maintained from the basolateral membrane including transcytosis, receptor recycling and lysosomal delivery (Ihrke et al., 1998). Their cytoskeleton mimics what is seen in hepatocytes *in situ* with a thick actin cortical web concentrated around the bile canaliculus and microtubule bundles radiating outward from the centrioles localized close to the apical membrane (Ihrke et al., 1993).

Importantly for our studies, WIF-B cells efficiently metabolize alcohol (Schaffert et al., 2004). They exhibit twice the ADH activity of freshly isolated hepatocytes and produce levels of acetaldehyde similar to that of ethanol-treated hepatocytes. The ALDH in these cells has a very low  $K_m$  which allows for a rapid conversion of acetaldehyde to acetate. While WIF-B cells express only 25% of the levels and activity of CYP2E1 compared to hepatocytes, it can be induced up to 65% with the addition of 4-methylpyrazole (4MP), an ADH inhibitor that stimulates CYP2E1 activity. Upon addition of ethanol, WIF-B cells exhibit an increased lactate:pyruvate ( $\text{NADH:NAD}^+$ ) ratio indicative of oxidative stress (Schaffert et al., 2004). This altered oxidative state leads to the formation of protein carbonyl adducts and the generation of  $\text{H}_2\text{O}_2$  (McVicker et al., 2009). Additionally, treated cells have increased triglyceride levels corresponding to the clinically observed fatty liver (Schaffert et al., 2004) and exhibit the hallmark characteristics of apoptosis including caspase activation and the upregulation of Fas protein (McVicker et al., 2006). Overall, both the maintenance of polarity and their ability to metabolize ethanol make WIF-B cells an excellent model system for studying the effects of long term, chronic ethanol consumption on liver hepatocytes.

**Lysine acetylation:**

In addition to protein modifications from ethanol metabolites, it has become apparent that alcohol exposure also induces protein covalent-modifications that are part of the natural repertoire. To date, these post-translational modifications include increased methylation, phosphorylation and acetylation (Kannarkat et al., 2006; Lee and Shukla, 2007; Lieber et al., 2008; Pal-Bhadra et al., 2007; Park et al., 2003; Picklo, 2008; You et al., 2008). In particular, numerous proteins have been identified that are hyperacetylated upon ethanol exposure, and this list is expanding rapidly. For over 40 years it has been recognized that proteins can be acetylated and that the modification comes in two forms (Polevoda and Sherman, 2002). One is the irreversible, co-translational N-terminal acetylation of  $\alpha$ -amino groups of mainly serine and alanine, but also of threonine, methionine and glycine. The other form is the reversible, post-translational modification of  $\epsilon$ -amino groups on lysine residues located within a polypeptide (Kouzarides, 2000; Polevoda and Sherman, 2002). The reversibility of lysine acetylation and its presence on an ever expanding list of nuclear and nonnuclear proteins have led some to postulate that it might rival phosphorylation in its ability to regulate cellular processes (Kouzarides, 2000). Thus, alcohol-induced protein hyperacetylation likely leads to major physiological consequences that contribute to the progression of hepatotoxicity.

Protein acetylation results from the coordinated activities of acetyltransferases and deacetylases (Kouzarides, 2000; Polevoda and Sherman, 2002). Histones were the first proteins known to be acetylated, and accordingly, the modifying enzymes were initially named histone acetyltransferases (HATs) and histone deacetylases (HDACs).

Although the list of acetylated proteins has since grown to include numerous nonhistone substrates, their names have remained. To date, there are at least 18 known deacetylases and 17 known families of HATs that are categorized based on sequence homology and cofactor/coenzyme dependence (Yang and Gregoire, 2005). Many of these modifying enzymes are found in the liver and generally reside in the nucleus. However, several HATs and HDACs have been found to shuttle between the nucleus and cytosol or reside completely in the cytosol for modification of non-nuclear proteins (Fig. 4). Of particular interest to these studies is the class II HDAC, HDAC6 which is the only exclusively cytosolic HDAC found in liver (Grozinger et al., 1999; Hubbert et al., 2002; Matsuyama et al., 2002; Shepard et al., 2008; Zhang et al., 2008; Zhang et al., 2003). One of its known substrates is  $\alpha$ -tubulin, one of the best characterized, nonnuclear, hyperacetylated proteins in ethanol exposed cells (Glozak et al., 2005; Kannarkat et al., 2006; Shepard et al., 2008; Shepard et al., 2009b; Zhang et al., 2008; Zhang et al., 2003) (see below and Part I).

Although most known HAT and HDAC substrates reside in the nucleus, a recent proteomics survey identified a diverse set of almost 200 lysine-acetylated proteins, many of which are non-nuclear (Kim et al., 2006). Remarkably, this survey also revealed that more than 20% of mitochondrial proteins are lysine-acetylated (Kim et al., 2006). To date, the lysine-acetylation of a handful of hepatic proteins has been reported to be induced by ethanol exposure (Shepard and Tuma, 2009). So far this list includes histone H3, tubulin, sterol response element binding protein-1c (SREBP), p53, peroxisome proliferator-activated receptor  $\gamma$  coactivator  $\alpha$  (PGC-1 $\alpha$ ) and acetyl CoA synthetase 2

(AceCS2) (Shepard and Tuma, 2009). A recent study also determined that numerous mitochondrial proteins (not yet identified) are hyperacetylated after ethanol exposure, and that the acetylation remained long after ethanol withdrawal (Picklo, 2008). With the growing number of known acetylated proteins and the large number of modifying enzymes, it is likely that numerous proteins are hyperacetylated in ethanol-exposed hepatocytes. The identification of novel, nonnuclear, ethanol-induced proteins is the subject of Part II of this dissertation.

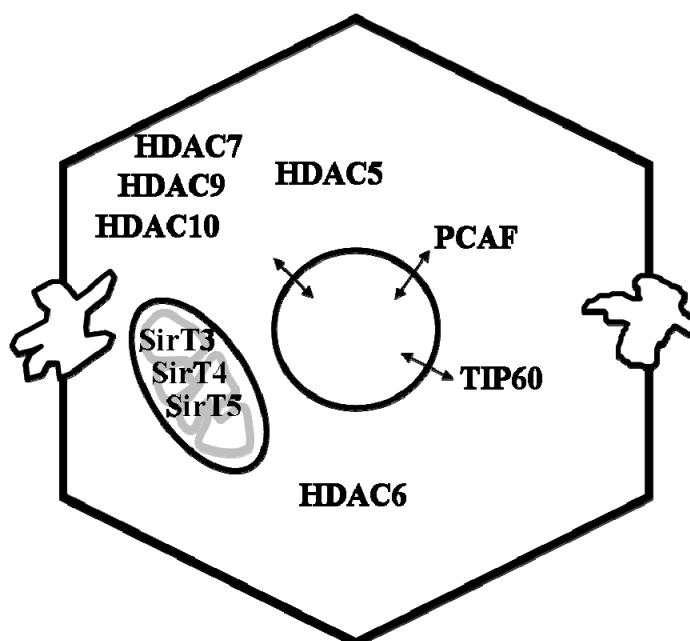


**Figure 4. Hepatic histone deacetylases (HDAC) and acetyltransferases (HAT) that may play a role in nonnuclear protein acetylation.** HDAC5, 7, 9 and 10 and acetyltransferases PCAF and TIP60 shuttle between the nucleus and cytoplasm in hepatocytes as indicated by the double arrow. HDAC6 is the only exclusively cytoplasmic deacetylase found in the liver and SirT3, 4 and 5 are all mitochondrial sirtuins.

#### **Ethanol-induced hepatic defects – A focus on the cytoskeleton:**

The hepatocyte cytoskeleton consists of three filamentous networks:

microtubules, actin microfilaments and keratin intermediate filaments. Because of the

abundance of the proteins that comprise each system and the central role each network plays in a variety of cellular processes, the three filament systems have been the focus of a host of studies aimed at understanding the progression of alcohol-induced liver injury (Fig. 5).

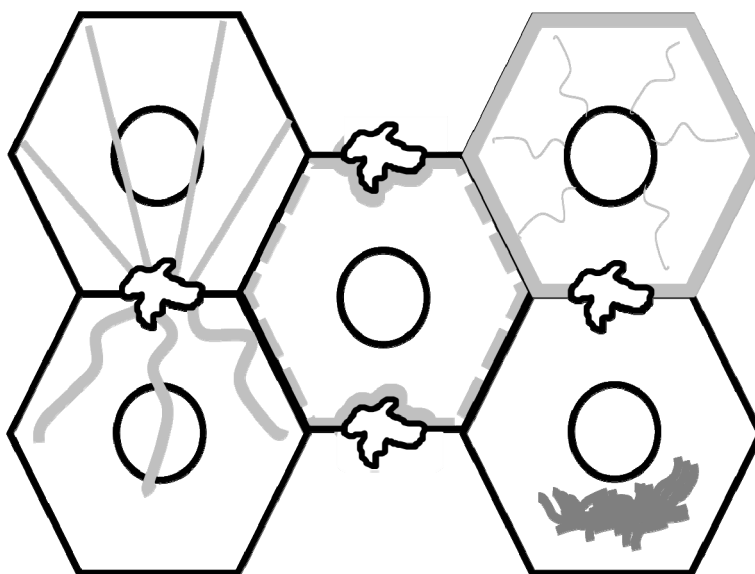


**Figure 5. Ethanol alters cytoskeletal organization in hepatocytes.** In control cells (top left cell), microtubules emanate from sites at or near the apical plasma membrane with their plus ends attached to or near the basolateral plasma membrane. In the presence of ethanol (bottom left cell), microtubules appear thicker, shorter and more gnarled. In contrast, ethanol does not alter actin filament organization (middle cell). Both control and ethanol-exposed actin filaments form a dense sub-cortical web at both the apical and basolateral plasma membranes. Keratin filaments normally form dense sub cortical networks originating from the apical and basolateral plasma membrane in hepatocytes (top right cell). In the presence of ethanol, keratin filaments accumulate in dense cytoplasmic inclusions known as Mallory-Denk Bodies (bottom right cell).

Microtubules are made of repeating units of  $\alpha$ - and  $\beta$ -tubulin heterodimers that form protofilaments, which in turn assemble into hollow tubes consisting of 13 protofilaments arranged in parallel. Microtubules exist as both dynamic and stable polymers. The latter population is characterized by a longer half-life, resistance to microtubule poisons (e.g. cold and nocodazole) and by specific post-translational

modifications on the  $\alpha$ -tubulin subunit(Westermann and Weber, 2003). In hepatocytes, cell surface polarity is reflected in the asymmetric organization of microtubules. In polarized cells, there is evidence that microtubules are organized from sites at or near the apical plasma membrane. The emanating microtubules are oriented with their minus ends at the apical surface and their plus ends attached to or near the basolateral membrane(Meads and Schroer, 1995) (Fig. 5).

Actin is a ubiquitous cytoskeletal protein that exists as both a monomer (G-actin) and a filamentous polymer (F-actin). The actin cytoskeleton has a unique organization in many polarized cells. In general, actin microfilaments extend to the basolateral membrane and form attachments through interactions with proteins of zonulae adherens, tight junctions and focal adhesions. At the apical surface, actin is found as the core filament of microvilli and also as a dense sub-cortical web(Bretscher, 1991; Fath et al., 1993; Mays et al., 1994). At the basolateral domain, actin-associated proteins form a scaffold that restricts the movement of membrane proteins, thereby contributing to the polarized separation of membrane proteins(Mays et al., 1994) (Fig. 5).

Lastly, the cytokeratin intermediate filament system is composed of polymerized dimers consisting of one acidic (Type I) and one basic (Type II) keratin subunit. Although over 50 keratin isoforms have been identified, hepatocytes express only keratin 8 (Type II) and keratin 18 (Type I). In the hepatocyte, apical and basolateral cortical keratin filaments are observed suggesting an important role in the establishment and maintenance of epithelial cell polarity and in polarized secretion(Oriolo et al., 2007). Several intermediate filament associated proteins (IFAPs) have also been identified that

are thought to modulate filament assembly and associations with actin filaments and microtubules(Strnad et al., 2008a). These associations are required for the polarized distribution of both actin and microtubules suggesting the role of keratins in regulating polarity and polarized protein trafficking is likely indirect by providing a polarized scaffold for filament orientation(Oriolo et al., 2007) (Fig. 5).

One of the best-studied target proteins for acetaldehyde is  $\alpha$ -tubulin(Tuma et al., 1991b). *In vitro*, soluble tubulin dimers purified from either bovine brain(Jennett et al., 1987; Jennett et al., 1980) or rat liver(Jennett et al., 1989) were found to be much more highly adducted than pre-formed microtubules. Adduction occurred preferentially on the  $\alpha$ -tubulin subunit at a highly reactive lysine(Jennett et al., 1987; Jennett et al., 1980). Further examination revealed that adduction of this highly reactive lysine on  $\alpha$ -tubulin drastically impaired *in vitro* microtubule polymerization(Jennett et al., 1987; Jennett et al., 1980). Assays using low acetaldehyde:tubulin dimer levels further revealed that impaired microtubule formation occurred at substoichiometric amounts of acetaldehyde (0.2 mol acetaldehyde/mol tubulin) suggesting that small levels of adduction can have far reaching effects on microtubule function(Smith et al., 1992). More recently it was shown that tubulin purified from ethanol-fed rat livers displayed impaired polymerization relative to control(Yoon et al., 1998). Although consistent with an acetaldehyde-induced impairment, the presence of adducts on the purified tubulin was not confirmed.

Impaired microtubule polymerization has also been examined in isolated hepatocytes from alcohol-fed rats(Yoon et al., 1998). After removing nocodazole (a reversible microtubule depolymerizing agent), microtubule regrowth was monitored

morphologically and was found to be significantly impaired in ethanol-treated hepatocytes. Ethanol-treated WIF-B cells exhibited a similar tubulin phenotype where microtubule regrowth after nocodazole washout was impaired (Kannarkat et al., 2006). Although the formation of tubulin-adducts has not been defined *in vivo*, these results are consistent with the effects of acetaldehyde on tubulin assembly *in vitro*.

In addition to acetaldehyde adduction,  $\alpha$ -tubulin is also one of the best characterized ethanol-induced hyperacetylated proteins. While acetaldehyde adduction prevents proper tubulin polymerization, when microtubules were examined morphologically, they resembled the so-called “stable” polymers (Fig. 5). Antibodies to acetylated lysine 40 on  $\alpha$ -tubulin confirmed their identity morphologically and revealed biochemically that ethanol-treated cells had approximately three-fold more acetylated  $\alpha$ -tubulin than control cells. Consistent with increased acetylated  $\alpha$ -tubulin levels, microtubules in ethanol-treated WIF-B cells were more stable. These results were confirmed in livers from ethanol-fed rats indicating the findings have physiologic importance (Kannarkat et al., 2006). Because microtubule hyperacetylation and stability increased with increased time of ethanol exposure or concentration, and was prevented by 4MP and potentiated by cyanamide, an ALDH inhibitor that leads to increased acetaldehyde levels, we conclude that increased acetylation requires alcohol metabolism and is likely mediated by acetaldehyde (Kannarkat et al., 2006). Thus, ethanol metabolism impairs tubulin polymerization, but once microtubules are formed they are hyperstabilized. Part I of this dissertation focuses on determining the mechanism(s) behind this observed microtubule hyperacetylation.

Like tubulin, actin contains several reactive lysines making it an attractive candidate for acetaldehyde-adduct formation. When the covalent binding of radiolabeled acetaldehyde to purified actin was examined, stable adducts were formed under both reducing and non-reducing conditions (Xu et al., 1989). Interestingly, G actin formed considerably more adducts with acetaldehyde than F actin, and the monomer efficiently competed for acetaldehyde adduction when co-incubated with albumin, another known adducted protein. However, despite the readily adducted G actin, actin polymerization was not impaired (Xu et al., 1989) (Fig. 5). This does not rule out the possibility that adduction can lead to altered actin dynamics *in vivo* or impair binding of actin to its binding partners or myosin motors that may explain some of the observed defects in protein trafficking (see below).

One of the pathological markers of alcoholic liver disease is the appearance of Mallory-Denk bodies. Morphologically, Mallory-Denk bodies are dense cytoplasmic inclusions formed of fibrillar keratin, chaperones, components of the protein degradation machinery and other proteins (Ku et al., 2007; Omary et al., 2009; Strnad et al., 2008a; Strnad et al., 2008b; Zatloukal et al., 2007) (Fig. 5). Interestingly, the keratin filaments in these inclusions are highly post-translationally modified. They are hyperphosphorylated, transamidated (via transglutaminase 2), ubiquitinated and partially degraded. These dense aggregates are thought to form in response to oxidative stress that triggers the upregulation and ubiquitinylation of keratins within the hepatocyte. The accumulated proteins overwhelm the degradative machinery that is already compromised by ethanol treatment (Osna and Donohue, 2007) resulting in the formation of dense inclusions.

### Ethanol-induced hepatic defects – A focus on protein trafficking:

While ethanol consumption leads to a multitude of hepatic defects, perhaps none is more well characterized than the impairments in protein trafficking. For over 30 years, defining the alcohol-induced defects in protein trafficking has been an active area of research in understanding liver injury. To date, numerous proteins are known to have alcohol-induced alterations in their dynamics. In general, two transport pathways appear to be affected: transport of newly-synthesized secretory or membrane glycoproteins from the Golgi to the basolateral membrane and clathrin-mediated endocytosis from the sinusoidal surface (Shepard et al., 2009a)(Fig. 6).

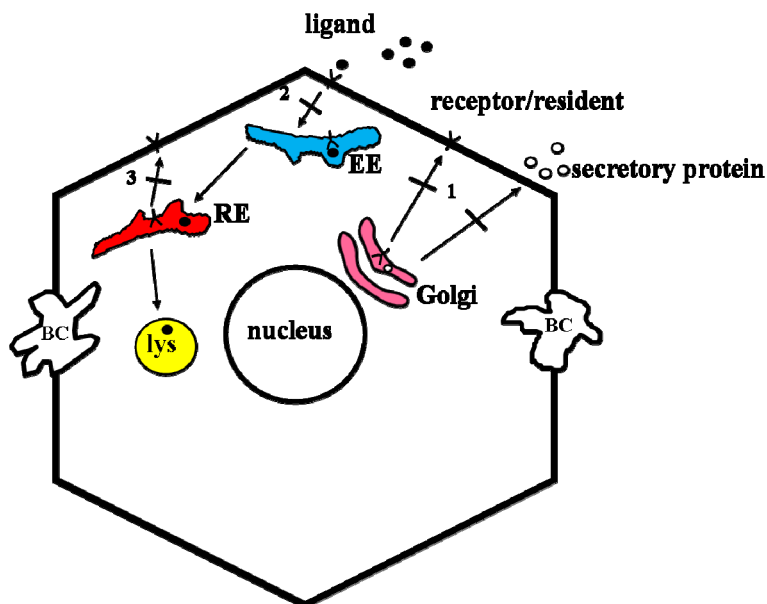


**Figure 6. Alcohol-induced defects in hepatic trafficking.** Secretion and delivery of newly synthesized basolateral proteins is impaired in ethanol-exposed hepatocytes (step 1). Also, three major steps in the itineraries of various receptors are impaired by ethanol metabolism: transport of newly synthesized receptors from the Golgi to the basolateral membrane (step 1); receptor internalization from the plasma membrane (step 2); and recycling of receptors from recycling endosomes (RE) back to the cell surface (step 3). EE, early endosome; RE, recycling endosome; lys, lysosome; BC, bile canaliculus.

The liver synthesizes the majority of serum proteins and lipoproteins and is characterized by robust constitutive secretion from the basolateral surface. In general, proteins destined for the secretory pathway and newly synthesized membrane-bound glycoproteins encode a signal sequence that directs their docking and cotranslational entry into the ER. During transit through the ER, these proteins are step-wise glycosylated, properly folded and eventually packaged into coatamer II-coated vesicles for delivery to the *cis*-Golgi. During transit through the Golgi, the proteins are further modified (e.g., sulfation or phosphorylation) and their carbohydrates further trimmed and modified. In the *trans*-Golgi network (TGN), the newly synthesized proteins are terminally glycosylated by the addition of N-acetylglucosamine, galactose, sialic acid and/or fucose moieties. While the mechanistic details regulating sorting at the TGN are not fully understood, secreted proteins and membrane-bound glycoproteins are packaged into discrete vesicles and delivered to the basolateral surface where they will either reside (membrane-bound proteins) or be released (secreted proteins) (Saucan and Palade, 1994).

Early studies relied on radiolabelling to identify and pinpoint the defect in transport from the Golgi. Radiolabeled leucine is incorporated into newly synthesized proteins and its release from the hepatocyte was measured. Studies found a decrease in release of radiolabeled leucine or terminal sugars with a reciprocal increase in hepatic protein content in the presence of ethanol suggesting that alcohol impairs post-Golgi sorting and vesicle delivery. More recent studies in both rat liver slices and polarized, hepatic WIF-B cells have also determined that ethanol exposure impairs albumin secretion (Joseph et al., 2008; Klassen et al., 2008). Addition of acetaldehyde also led to

impaired hepatic secretion indicating that ethanol metabolism is required for the defect (Volentine et al., 1987). This is consistent with findings where addition of cyanamide potentiated the impairment while 4-MP prevented the observed secretion defects (Sorrell et al., 1977; Volentine et al., 1987; Volentine et al., 1984). Together, these early studies indicate that ethanol significantly impairs both hepatic protein secretion and glycoprotein delivery and the defect is likely mediated by acetaldehyde (Fig. 5).

There are at least three major internalization routes in mammalian cells: clathrin-mediated, caveolae/raft-mediated and non-clathrin/non-raft mediated (Conner and Schmid, 2003; Doherty and McMahon, 2009; Mayor and Pagano, 2007) that are characterized by specific molecular players, cargoes and regulators. Previously, we found that ethanol impairs the clathrin-mediated internalization of asialoglycoprotein receptor (ASGP-R) and the transcytosis of a single spanning apical resident, aminopeptidase N (APN). However, no changes were observed in the trafficking of the glycosphosphatidylinositol (GPI)-anchored protein, 5' nucleotidase (5'NT), suggesting that the major routes of internalization are differentially affected by ethanol (Joseph et al., 2008). This hypothesis was confirmed when the basolateral internalization of selected proteins/compounds endocytosed by different mechanisms was monitored in the presence of ethanol (Fernandez et al., 2009). In this study, both polymeric IgA-receptor (pIgA-R) and transferrin receptor (Tf-R), two additional markers of clathrin internalization, accumulated at the plasma membrane consistent with decreased internalization. Conversely, those markers taken up either by caveolae/raft, fluid phase or non-vesicle mediated internalization were not affected by ethanol. In support of a clathrin-specific

defect, ethanol treatment led to an accumulation of clathrin heavy chain in discrete puncta at the basolateral plasma membrane. These findings strongly argue that ethanol specifically impairs clathrin-mediated internalization likely at the stage of vesicle fission, not coat assembly (Fernandez et al., 2009).

There are three core proteins and a multitude of accessory factors that are required for efficient clathrin-mediated internalization (Apodaca, 2001; Conner and Schmid, 2003; McNiven and Thompson, 2006). Briefly, the clathrin triskelion comprised of three heavy chains and three light chains assemble to form a basket-like coat that surrounds internalized vesicles. The assembly of these triskelions requires other proteins, mainly the adaptor protein, AP2. This multisubunit molecule is comprised of 4 subunits ( $\alpha$ ,  $\beta$ 2,  $\mu$ 2 and  $\sigma$ 2) and participates in the coordination of the receptors and clathrin at the plasma membrane. Clathrin-mediated internalization progresses through three major stages. Assembly is initiated upon ligand binding and the subsequent AP2 recruitment to the plasma membrane where the  $\alpha$  subunit binds at sites enriched in phosphatidylinositol 4,5-bisphosphate (PIP<sub>2</sub>) lipids. The  $\mu$ 2 subunit recognizes dileucine or tyrosine-based motifs on the receptor cytoplasmic tails, allowing the  $\beta$  subunit to interact with clathrin which in turn promotes assembly. As the coated pit matures, it becomes remodeled and deeply invaginated with the help of membrane curvature Bin/Amphiphysin/Rvs (BAR) domain proteins such as epsin and amphiphysin. Lastly, scission occurs when the coated pit is highly invaginated. This step is characterized by actin polymerization and the recruitment of the GTPase, dynamin whose oligomerization and GTPase activity promotes membrane pinching resulting in vesicle release (Apodaca, 2001; Conner and

Schmid, 2003; McNiven and Thompson, 2006). Newly budded vesicles are rapidly uncoated allowing for coat recycling and vesicle fusion with its target organelle.

The defect in clathrin-mediated internalization has been studied by examining several different receptors or ligands in different systems that include isolated hepatocytes, intact perfused rat liver, rat liver slices and WIF-B cells. Initially examined by studying the trafficking of both ASGP-R and its ligand, ethanol was found to impair both receptor-mediated internalization as well as receptor recycling from recycling endosomes. In most cases, both chronic and acute ethanol consumption led to the retention of clathrin-specific receptors on the surface of the hepatocyte with a decrease in the intracellular population. Addition of 4MP prevented the endocytic defect in both HepG2 cells stably expressing alcohol dehydrogenase and in WIF-B cells indicating the effect requires ethanol metabolism and is likely mediated by acetaldehyde (Clemens et al., 1996), 35] (Fig. 5). Determining the exact mechanism(s) for this defect is the focus of Part III of this dissertation.

## MATERIALS AND METHODS

**Reagents and Antibodies.** F12 (Coon's modification) medium, 4MP, trichostatin A (TSA), nocodazole, nicotinamide (NTA), sodium butyrate, taxol and bovine serum albumin (BSA) were purchased from Sigma-Aldrich (St. Louis, MO). Purified bovine brain tubulin was purchased from Cytoskeleton (Denver, CO) and was stored as a 10 mg/ml stock in PEM (100 mM Pipes, 1 mM EGTA, 1 mM MgSO<sub>4</sub>, pH 6.6) at -70°C. Fetal bovine serum (FBS) was purchased from Gemini Bio-Products (Woodland, CA) and HEPES was from HyClone (Logan, Utah). Acetylated BSA was purchased from USB (Cleveland, OH) and the polyclonal acetylated lysine antibodies were from Cell Signaling Technology (Danvers, MA). Cy3, alexa-488 and 568-conjugated secondary antibodies were purchased from Invitrogen (Carlsbad, CA). Horse radish peroxidase (HRP)-conjugated secondary antibodies and monoclonal antibodies against  $\alpha$ -tubulin or acetylated  $\alpha$ -tubulin were purchased from Sigma-Aldrich. Antibodies for histone H3, acetylated histone H3, glutathione peroxidase-1 (GPx-1), the HDAC6 C-terminus (H-300) and the Sirtuin 2 (SirT2) N-terminus were from Santa Cruz Biotechnologies (Santa Cruz, CA). The polyclonal antibody against the SirT2 C-terminus (PA3-200) was from Affinity Bio Reagents (Golden, CO). The clathrin heavy chain (CHC) (X22) and  $\alpha$ -adaptin (AP6) antibodies were purchased from Novus Biologicals (Littleton, CO) and the dynamin antibody was purchased from BD Biosciences (San Jose, CA). The actin and cortactin antibodies were purchased from Abcam (Cambridge, MA) and Millipore (Billerica, MA), respectively. The ASGP-R, pIgA-R, 5'NT and CE9 antibodies were kindly provided by A. Hubbard (Johns Hopkins University School of Medicine,

Baltimore, MD). HDAC colorimetric activity assay kits were purchased from BioMol International (Plymouth Meeting, PA).

***Cell Culture, Virus Production and Infection.*** HeLa cells were grown in a humidified incubator in 5% CO<sub>2</sub> at 37<sup>0</sup>C in Dulbecco's Modified Eagle Medium (DMEM) supplemented with 10% FBS and were seeded at 1x10<sup>6</sup> cells/10 cm dish and cultured for 4-5 days. WIF-B cells were grown in 7% CO<sub>2</sub> in Coon's-modified F-12, pH 7.0, supplemented with 5% FBS, 10 μM hypoxanthine, 40 nM aminopterin and 1.6 μM thymidine (Ihrke et al., 1993). Cells were seeded onto glass coverslips at 1.3x10<sup>4</sup> cells/cm<sup>2</sup> or at 1x10<sup>6</sup> cells/10 cm dish and cultured for 8-12 days until they reached maximum density and polarity. Cells grown on dishes or coverslips were treated on day 3 or 7, respectively, with 50 mM ethanol buffered with 10 mM Hepes, pH 7.0 at 37<sup>0</sup>C for 72 h as described (Schaffert et al., 2004).

Recombinant adenovirus encoding V5/myc-tagged pIgA-R that was generated using the Cre-Lox system (Bastaki et al., 2002) was provided by Dr. A. Hubbard (Johns Hopkins University School of Medicine, Baltimore, MD). For alcohol studies, WIF-B cells were infected after 48 h of ethanol treatment for 60 min at 37<sup>0</sup>C as described (Bastaki et al., 2002). The cells were washed with complete medium and incubated for an additional 18-20 h in the continued absence or presence of ethanol to allow for protein expression.

***Immunofluorescence Microscopy and Imaging.*** In general, WIF-B cells were fixed on ice with phosphate buffered saline (PBS) containing 4% paraformaldehyde for 1 min and permeabilized with methanol for 10 min (Ihrke et al., 1993). Cells were processed for

indirect immunofluorescence as described (Ihrke et al., 1993) using polyclonal antibodies to HDAC6 (1:100), ASGP-R (1:1000) and pIgA-R (1:200), or monoclonal antibodies to  $\alpha$ -adaptin (1:100) and CHC (1:1000). Cy3- and alexa-488 and 568-conjugated secondary antibodies were added at 5  $\mu$ g/ml. To stain using the monoclonal anti-cortactin antibody (1:100), cells were permeabilized with 0.1% saponin in PEM/sucrose for 2 min and fixed at room temperature with PBS containing 4% paraformaldehyde for 30 min. Washes and antibody dilutions were done in the continued presence of 0.1% saponin. To visualize membrane-associated dynamin (1:100), WIF-B cells were first permeabilized with 0.1% Triton X-100 (Tx-100) for 2 min in PEM/sucrose at room temperature and fixed in methanol for 5 min at 4°C. Labeled cells were visualized by epifluorescence using an Olympus BX60 Fluorescence Microscope (OPELCO, Dulles, VA). Images were taken using a SPOT digital camera and software (Diagnostic Instruments, Sterling Heights, MI) or a Coolsnap HQ2 digital camera (Photometrics, Tucson, AZ) and IPLabs image analysis software (Biovision, Exton, PA). Visualization of confocal images was performed on a Zeiss Axiovert 200 inverted microscope with a 510 meta laser scanning confocal module. Images were processed and figures compiled using Adobe Photoshop (Adobe Systems Inc, Mountain View, CA).

***Total Internal Reflection Fluorescence (TIRF) Microscopy.*** WIF-B cells were fixed and labeled as described above and mounted in 5% glycerol/tris buffered saline (TBS) containing 4 mg/ml phenylenediamine. Fluorophores were excited at 488 nm and 568 nm with a high-power 2.5W Kr/Ar laser (Spectra Physics, Irvine, CA) and visualized by TIRF microscopy using an Olympus 1X 71 inverted microscope and Olympus TIRF

illuminator with fiber optic input (Center Valley, PA). Images were taken using a Photometrics Evolve EM-CCD camera (Tucson, AZ) and Metamorph software (Molecular Devices, Sunnyvale, CA).

**Western Blotting.** In general, cells were lysed directly into Laemmli sample buffer (Laemmli, 1970) and boiled for 3 min. Proteins were electrophoretically separated using sodium dodecyl sulfate polyacrylamide gel electrophoresis (SDS-PAGE) and transferred to nitrocellulose. Samples were immunoblotted with antibodies specific to  $\alpha$ -tubulin (1:7500), acetylated- $\alpha$ -tubulin (1:4000), HDAC6 (1:2000), the SirT2 N-terminus (1:4000),  $\alpha$ -adaptin (1:1000), CHC (1:2000), cortactin (1:2500), actin (1:2500), or dynamin (1:2500). Immunoreactivity was detected using enhanced chemiluminescence (PerkinElmer, Crofton, MD). Relative levels of tubulin or HDAC6 were determined by densitometric analysis of immunoreactive bands.

**HDAC Activity.** Cells grown on 10 cm dishes were rinsed with PBS, detached with trypsin for 2 min at 37<sup>0</sup>C and pelleted by centrifugation. Cells from two dishes were pooled, resuspended in 5 ml ice-cold swelling buffer (1 mM MgCl<sub>2</sub>, 1 mM dithiothreitol (DTT), 1 mM ethylene glycol tetraacetic acid (EGTA)) and incubated 5 min on ice. Cells were pelleted by centrifugation and resuspended in 500  $\mu$ l of 0.25 M sucrose with added protease inhibitors (1  $\mu$ g/ml each of leupeptin, antipain, phenylmethanesulfonylfluoride (PMSF) and benzamidine) and Dounce-homogenized with a tight fitting pestle for 20 strokes. Homogenates were centrifuged at 900 x g at 4<sup>0</sup>C for 5 min, the pellet was washed and recentrifuged at 14,200 x g at 4<sup>0</sup>C for 10 min to collect nuclei. The post nuclear supernatant was centrifuged at 150,000 x g at 4<sup>0</sup>C for 60

min to prepare the cytosolic fraction. The colorimetric activity assay was performed according to the manufacturer's specifications. Total protein in each sample was determined using bicinchronic acid (BCA) reagent (Pierce, Rockford, IL) and activity was calculated as nmol/min/ $\mu$ g of total protein. Sodium butyrate, TSA or tubulin were added as described in the legends.

To determine tubulin deacetylase activity directly, cytosolic extracts were incubated with 1.8  $\mu$ M purified bovine brain tubulin for the indicated times at 37<sup>0</sup>C. Reactions were stopped by the addition of Laemmli sample buffer and boiling for 3 min. Samples were immunoblotted for acetylated- $\alpha$ -tubulin and the relative amounts were determined using densitometry. 0 min time point values were set to 100% from which the percent deacetylation (decreased immunoreactivity) was determined.

***Solubility Assay.*** WIF-B cells were pretreated with 50 mM ethanol for 72 h or 50 nM TSA for 15 min. In the continued absence or presence of ethanol or TSA, cells were treated with 33  $\mu$ M nocodazole for the indicated times then extracted in prewarmed PEM containing 0.15% TX-100 for 1 min at 37<sup>0</sup>C. Supernatants containing the released soluble (S) tubulin and other cytosolic proteins were collected. The permeabilized cells containing intact microtubule polymers (P) and microtubule-associated proteins were washed in PEM without and lysed directly into sample buffer. Samples were immunoblotted for HDAC6 and the percent soluble was determined by densitometry.

***Microtubule Binding.*** Microtubules were purified based on two previously published methods (Meads and Schroer, 1995; Zhang et al., 2003). Briefly, cells grown on 10 cm

dishes were resuspended in 500  $\mu$ l ice-cold PEM and homogenized as described above. The homogenate was centrifuged for 60 min at 4<sup>0</sup>C at 150,000 x g to prepare a cytosolic extract. 10  $\mu$ M taxol was added to the supernatant for 15 min at 37<sup>0</sup>C to polymerize microtubules. The microtubules were pelleted through a 10% sucrose cushion at 150,000 x g at 20<sup>0</sup>C for 30 min. The resultant supernatant and pelleted fraction containing the microtubules and associated proteins were immunoblotted for HDAC6 and  $\alpha$ -tubulin. The distributions of HDAC6 in the soluble or pelleted fractions were determined by densitometry.

***Rat Ethanol Treatment.*** Male Wistar rats (Charles River Laboratories, Wilmington, MA) were pair-fed control and ethanol Lieber-DeCarli liquid diets for 5 weeks as described (Lieber and DeCarli, 1989). The nutritionally adequate Lieber-DeCarli control and ethanol liquid diets were purchased from Dyets, Inc (Bethlehem, PA). The ethanol-containing diet consisted of 18% protein, 35% fat, 11% carbohydrate, and 36% ethanol. In the control diet, ethanol was replaced isocalorically with carbohydrate such that both ethanol-fed and control rats ingested identical amounts of all nutrients except carbohydrates. At time of sacrifice, the livers were excised and frozen at -70<sup>0</sup>C.

***Liver Fractionation and Blotting.*** Liver was Dounce-homogenized in 0.25 M sucrose containing 10 mM Tris and protease inhibitors (2  $\mu$ g/ml each of leupeptin, antipain, PMSF and benzamidine) (20% w/v). Homogenates were centrifuged at 900 x g at 4<sup>0</sup>C for 5 min. The supernatant was centrifuged at 150,000 x g at 4<sup>0</sup>C for 60 min to prepare the cytosolic and total membrane fractions. The nuclear pellet was washed by

resuspending to volume and centrifuged at 14,200 x g at 4°C for 10 min. Samples were mixed with 2X Laemmli sample buffer (Laemmli, 1970) and boiled for 3 min. Proteins were separated using SDS-PAGE, transferred to nitrocellulose and immunoblotted with antibodies specific to acetylated lysine (1:1000), acetylated histone H3 (1:1000), tubulin (1:7500), CE9 (1:10,000), GPx-1 (1:2000), actin (1:2500) or cortactin (1:2000). The acetylated lysine and acetylated histone H3 antibodies were diluted in PBS containing 1% (w/v) BSA and 0.1% (v/v) Tween 20 (PBS-BT) and incubated overnight at 4°C. Immunoreactivity was detected using enhanced chemiluminescence (PerkinElmer, Crofton, MD). The fold increase in acetylation of 10 selected immunoreactive species in whole homogenate samples or of acetylated histone H3 in nuclear fractions was determined by densitometric analysis. Histone H3 acetylation levels were normalized to total histone H3 levels. Eight sets of pair-fed animals were examined in the whole homogenate analysis.

The anti-tubulin, CE9, GPx-1, actin and cortactin antibodies were diluted in PBS containing 5% (w/v) milk and 0.1% (v/v) Tween 20 for 1 h at RT and processed as described above. For the preabsorption assays, 0.4 µg of the anti-acetylated lysine antibodies were incubated with 1.6 mg acetylated BSA diluted in PBS-BT for 2 h on ice as described (Kim and Shukla, 2006). The mixture was diluted in an additional 3 ml PBS-BT and incubated overnight at 4°C and processed for immunoblotting as described above.

**2D Gel Electrophoresis.** Protein concentrations were determined using BCA Reagent (Thermo Scientific, Rockford, IL). 2D electrophoresis was performed by Kendrick Labs,

Inc. (Madison, WI) using the carrier ampholine method of isoelectric focusing (O'Farrell, 1975). 645  $\mu$ g of cytosolic proteins or 360  $\mu$ g of total membrane proteins were loaded on each gel. Isoelectric focusing was carried out in a glass tube of inner diameter 3.0 mm using 2.0% pH 3.5-10 ampholines (GE Healthcare, Piscataway, NJ) for 20,000 volt-hrs. After equilibrium for 10 min in buffer "0" (10% glycerol, 50 mM DTT, 2.3% SDS and 62.5 mM Tris, pH 6.8), the tube gel was sealed to the top of a stacking gel overlaying a 10% acrylamide slab gel. SDS slab gel electrophoresis was performed and the gel was dried between sheets of cellophane paper. Duplicate gels were transferred onto polyvinylidene fluoride (PVDF) and immunoblotted with the acetylated lysine antibodies (1:2000).

To determine the fold increase in acetylation of proteins in samples from ethanol-fed animals, the density of individual spots on both the gels and immunoblots were determined. Because not all proteins were resolved in 2 dimensions into discrete spots, there were many smeared regions on both the gels and immunoblots that were excluded from our analysis. Thus, the numbers represent only the resolved spots. The level of each of the selected immunoreactive spots was normalized to the relative protein level of its corresponding spot in the gel. Fold-increase in acetylation was calculated by comparing the control ratios to those from ethanol-treated samples.

***Matrix-assisted laser desorption/ionization mass spectrometry (MALDI-MS) Analysis.***

Mass spectrometry was performed by the Protein Chemistry Core Facility at Columbia University (New York, NY). In general, gel spots were prepared for digestion by washing twice with 50 mM Tris, pH 8.5/30% acetonitrile. Gel pieces were subsequently

dried in a Speed-Vac concentrator and digested with trypsin (Roche Molecular Biochemicals, Indianapolis, IN) in 25 mM Tris, pH 8.5. Tubes were placed in a heating block at 32°C and left overnight. Peptides were extracted with 50% acetonitrile/2% trifluoroacetic acid (TFA) and suspended in a matrix solution containing 10 mg/ml 4-hydroxy- $\alpha$ -cyanocinnamic acid and 50% acetonitrile/0.1% TFA. The dried sample was analyzed by MALDI-MS analysis (Applied Biosystems Voyager DE Pro Mass spectrometer in linear mode). The MALDI spectra were manually searched against the National Center for Biotechnology Information (NCBI) database for protein matches. Parameters used in the search were Database: NCBI, taxonomy: rattus, enzyme: trypsin. Molecular weight search (MOWSE) scores were generated from the MS-Fit program of Protein Prospector, v 5.3.0 (USCF Mass Spectrometry Facility). Mascot scores (probability based MOWSE scores) and expect values were generated from the Mascot search program ([www.matrixscience.com](http://www.matrixscience.com)). Up to one missed tryptic cleavage was allowed and cysteine propionamidation and methionine oxidation were considered. The peptide mass tolerance was 0.5 Da.

***Immunoprecipitations from Liver.*** Cytosolic liver fractions (30  $\mu$ l) were diluted to 500  $\mu$ l with RIPA buffer (150 mM NaCl, 1% NP-40, 0.5% deoxycholic acid, 0.1% SDS, 50 mM Tris, pH 8.0) containing protease inhibitors (2  $\mu$ g/ml each of leupeptin, antipain, PMSF and benzamidine). Anti-GPx-1 antibodies (0.5  $\mu$ g) were added and samples incubated overnight at 4°C on a rotating shaker. Prewashed protein G-agarose (30-60  $\mu$ l of a 50% slurry) (Thermo Scientific) was added and incubated for an additional 2-4 h at 4°C on a rotating shaker. Agarose was collected by centrifugation. Unbound fractions

were made into gel samples by addition of 5X Laemmli sample buffer. The bound fractions were resuspended in 10  $\mu$ l of 1X Laemmli sample buffer. In general, 10  $\mu$ l of each unbound fraction and the entire bound sample were loaded on the gels.

***Two-antibody Sandwich enzyme-linked immunosorbent assay (ELISA).*** 20  $\mu$ g of the indicated antibodies were diluted in PBS and added to ELISA microplate strip wells (BioRad, Hercules, CA). The antibodies were allowed to adhere for 2 h in a humidified chamber, and non-labeled sites were blocked with 1% BSA for 1 h. The wells were washed with PBS and incubated with  $\sim$ 100  $\mu$ g liver lysate for 2 h. The bound protein was probed with the anti-acetylated lysine antibodies diluted 1:500 in 1% BSA for 2 h and detected with anti-rabbit HRP-conjugated secondary antibodies. HRP levels were detected with the 1-step 2,2'-azino-di (3-ethyl-benzthiazoline-6-sulfonate) (ABTS) HRP detection solution (Thermo Scientific) and absorbance was measured at 405 nm.

***Immunoprecipitations from WIF-B cells.*** WIF-B cells grown on coverslips were lysed in 0.5 ml lysis buffer containing 1 mM ethylenediaminetetraacetic acid (EDTA), 150 mM NaCl, 50 mM Tris, 1% NP-40 pH 7.5 with protease inhibitors (2  $\mu$ g/ml each of leupeptin, antipain, PMSF and benzamidine) on ice for 30 min. Lysates were cleared by centrifugation at 120,000 x g for 30 min at 4°C. Anti-cortactin and dynamin antibodies (0.5-1  $\mu$ g) were added to the samples and incubated overnight at 4°C on a rotating shaker. Prewashed protein G-agarose (30-60  $\mu$ l of a 50% slurry) (Thermo Scientific) was added and incubated for an additional 2-4 h at 4°C on a rotating shaker. Agarose was collected by centrifugation. Unbound fractions were made into gel samples by addition of 5X

Laemmli sample buffer. The bound fractions were resuspended in 35  $\mu$ l of 1X Laemmli sample buffer. In general, 10  $\mu$ l of each unbound fraction and 15  $\mu$ l of the bound sample were loaded on the gels.

***K<sup>+</sup> depletion/repletion Assays.*** WIF-B cells treated with either ethanol for 72 h or TSA for 30 min were rinsed 3x with PBS and incubated in prewarmed K<sup>+</sup> depletion buffer (150 mM NaCl, 50 mM Hepes pH 7.4) for 30 min at 37°C to disrupt clathrin-coated pit formation. For ASGP-R trafficking studies, depleted cells were placed in a prechilled dish and chilled for 5 min in the presence of depletion buffer and surface labeled with the anti-ASGP-R polyclonal antibody at 1:25 for 20 min on ice. For repletion, cells were placed back into WIF-B medium supplemented with 10 mM KCl and ASGP-R was allowed to traffic for 0, 5, 15 or 30 min at 37°C. The trafficked ASGP-R antibody was labeled with a cy3-conjugated secondary antibody. For dynamin recruitment assays, WIF-B cells were depleted as described above and then placed back into repletion medium for 0, 5, 15 or 30 min to allow for coat reassembly and dynamin recruitment. After repletion, cells were permeabilized with TX-100 and stained with the monoclonal anti-dynamin antibody.

***Statistical Analysis.*** Results are expressed as the mean  $\pm$  SEM. The student t-test was performed for paired data to assess statistical significance. P values  $\leq$  0.05 were considered significant. The Pearson's coefficient was calculated from 8 bit split images in ImageJ using the Just Another Colocalization Plugin (JACoP).

**Part I: Alcohol-induced alterations in hepatic microtubule dynamics can be explained by impaired histone deacetylase 6 function**

Previously, we determined that microtubules were more stable and hyperacetylated in ethanol-treated WIF-B cells and this phenotype required alcohol metabolism and was likely mediated by acetaldehyde (Kannarkat et al., 2006). We also determined that microtubules were acetylated to the same extent in livers from ethanol-fed rats indicating the effect has physiologic relevance (Kannarkat et al., 2006). However, the mechanism for the ethanol-induced increase in microtubule acetylation and stability is not known.

Although it is known that  $\alpha$ -tubulin is acetylated on lysine 40, the identity of the acetyltransferase is not known (Westermann and Weber, 2003). However, there are two known microtubule deacetylases, HDAC6 and SirT2 (Hubbert et al., 2002; Matsuyama et al., 2002; North et al., 2003; Zhang et al., 2003). HDAC6 (a class II member) and SirT2 (a class III member) are exclusively cytosolic deacetylases that colocalize with microtubules in some cell types (Hubbert, 2002 #206). Overexpression of either enzyme led to a specific loss of acetylated microtubules and decreased microtubule stability (Hubbert et al., 2002; Matsuyama et al., 2002; North et al., 2003; Zhang et al., 2003). Conversely, when the deacetylases were inactivated or their expression knocked down, microtubules were hyperacetylated and more stable (Hubbert et al., 2002; Matsuyama et al., 2002; North et al., 2003; Zhang et al., 2003). Because HDAC6 is enriched in liver (Grozingier et al., 1999) (its expression in hepatic cell lines and isolated hepatocytes has

not been examined) and because class III enzymes, including SirT2, require  $\text{NAD}^+$  for activity ( $\text{NAD}^+$  is a coenzyme for both ADH and ALDH) (North et al., 2003), both HDAC6 and SirT2 are good candidates for mediating the alcohol-induced hyperacetylation of microtubules.

We found that WIF-B cells do not express SirT2, consistent with reports that SirT2 expression is enriched in brain (Li et al., 2007; Tang and Chua, 2008). However, HDAC6 was abundantly expressed in WIF-B cells and its inhibition with TSA led to increased microtubule acetylation comparable to that observed in ethanol-treated cells. Although alcohol or TSA did not alter HDAC6 subcellular distribution, it led to decreased HDAC6 protein levels. Furthermore, HDAC6 binding to microtubules was significantly impaired in ethanol-treated cells. HDAC6 from ethanol treated cells bound to and deacetylated exogenous tubulin to the same extent as HDAC6 from control cells. Thus, impaired binding of HDAC6 to microtubules is likely due to ethanol-induced tubulin modifications that prevented associations. Together these results indicate that the alcohol-induced increases in microtubule acetylation and stability in WIF-B cells are due, in part, to decreased HDAC6 protein levels and decreased microtubule binding.

## RESULTS

### *HDAC6 is abundantly expressed and is a tubulin deacetylase in WIF-B cells*

We first determined HDAC6 and SirT2 protein expression by immunoblotting. We began with HeLa cells, a cell line known to be positive for both proteins. As shown in Fig. 7A, an 160 kDa immunoreactive doublet and a 43 kDa band were detected corresponding to the predicted molecular weights of HDAC6 and SirT2, respectively. However, only the 160 kDa HDAC6 doublet was detected in WIF-B cells (Fig. 7A). To further confirm that SirT2 was absent in WIF-B cells, we assayed microtubules for increased acetylation in the presence of the SirT2 inhibitor, NTA. No increased acetylation was observed with increased time of NTA incubation, and in fact, a slight (but not statistically significant) decrease was observed (Fig. 7B). This result was also observed with 50 mM NTA (data not shown). Furthermore, when cells were immunolabeled for SirT2, no specific signal was detected (data not shown). We failed to detect SirT2 using five fixation methods, antibodies to the SirT2 N- or C-terminus, or increased antibody concentrations (data not shown). From these results, we conclude that WIF-B cells lack SirT2, a finding that is consistent with reports that SirT2 expression is enriched in brain (Li et al., 2007; Tang and Chua, 2008).

Since HDAC6 inactivation has been shown to increase microtubule acetylation (Hubbert et al., 2002; Matsuyama et al., 2002; Zhang et al., 2003), we examined whether its inactivation with TSA in WIF-B cells led to the same effect. As shown in Fig. 7C, 50 nM TSA for 30 min led to a 2.3 fold increase in acetylated tubulin, similar to the

increased acetylation observed in ethanol-treated cells ( $2.62 \pm 0.48$ ) (Joseph et al., 2008; Kannarkat et al., 2006). Importantly, total tubulin levels did not change indicating that the hyperacetylation was not due to increased protein levels. Thus, we conclude that HDAC6 is an abundant tubulin deacetylase in WIF-B cells.

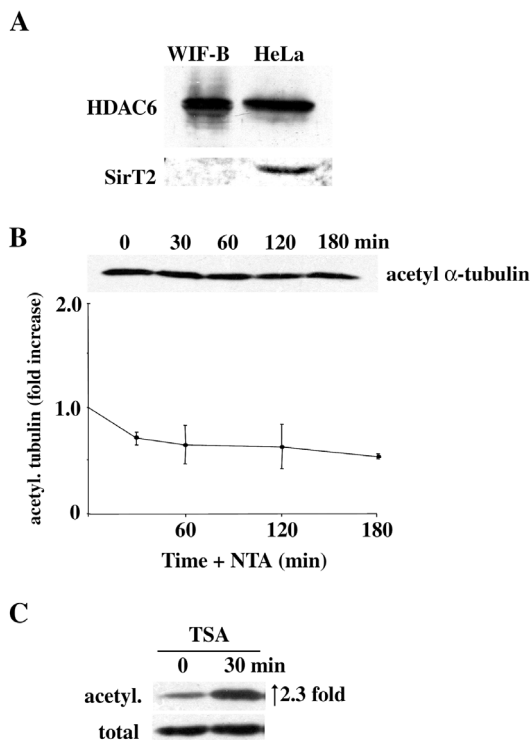


**Figure 7. HDAC6 is an abundant microtubule deacetylase in WIF-B cells.** *A.*, 35  $\mu$ g protein from WIF-B or HeLa lysates was immunoblotted for HDAC6 or SirT2. *B.*, WIF-B cells were treated with 25 mM NTA for the indicated times and blotted for acetylated and total  $\alpha$ -tubulin. The level of acetylated tubulin was normalized to the total tubulin present and the fold-increase plotted. Values represent the mean  $\pm$  SEM from at least 3 independent experiments. *C.*, Cells were treated with 50 nM TSA for 30 min and blotted for acetylated and total  $\alpha$ -tubulin. The fold increase in acetylation is indicated. A representative blot from 3 independent experiments is shown.

### ***Ethanol decreases HDAC6 protein levels***

One simple explanation for increased microtubule acetylation in ethanol-treated cells is

decreased HDAC6 protein levels. To test this, we immunoblotted control and ethanol-treated cell lysates for HDAC6 (Fig. 8A). After incubation for 24 h with ethanol, HDAC6 protein levels decreased to  $92.0 \pm 7.4\%$  (Fig. 8B). Levels continually declined, and after 72 h, there was  $75.0 \pm 6.1\%$  of HDAC6 control levels ( $P < 0.05$ ). This decrease in HDAC6 was not the result of overall decreased total protein levels because the cytosolic protein concentration in ethanol-treated cells was  $96.5 \pm 3.14\%$  of control, far less than the decrease in HDAC6 protein.

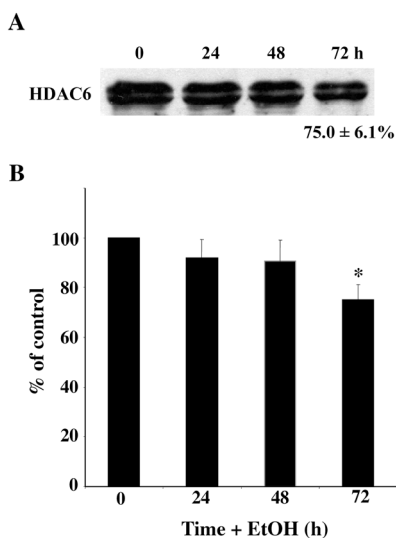


**Figure 8. HDAC6 protein levels decrease upon ethanol exposure.** *A.*, WIF-B cells were treated with 50 mM ethanol for 0, 24, 48 or 72 h, lysed directly into sample buffer and immunoblotted for HDAC6. A representative immunoblot from 3 independent experiments is shown. *B.*, The relative levels of HDAC6 were calculated. Values represent the mean  $\pm$  SEM from at least 3 independent experiments. \*  $P < 0.05$ .

### ***HDAC6 is less tightly associated with microtubules in ethanol-treated cells***

Another possible mechanism for alcohol-induced microtubule hyperacetylation is changes in HDAC6 microtubule binding. To test this possibility, we first immunolabeled

control and treated cells for HDAC6 and tubulin. Previously, we observed that ethanol promoted the formation of microtubules that appeared thicker and more gnarled, features of stable microtubules (Kannarkat et al., 2006) whereas in TSA-treated cells, the change in morphology was much less pronounced (Joseph et al., 2008). Similar results were obtained here (Fig. 9). Although HDAC6 has been shown to colocalize with microtubules in other cell types (Hubbert et al., 2002; Matsuyama et al., 2002; Zhang et al., 2003), we observed only diffuse cytosolic staining in WIF-B cells (Fig. 9A and B; unlabeled BCs are marked with asterisks). In cells treated with TSA (Fig. 9A) or ethanol (Fig. 9B), no overt changes in HDAC6 cytosolic distributions were observed.

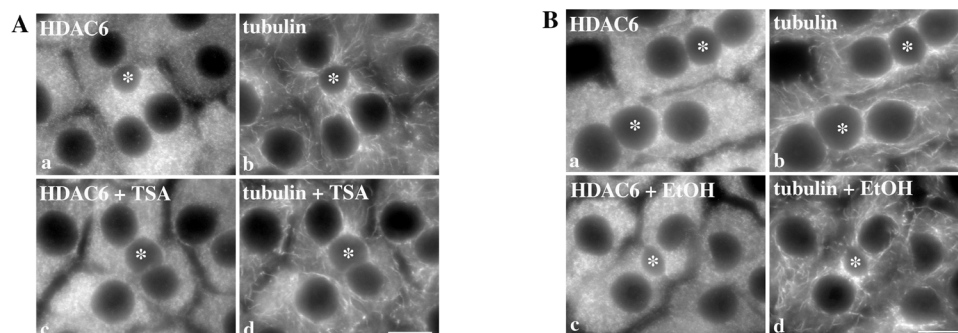


**Figure 9. HDAC6 cytosolic distributions are not altered in ethanol or TSA-treated cells.** A., Cells were incubated in the absence (a, b) or presence (c, d) of 50 nM TSA for 30 min. Cells were fixed and stained for HDAC6 and  $\alpha$ -tubulin. B., Cells were incubated in the absence (a,c) or presence (c,d) of 50 mM ethanol (EtOH) for 72 h. Cells were fixed and stained for HDAC6 and  $\alpha$ -tubulin. In all conditions, HDAC6 cytosolic staining was detected. Representative images of 6 independent experiments are shown.

Because the high level of cytosolic HDAC6 may have obscured its microtubule association, we examined HDAC6–microtubule binding by two methods. First, we used an indirect method where microtubules in intact cells were depolymerized with nocodazole and cells assayed for released HDAC6. Cells were pretreated for 72 h with

50 mM ethanol or 15 min with 50 nM TSA. In the continued absence or presence of either agent, 33  $\mu$ M nocodazole was added to depolymerize microtubules. WIF-B cells were lysed in a microtubule stabilizing buffer containing 0.15% TX-100 releasing soluble tubulin (and other soluble proteins) leaving the stable polymeric tubulin and associated proteins in the intact cells. In control cells, ~45% of HDAC6 was soluble, and in the presence of nocodazole, solubility was slightly increased to ~55% after 60 min (Fig. 10). In ethanol-treated cells, significantly more HDAC6 was soluble, and after 60 min in nocodazole, >80% of HDAC6 was released ( $P < 0.02$ ). Similarly, in TSA-treated cells, ~90% of HDAC6 was soluble after 60 min ( $P < 0.05$ ) suggesting impaired microtubule binding.

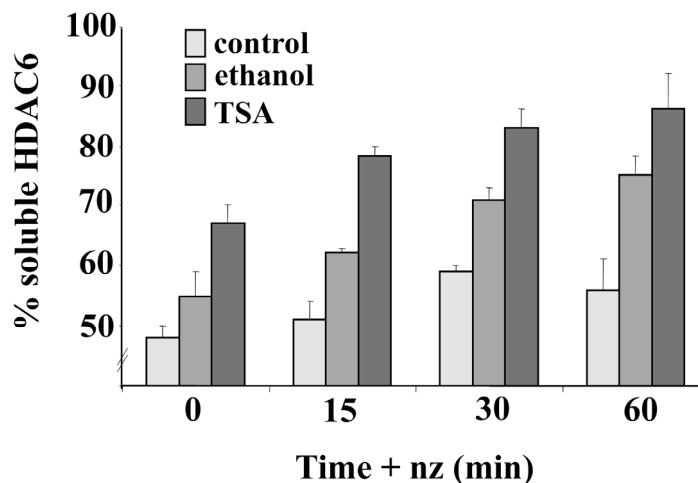


**Figure 10. HDAC6 is less stably associated with microtubules in ethanol and TSA-treated cells.** WIF-B cells were pretreated with 50 mM ethanol for 72 h (light gray) or 50 nM TSA for 15 min (dark gray) and microtubules were depolymerized with nocodazole (nz) for the indicated times in the continued absence or presence of either agent. The cells were lysed in a microtubule stabilizing buffer containing 0.15% Triton X-100 for 1 min at 37°C. The supernatant containing the soluble tubulin (S) and other solubilized proteins was collected. The permeabilized cells containing polymeric microtubules (P) and associated proteins were lysed. The fractions were immunoblotted for HDAC6 and the percent of soluble HDAC6 is plotted. Values represent the mean  $\pm$  SEM from 3 independent experiments.

We next measured direct microtubule binding. We prepared cytosolic fractions from control and treated cells and added taxol to polymerize microtubules. The stabilized microtubules and associated proteins were pelleted through a sucrose cushion and samples were immunoblotted for HDAC6 and  $\alpha$ -tubulin. In both control and ethanol-treated cells, all of the tubulin was pelleted indicating complete polymerization (Fig. 11A). In contrast, much less HDAC6 was detected in the microtubule pellet from ethanol-treated cells. In control cells,  $60.7 \pm 11.5\%$  of HDAC6 was detected in the pellet whereas less than half that amount ( $21.9 \pm 4.1\%$ ,  $P < 0.03$ ) bound microtubules in ethanol-treated cells. When cells were treated with ethanol and 4MP, HDAC6 microtubule association remained closer to control levels ( $\sim 40\%$ ) (Fig. 11B) indicating that HDAC6's altered microtubule binding partially required ethanol metabolism and may be mediated by acetaldehyde.

***Ethanol-induced tubulin modifications likely prevent HDAC6 microtubule binding***

Another possible mechanism for increased microtubule acetylation in ethanol-treated cells is that HDAC6 activity was impaired. To test this, we assayed total deacetylase activity using a colorimetric assay with acetylated lysine as the substrate. Because this assay cannot discriminate between nuclear and cytoplasmic HDAC isoforms, we prepared both fractions from control and ethanol-treated WIF-B cells. Consistent with our hypothesis, nuclear HDAC activity was decreased ( $67.8 \pm 5.5\%$  of control,  $P < 0.003$ ) in ethanol-treated cells. In contrast, cytosolic HDAC activity was increased ( $125.6 \pm 8.3\%$  of control,  $P < 0.007$ ) (Fig. 12A).

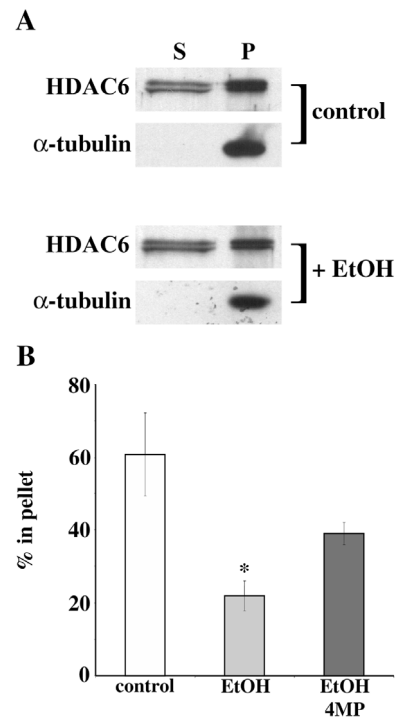
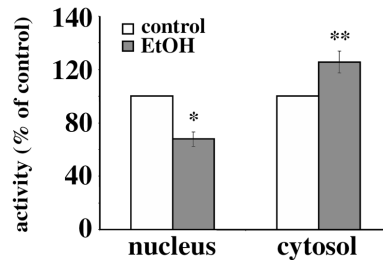


**Figure 11. HDAC6 microtubule binding is impaired in ethanol-treated cells.** *A.*, WIF-B cells were assayed for HDAC6 microtubule binding in control (top) and ethanol-treated cells (bottom). Microtubules were polymerized and pelleted from cytosolic extracts (see Materials and Methods). The supernatant (S) and microtubule pellet (P) were immunoblotted for HDAC6 and  $\alpha$ -tubulin as indicated. Representative immunoblots from 5 independent experiments are shown. *B.*, The percent HDAC6 found in the microtubule pellet was quantified. \*  $P < 0.03$ .

To characterize this somewhat surprising finding, we first confirmed that the cytosolic activity was predominantly due to HDAC6. Although HDAC6 is exclusively cytosolic (Bertos et al., 2001; Hubbert et al., 2002; Verdel et al., 2000; Zhang et al., 2003), some of the HDAC family members shuttle between the nucleus and cytosol (Hildmann et al., 2007) (Fig. 4). Because all of the HDAC family members are sensitive to TSA and sodium butyrate while HDAC6 is sensitive only to TSA (Hubbert et al., 2002), we measured HDAC activity in the presence of these inhibitors. As predicted, both TSA and

sodium butyrate inhibited nuclear activity by ~50% (Fig. 12B). In contrast, only TSA inhibited the cytosolic activities; sodium butyrate had no effect (Fig. 12B). Thus, the cytosolic deacetylase activity we were measuring was mainly due to HDAC6.

**A**



**B**

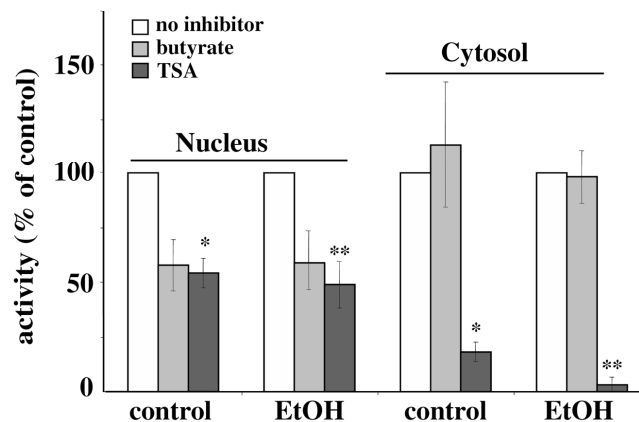


**Figure 12. Cytosolic HDAC activity is increased in ethanol-treated WIF-B cells while nuclear HDAC activity is decreased.** *A.*, Cytosolic and nuclear fractions were assayed for HDAC activity using acetylated lysine as the substrate (see Materials and Methods). Control (white) and the ethanol-treated (EtOH) (gray) activities are shown. Values represent the mean  $\pm$  standard error of the mean (SEM) from at least 3 independent experiments. \*  $P < 0.003$ ; \*\*  $P < 0.007$ . *B.*, Nuclear and cytosolic HDAC activities were measured in the presence of 0.2 mM sodium butyrate (light gray) or 50 nM TSA for 15 min (dark gray) as indicated. For nuclear fractions, \*  $P < 0.007$ ; \*\*  $P < 0.02$ . For the cytosolic fractions, \*  $P < 0.03$ ; \*\*  $P < 0.001$ .

Our next step to explain increased cytosolic activity in ethanol-treated cells was to consider the reaction mixtures. Both the acetylated lysine (supplied by the manufacturer) and tubulin (copurified in the cytosolic fraction) were present, both of which are

substrates for HDAC6. As shown in Figs. 10 and 11, ethanol-treatment leads to decreased HDAC6 binding to microtubules. Thus, one possibility is that in the ethanol-treated samples, more HDAC6 was dissociated from tubulin and therefore more available for binding to the acetylated lysine substrate leading to an apparent increase in activity. To test this hypothesis, we added increasing concentrations of bovine brain tubulin (which is acetylated; data not shown) to the assay mixtures to compete for HDAC6 binding to acetylated lysine. Importantly, the exogenous tubulin concentrations (0.9-4.5  $\mu\text{M}$ ) were far lower than the concentrations of acetylated lysine (1.5 mM) or endogenous tubulin (10  $\mu\text{M}$ ) ( $\sim$ 350-1700-fold and  $\sim$ 2.5-10-fold, respectively). As shown in Fig. 13A, tubulin addition had no significant effect on HDAC6 activity in control cells. In contrast, there was a dose-dependent decrease in activity in ethanol-treated samples. Thus, HDAC6 preferentially associates with the low levels of exogenous tubulin preventing interactions with the acetylated lysine substrate leading to a decrease in apparent activity. These results further suggest that HDAC6's ability to bind and deacetylate exogenous tubulin activity is not altered by ethanol-treatment. To test this directly, cytosolic fractions from control and ethanol-treated WIF-B cells were incubated with 1.8  $\mu\text{M}$  exogenous tubulin for the indicated times and immunoblotted for acetylated tubulin. In both control and ethanol-treated samples, there was a time-dependent increase in tubulin deacetylation (Fig. 13B). When quantitated (Fig. 13C), no change in the tubulin deacetylase activity in the ethanol-treated samples was observed; the plots were nearly superimposable. These results indicate that HDAC6 binding and deacetylation of *exogenous* tubulin is not changed by ethanol treatment. We conclude that ethanol

treatment is not impairing HDAC6 deacetylase or microtubule binding activities directly. Rather, we propose that tubulin from ethanol-treated cells is modified (see Discussion) preventing HDAC6 microtubule binding.

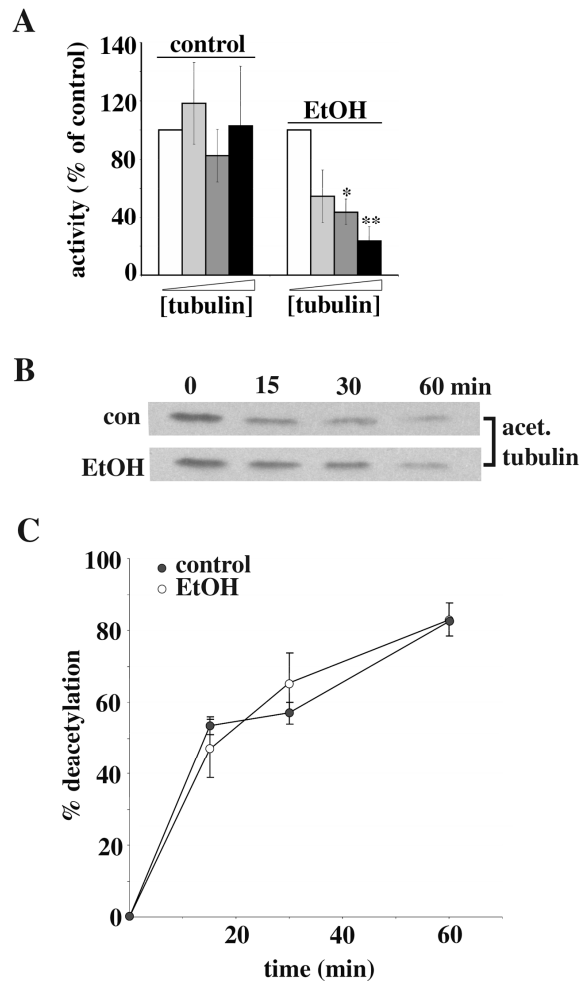


**Figure 13. Ethanol-induced tubulin modifications prevent HDAC6 binding.** *A.*, Cytosolic fractions from control or ethanol-treated WIF-B cells were assayed for HDAC activity with acetylated lysine as the substrate in the presence of 0, 0.9, 1.8 or 4.5  $\mu$ M bovine brain tubulin. Values represent the mean  $\pm$  SEM from 3 independent experiments. \*  $P < 0.01$ ; \*\*  $P < 0.004$ . *B.*, Cytosolic fractions were incubated with 1.8  $\mu$ M purified bovine brain tubulin for the indicated times and reactions stopped by addition of Laemmli sample buffer and boiling. Samples were blotted for acetylated tubulin. Representative immunoblots are shown. *C.*, The percent tubulin deacetylation for each time point was determined by densitometry. Values represent the mean  $\pm$  SEM from 3 independent experiments.

## ***CONCLUSIONS***

Previously, we determined that microtubules were more highly acetylated and more stable in ethanol-treated WIF-B cells and in livers from ethanol-fed rats (Kannarkat et al., 2006). In this study, we sought to identify the mechanism by which microtubules became hyperacetylated. Since a tubulin acetyltransferase has not been identified, and because tubulin acetylation appears more tightly regulated by deacetylases, we focused on the two known tubulin deacetylases, HDAC6 and SirT2. We found that only HDAC6 was expressed in WIF-B cells, and that its protein levels decreased by 25% in ethanol-treated cells. We also found that HDAC6 binding to endogenous microtubules was significantly impaired in ethanol-treated cells and that this impairment partially required ethanol metabolism. Measuring HDAC6 tubulin deacetylase activity by two methods further revealed that ethanol did not impair HDAC6's ability to bind or deacetylate exogenous tubulin. This suggests that tubulin from ethanol-treated cells is modified thereby preventing HDAC6 binding.

### ***Our working model***

Our studies revealed that HDAC6 protein levels are decreased by ethanol treatment and its ability to bind microtubules is impaired. These two findings may explain the increased microtubule acetylation and stability observed in ethanol-treated WIF-B cells. Although decreased HDAC6 protein levels are a simple explanation for increased tubulin acetylation, we propose it is the impaired microtubule binding that has more impact. HDAC6 is abundant in the liver (Grozingler et al., 1999; Zhang et al., 2007) such that a

25% decrease in levels may not likely have profound effects on tubulin acetylation.

Rather, the 70% impairment in HDAC6 binding to microtubules may have a more dramatic effect; much less of the available enzyme can bind its substrate leading to decreased deacetylation. However, our studies cannot rule out the possibility that increased acetyltransferase activity is also contributing to increased tubulin acetylation.

Based on the results from our efforts to explain the somewhat surprising finding that deacetylase activity was enhanced in ethanol cytosolic extracts, we propose that alcohol-induced tubulin modifications prevent HDAC6 binding to microtubules. We determined that addition of exogenous tubulin to our reaction mixtures impaired deacetylase activity in ethanol-treated samples only. Importantly, the exogenous tubulin concentrations were ~350-1700-fold lower than the concentrations of acetylated lysine or ~2.5-10-fold lower than endogenous tubulin. Thus, the decreased activity in the ethanol-treated samples strongly argues that HDAC6 preferentially bound the exogenous tubulin, displacing it from the acetylated lysine substrate. In control samples, where HDAC6 microtubule binding properties were not changed, the low amounts of exogenous tubulin did not further displace HDAC6 from the acetylated lysine (or the unmodified endogenous tubulin) such that activity remained the same. When assayed directly, there was no difference between control or treated HDAC6 activity using exogenous tubulin indicating that ethanol does not alter HDAC6 microtubule binding or catalytic activity directly. Rather, we conclude that endogenous tubulin from the ethanol-treated samples is modified thereby preventing HDAC6 binding.

## **Part II: Chronic Ethanol Consumption Induces Global Hepatic Protein Hyperacetylation**

To date, the lysine-acetylation of a handful of hepatic proteins has been reported to be induced by ethanol exposure (Shepard and Tuma, 2009). So far this list includes histone H3, tubulin, SREBP-1c, p53, PGC-1 $\alpha$  and AceCS2 (Shepard and Tuma, 2009). A recent study also determined that numerous mitochondrial proteins (not yet identified) are hyperacetylated after ethanol exposure, and that the acetylation remained long after ethanol withdrawal (Picklo, 2008). With the growing number of known acetylated proteins and the large number of modifying enzymes, it is likely that numerous proteins are hyperacetylated in ethanol-exposed hepatocytes.

To identify other ethanol-induced hyperacetylated proteins, we immunoblotted liver samples from control and ethanol-fed rats with antibodies generated against acetylated lysine. In whole homogenates from ethanol-fed animals, a striking increase in lysine acetylation was detected. We also immunoblotted nuclear, cytosolic, and membrane fractions from control and ethanol-fed livers and determined that all fractions contained numerous hyperacetylated proteins. We further analyzed the cytosolic and membrane fractions by 2D electrophoresis and immunoblotting. Selected hyperacetylated proteins were identified by mass spectrometry. In all, 40 non-nuclear proteins were identified, half of which were from the cytosol and half from the membrane fraction. Remarkably, almost all of the hyperacetylated proteins in the latter fraction were from mitochondria and most were metabolic enzymes. Hyperacetylation of two identified proteins, GPx-1

and actin, was confirmed by immunoprecipitations and ELISAs. Further analysis also revealed that alcohol induced the hyperacetylation of cortactin, a known acetylated actin binding protein. Thus, alcohol-induced hyperacetylation may be a key factor in the development of liver injury.

## RESULTS

### *Ethanol Induces Global Hepatic Protein Hyperacetylation*

To determine whether other hepatic proteins are hyperacetylated by ethanol exposure, we began by immunoblotting whole homogenate samples from control or ethanol-fed livers with antibodies specific for acetylated lysine residues. Analysis was performed on eight pair-fed liver sets from several different studies. In Figure 14A, three representative pairs are shown. A striking increase in acetylation is apparent in the samples from ethanol-fed rats (Fig. 14A). In general, the same 10 proteins ranging in molecular weight from 17-175 kDa were more highly acetylated in ethanol-treated homogenates (Table 1). Among all samples examined, a cluster of 5 bands ranging from 30-50 kDa and a protein of 17 kDa were consistently hyperacetylated. For most proteins, acetylation was enhanced 2-3 fold, but in some cases, acetylation was increased to as much as ~14-fold (Table 1). To confirm the specificity of the anti-acetylated lysine antibodies, we preabsorbed them with 1% BSA in the absence or presence of 0.04% acetylated BSA (Fig. 14B). In the absence of the acetylated BSA, a similar pattern of hyperacetylation was observed in the ethanol-exposed samples (Fig. 14B). In contrast, addition of the acetylated BSA virtually abolished immunoreactivity (Fig. 14B).

To further characterize the hyperacetylated proteins in the ethanol-fed rat livers, we prepared nuclear, cytosolic, and membrane fractions (excluding nuclei) by differential centrifugation (Fig. 15). As for the whole homogenates, multiple proteins were hyperacetylated in the various fractions. Although the 175 kDa protein equally

distributed among all fractions, other proteins fractionated into distinct fractions. For example, 48, 62, and 85 kDa proteins were detected only in the total membrane fraction whereas a 30-35 kDa protein cluster distributed mainly to the cytosolic fraction (Fig. 15A).

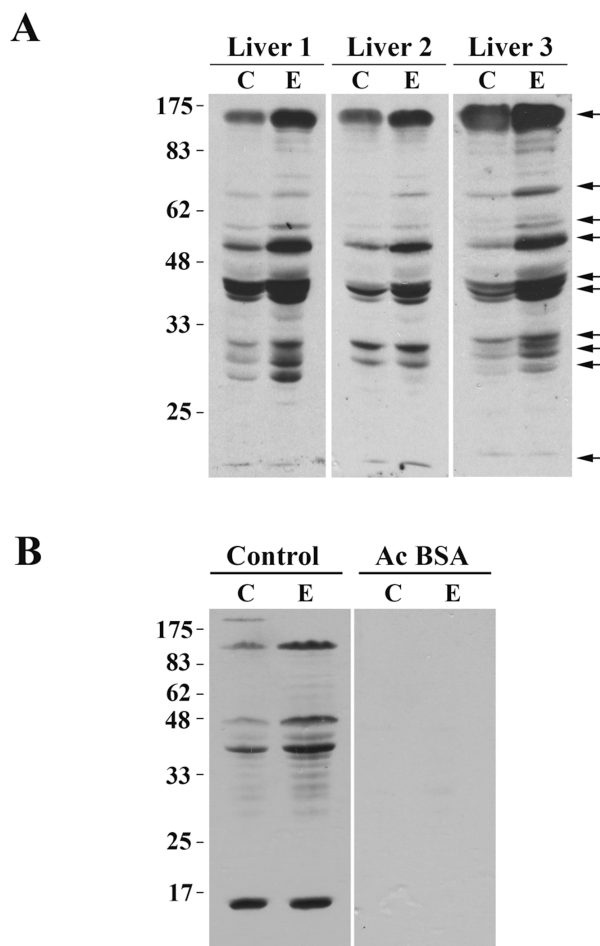


**Figure 14. Chronic ethanol treatment induces global hepatic protein hyperacetylation.** A, Livers from control (C) and ethanol (E) pair-fed rats were immunoblotted with the anti-acetylated lysine antibodies. Molecular weight standards are indicated on the left and arrows on the right indicate proteins with a 2-fold or greater increase in acetylation. Three representative pairs are shown. B, The anti-acetylated lysine antibodies were preabsorbed in 1% BSA in the absence or presence of 0.04% acetylated BSA (Ac BSA) prior to immunoblotting the liver whole homogenate samples.

**Table 1. Increased immunoreactivity is observed in a conserved set of proteins in livers from ethanol-fed rats**

<b>kDa</b>	<b>Fold Increase</b>	<b>Subcellular Location</b>
175	2.9 ± 1.3	N, C, M
85	13.1 ± 11.1	M
62	5.5 ± 3.2	N, M
55	2.8 ± 1.0	C
50	2.0 ± 0.5	N, C, M
45	1.8 ± 0.3	N, C, M
40	2.7 ± 1.1	N, C, M
32	2.3 ± 0.8	C
30	1.6 ± 0.4	M
17	14.3 ± 9.9	N

The relative levels of 10 selected hyperacetylated proteins were determined by densitometric analysis of immunoreactive species of the indicated molecular weights. Values are averages ± SEM from 8 independent sets of pair-fed rats. The subcellular distribution of each of the species is also indicated. N, nucleus; C, cytosol; M, membranes (without nuclei).

To assess the purity of the three fractions, we immunoblotted them with acetylated histone H3 (a nuclear marker protein), tubulin (a cytosolic marker protein) and the basolateral resident protein, CE9 (a membrane marker protein). As shown in Fig. 15B, the marker proteins distributed to their corresponding fractions indicating their purity. Because the CE9 antibodies are extremely sensitive, we believe that the amount detected in the nuclear fraction likely reflects incomplete cell homogenization and sedimentation

of intact cells at low speed. However, importantly, the cytosolic and membrane fractions are free of nuclei thereby allowing further analysis to identify non-nuclear hyperacetylated proteins in livers from ethanol-fed rats.

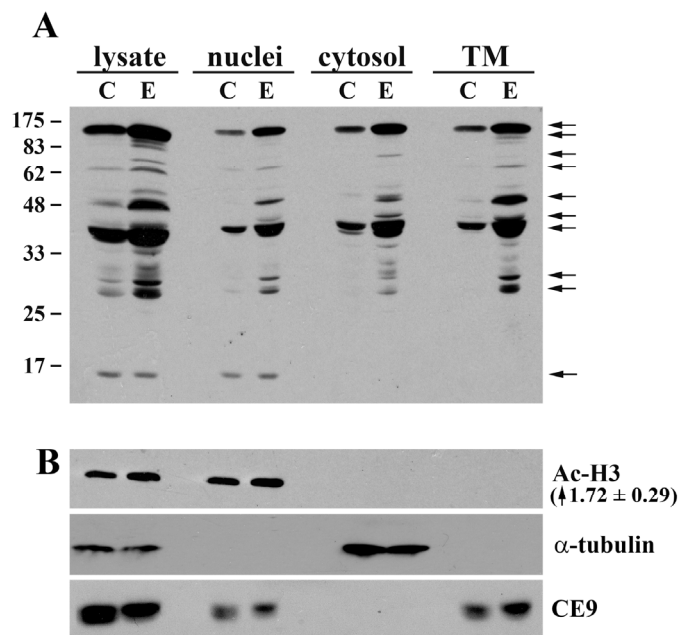


**Figure 15. Chronic ethanol treatment induces acetylation of nuclear, cytosolic and membrane proteins.** Liver homogenates from control (C) and ethanol (E) pair-fed rats were separated by differential centrifugation to prepare nuclei, cytosol or total membranes (TM). A, Fractions were immunoblotted with anti-acetylated lysine antibodies to detect hyperacetylated proteins (marked by arrows). Molecular weight standards are indicated on the left. B, Fractions were immunoblotted for acetylated histone H3 (Ac-H3; a nuclear marker protein), tubulin (a cytosolic marker protein) and the basolateral resident protein, CE9, (a membrane marker protein) as indicated. The ethanol-induced increase in histone H3 acetylation is indicated in parentheses. The value is the average  $\pm$  SEM from three independent sets of pair-fed animals.

A low molecular weight protein was found exclusively in the nuclear fraction that was hyperacetylated in ethanol-treated samples. This low molecular weight and nuclear distribution suggested that it might be histone H3, a protein known to be hyperacetylated by ethanol exposure (Bardag-Gorce et al., 2007; Choudhury and Shukla, 2008; Kim and Shukla, 2005; Kim and Shukla, 2006; Park et al., 2005; Park et al., 2003). The

acetylated histone H3 immunoblots confirmed this possibility (Fig. 15B) revealing an  $1.72 \pm 0.29$ -fold increase in acetylation in ethanol-fed samples.

### ***Ethanol induces non-nuclear protein acetylation***

Because most known acetylated proteins are nuclear, we chose to further analyze cytosolic and total membrane fractions (excluding nuclei) to increase the likelihood of identifying novel acetylated proteins. We began by analyzing the cytosolic samples. 645  $\mu$ g of total cytosolic protein from control or ethanol-treated livers was resolved on 2D gels and immunoblotted with the anti-acetylated lysine antibodies. Coomassie blue-stained gels revealed that the gels were equally loaded and displayed similar staining patterns (Fig. 16). In both the control and ethanol-treated gels, 426 discrete spots were resolved (Fig. 16). In the control gel, 191 acetylated spots were detected whereas 325 acetylated spots were detected in the gel loaded with the ethanol-treated sample indicating robust hyperacetylation (see Table 2).

In general, cytosolic proteins from the ethanol-fed rats ranging from 40-45 kDa with a pI of 7-10 exhibited substantial hyperacetylation (Fig. 16). A few distinct bands were also detected around 25 kDa. To better visualize individual hyperacetylated proteins, we enlarged portions of both the control and ethanol immunoblots (Fig. 17). In some cases, ethanol induced acetylation of proteins that were not detected in control blots (e.g., see spot a in Box 1). Many other proteins exhibited baseline acetylation levels that were either significantly increased in the presence of ethanol (e.g., see spot c in Box 1) or did

not change (e.g., see the large immunoreactive species marked with asterisks in Box 1). The proteins exhibiting substantial hyperacetylation that were selected for MALDI-MS are indicated with arrowheads and are labeled (see Table 2). The corresponding spots in the control immunoblots are indicated with arrowheads.

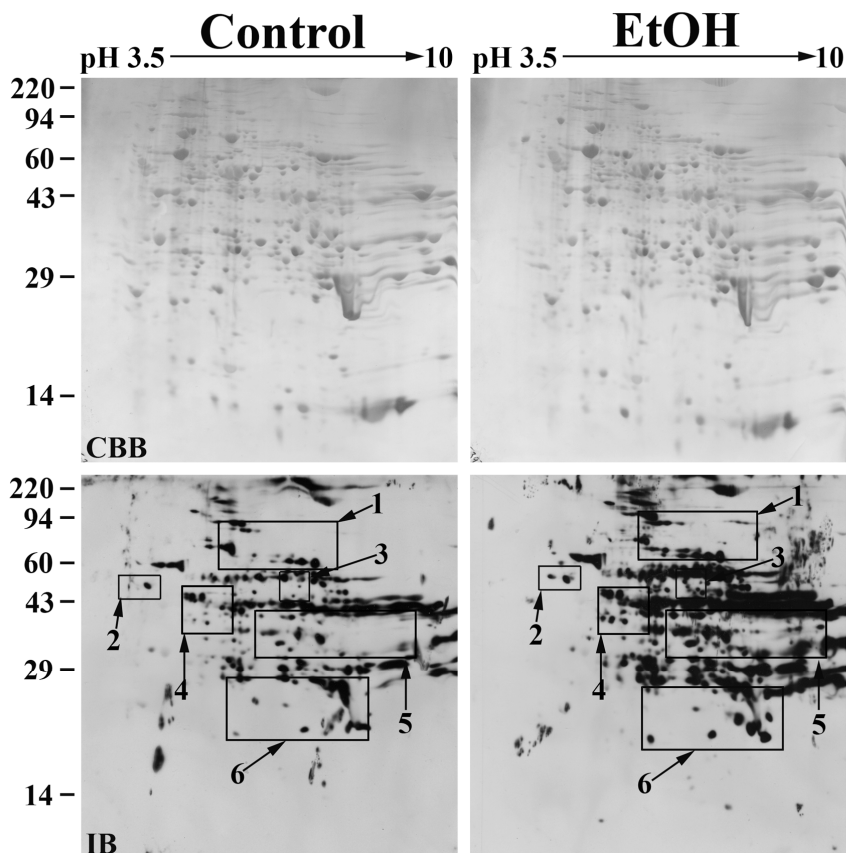


**Figure 16. Numerous cytosolic proteins are hyperacetylated in livers from ethanol-fed rats.** Liver cytosolic extracts from control and ethanol pair-fed rats were prepared by differential centrifugation. 645  $\mu\text{g}$  of total protein from each sample were subjected to 2D electrophoresis and immunoblotted with the anti-acetylated lysine antibodies. The pH gradient of the first dimension is indicated across the top and the molecular weight standards are indicated on the left. The Coomassie blue stained gels (CBB) are shown in the upper panels and the corresponding immunoblots (IB) are shown below. Regions of hyperacetylation are boxed and numbered. These boxes correspond with the regions of the blot enlarged in Figure 17.

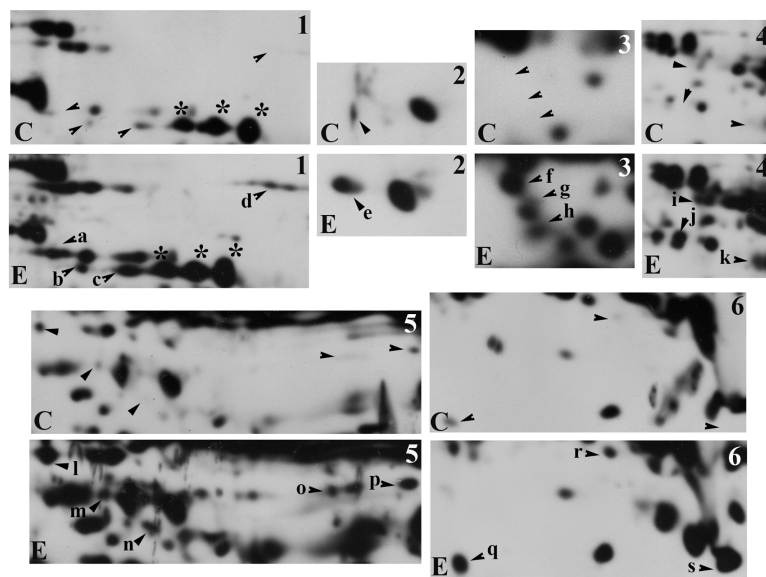


**Figure 17. Ethanol induces cytosolic protein hyperacetylation.** Regions of hyperacetylation seen in the cytosolic 2D gels in Figure 16 were boxed and enlarged. Control (C) and ethanol (E) samples were compared and hyperacetylated proteins were selected (marked with arrows) for mass spectrometric analysis. The labels on the blots from ethanol-treated samples correspond to the entries in Table 2. Asterisks are marking examples of acetylated proteins that were not changed by ethanol treatment.

Although much less membrane protein was loaded (360  $\mu$ g) than for the cytosolic samples, similar numbers of individual spots were resolved on both the control and ethanol gels (397 and 395 spots, respectively) (Fig. 18). Interestingly, the membrane samples displayed much less acetylation than the cytosolic samples, both in control (60 immunoreactive species) and in ethanol-treated (83 immunoreactive species) membranes. Nonetheless, robust hyperacetylation was observed in the ethanol-treated samples (see Table 2). In general, the hyperacetylated proteins were clustered in the middle of the gel ranging from 30-60 kDa with a pI of 5-9 (Fig. 18). When this region was enlarged, 18 hyperacetylated proteins were detected in the presence of ethanol and are marked with arrows (Fig. 19). Some proteins were significantly hyperacetylated (see spots w, x, y and

z) while others were not additionally modified (e.g., see the streak of proteins on the far right). Interestingly, ethanol also decreased acetylation of two proteins at 25 and 30 kDa. Only one was successfully identified as carbonic anhydrase 3 (Fig. 19, marked with an asterisk). The labeled spots were selected for MALDI-MS analysis (see Table 2). The corresponding spots in the control immunoblots are indicated with arrowheads.

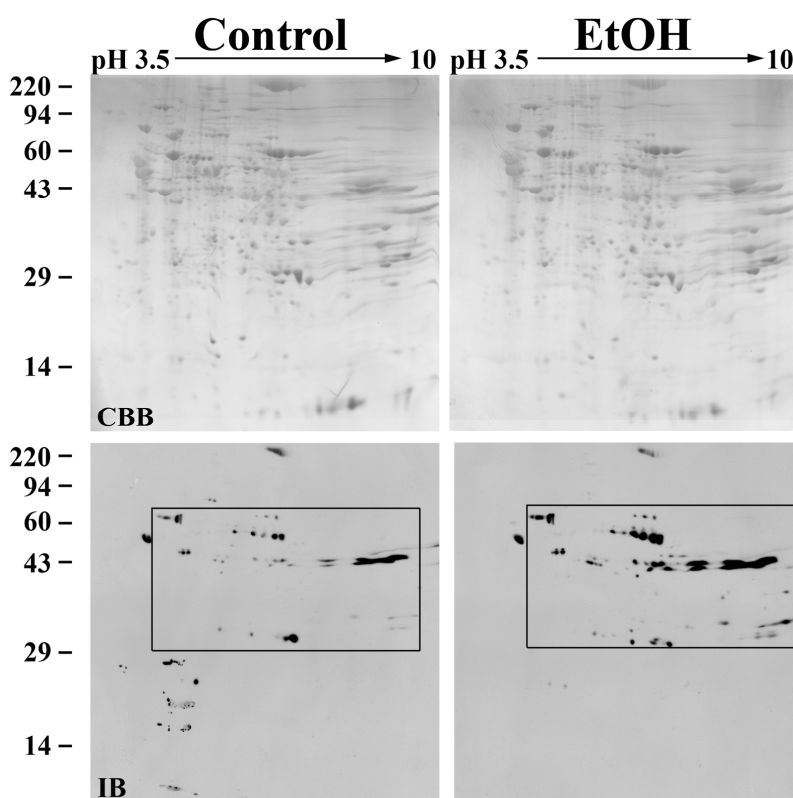


**Figure 18. Numerous membrane proteins are hyperacetylated in livers from ethanol-fed rats.** Liver total membrane fractions from control and ethanol pair-fed rats were prepared by differential centrifugation. 360  $\mu$ g of total protein from each sample was subjected to 2D electrophoresis and immunoblotted with the anti-acetylated lysine antibodies. The pH gradient of the first dimension is indicated across the top and the molecular weight standards are indicated on the left. The Coomassie blue stained gels (CBB) are shown in the upper panels and the corresponding immunoblots (IB) are shown below. The middle region of hyperacetylation is boxed and corresponds with the region enlarged in Figure 19.

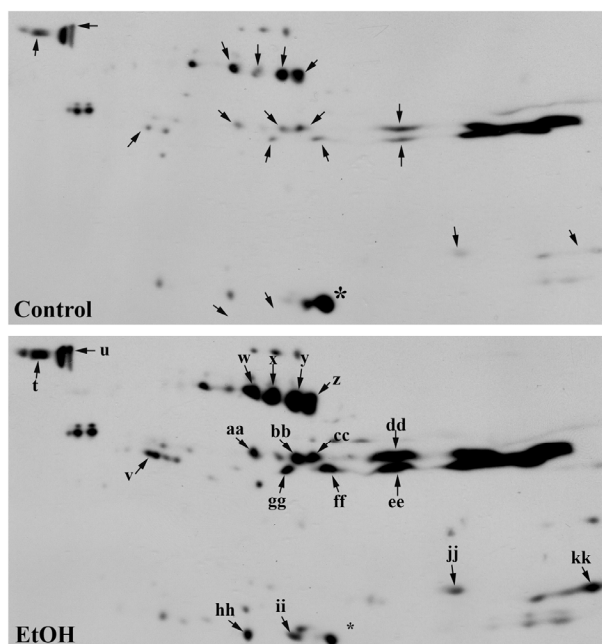


**Figure 19. Ethanol induces total membrane protein hyperacetylation.** The region of significant hyperacetylation found in Figure 18 was boxed and enlarged. Control and ethanol samples were compared and hyperacetylated proteins were selected (marked with arrows) for mass spectrometric analysis. The labels on the blots from ethanol-treated samples correspond to the entries in Table 2. The asterisk indicates a hypoacetylated protein in ethanol treated samples.

From the spots selected for mass spectrometric analysis, 40 proteins were positively identified. Table 2 provides a complete list of the selected proteins labeled in Figures 17 and 19. Table 3 groups the identified proteins by subcellular location and function.

Although our MALDI-MS approach used in these studies could not detect individual acetylated residues, 11 of these proteins were previously identified as acetylated proteins in a recent proteomic survey for acetylated residues (Kim et al., 2006) (Table 3, indicated with a “+”). Many of the cytosolic proteins were metabolic enzymes participating in amino acid metabolism, glycolysis or gluconeogenesis. Of particular interest was the finding that GPx-1, glutathione S-transferase  $\mu$ 2 (GST  $\mu$ 2) and superoxide dismutase 1

**Table 2. Non-nuclear hyperacetylated proteins identified in livers from ethanol-fed rats**

Spot	Protein	NCBI Accession	App MW	Calc MW	Calc PI	Peptides Matched	Sequence Coverage (%)	MOWSE Score	Mascot Score	Expect Value
a	Butyryl CoA synthetase 1	GI:197245828	65	65	7.6	16	44	1.32x10 <sup>11</sup>	123	3.4x10 <sup>-8</sup>
b	1-pyrroline-5-carboxylate dehydrogenase	GI:149024431	67	62	8.3	12	32.6	1.05x10 <sup>7</sup>	70	6.4x10 <sup>-3</sup>
c	Keratin contamination									
d	Aconitate hydratase	GI:40538860	93	85	7.9	27	40	6.21x10 <sup>14</sup>	170	6.9x10 <sup>-13</sup>
e	ATP synthase $\beta$ subunit	GI:54792127	55	56	5.1	37	69.6	1.72x10 <sup>18</sup>	267	1.1x10 <sup>-22</sup>
f	4-trimethylamino- butyraldehyde dehydrogenase	GI:149058126	58	56	6.9	19	46.3	6.87x10 <sup>9</sup>	147	1.4x10 <sup>-10</sup>
g	Succinate-semialdehyde dehydrogenase	GI:182676407	53	56	8.4	19	46.1	3.06x10 <sup>10</sup>	121	5.4x10 <sup>-8</sup>
h	Ethanolamine-phosphate cytidyltransferase	GI:50925459	50	43	6.4	17	45.9	9.01x10 <sup>9</sup>	117	1.4x10 <sup>-7</sup>
i	Adenosine kinase	GI:149031258	43	38	5.8	15	43.8	7.18x10 <sup>6</sup>	101	5.4x10 <sup>-6</sup>
	$\beta$ -Actin	GI:4501885	43	42	5.3	9	28.8	4.07x10 <sup>4</sup>	43	3.4
j	Fructose-1,6-bisphosphatase 1	GI:51036635	38	40	5.9	14	47.9	5.01x10 <sup>8</sup>	145	2.2x10 <sup>-10</sup>
k	$\delta$ -Aminolevulinic acid dehydratase	GI:6978483	36	36	6.3	17	54.5	5.80x10 <sup>8</sup>	126	1.7x10 <sup>-8</sup>
	Transaldolase	GI:149061610	36	36	8.2	11	25.3	2.57x10 <sup>4</sup>	74	3.1x10 <sup>-3</sup>
l	$\alpha$ -methylacyl-CoA racemase	GI:6981184	41	40	6.2	11	39.3	1.39x10 <sup>6</sup>	89	9.0x10 <sup>-5</sup>
m	3-oxo-5- $\beta$ -steroid-4- dehydrogenase	GI:20302063	36	37	6.2	14	45.4	4.65x10 <sup>9</sup>	62	3.9x10 <sup>-2</sup>
	Transaldolase	GI:149061610	36	36	8.2	15	29.4	1.12x10 <sup>6</sup>	55	2.1x10 <sup>-1</sup>
	Ornithine transcarbamylase	GI:6981312	36	36	8.2	10	45.2	1.38x10 <sup>6</sup>	45	2.1
n	Dihydropicolinate synthase	GI:157822207	32	34	8.5	12	55.5	3.48x10 <sup>5</sup>	66	1.7x10 <sup>-2</sup>
o	Trans-2-enoyl-CoA reductase	GI:8393848	36	40	8.9	7	23.3	5.31x10 <sup>3</sup>		
	Fructose-bisphosphate aldolase B	GI:158081751	36	40	8.7	15	50.8	1.03x10 <sup>7</sup>	92	3.9x10 <sup>-5</sup>

p	Fructose-bisphosphate aldolase B	GI:158081751	38	40	8.7	8	30.1	1.92x10 <sup>4</sup>	72	4.9x10 <sup>-3</sup>
	Peroxisomal $\delta$ 3, $\delta$ 2-enoyl CoA isomerase	GI:55741520	38	43	9.1	11	31.7	2.05x10 <sup>7</sup>	75	2.1x10 <sup>-3</sup>
	Peroxisomal $\delta$ 3, $\delta$ 2-enoyl CoA isomerase	GI:55741520	38	43	9.1	11	31.7	2.05x10 <sup>7</sup>	75	2.1x10 <sup>-3</sup>
q	Glutathione peroxidase 1	GI:2654236	20	22	7.7	9	63.2	3.29x10 <sup>5</sup>	125	2.2x10 <sup>-8</sup>
r	Glutathione S-transferase $\mu$ 2	GI:62653546	27	26	6.9	16	55.0	1.32x10 <sup>9</sup>	143	3.4x10 <sup>-10</sup>
s	Superoxide dismutase	GI:8394331	24	25	9.0	5	33.3	9.07x10 <sup>3</sup>	58	1.1x10 <sup>-1</sup>
t	60 kDa heat shock protein	GI:1334284	63	58	5.3	30	57.8	5.60x10 <sup>17</sup>	220	6.9x10 <sup>-18</sup>
u	60 kDa heat shock protein	GI:1334284	63	58	5.3	31	60	1.90x10 <sup>18</sup>	219	8.6x10 <sup>-18</sup>
v	Isovaleryl-CoA dehydrogenase	GI:6981112	42	43	8.0	17	43.9	7.81x10 <sup>10</sup>	105	2.2x10 <sup>-6</sup>
w	Glutamate dehydrogenase 1	GI:6980956	55	61	8.1	17	39.6	2.49x10 <sup>8</sup>	119	8.6x10 <sup>-8</sup>
x	Glutamate dehydrogenase 1	GI:6980956	55	61	8.1	25	50.0	3.78x10 <sup>12</sup>	186	1.7x10 <sup>-14</sup>
y	Glutamate dehydrogenase 1	GI:6980956	55	61	8.1	22	48.9	2.41x10 <sup>12</sup>	170	6.9x10 <sup>-13</sup>
z	Glutamate dehydrogenase 1	GI:6980956	55	61	8.1	27	51.1	1.75x10 <sup>15</sup>	205	2.2x10 <sup>-16</sup>
aa	4-hydroxyphenyl pyruvate dioxygenase	GI:8393557	42	45	6.3	13	42.2	5.52x10 <sup>8</sup>	94	2.7x10 <sup>-5</sup>
	Acyl-CoA thioesterase 2	GI:48675862	42	50	8.2	7	31.8	2.62x10 <sup>5</sup>	45	2.0
bb	Acyl-CoA thioesterase 2	GI:48675862	42	50	8.2	13	39.5	2.76x10 <sup>5</sup>	86	1.6x10 <sup>-4</sup>
cc	Acyl-CoA thioesterase 2	GI:48675862	42	50	8.2	9	33.8	2.18x10 <sup>4</sup>	60	6.2x10 <sup>-2</sup>
	3-ketoacyl-CoA thiolase	GI:149027156	42	50	8.2	13	46.3	8.50x10 <sup>8</sup>	77	1.3x10 <sup>-3</sup>
dd	3-ketoacyl-CoA thiolase	GI:149027156	42	50	8.2	9	35.6	1.47x10 <sup>7</sup>	60	6.2x10 <sup>-2</sup>
	Argininosuccinate synthase	GI:25453414	42	46	7.6	13	41.5	2.67x10 <sup>9</sup>	75	2.4x10 <sup>-3</sup>
ee	Cystathionine $\gamma$ -lyase	GI:13699175	41	54	7.5	13	51.3	6.29x10 <sup>7</sup>	82	4.5x10 <sup>-4</sup>
	Acetyl-CoA acetyltransferase	GI:135757	41	42	8.4	11	30.7	2.06x10 <sup>7</sup>	40	6.2
	Medium-chain specific acyl-CoA dehydrogenase	GI:8392833	41	47	8.6	11	28.0	2.94x10 <sup>6</sup>	64	3.1x10 <sup>-2</sup>
ff	26S protease regulatory Subunit S10 B	GI:81294202	41	43	7.2	22	56.7	5.65x10 <sup>12</sup>	113	3.4x10 <sup>-7</sup>
gg	$\beta$ -Ureidopropionase	GI:16758704	41	44	6.5	9	33.8	5.16x10 <sup>5</sup>	45	2.3
	Glutamine synthetase	GI:142349612	41	42	6.6	11	33.5	2.29x10 <sup>7</sup>	49	8.4x10 <sup>-1</sup>
	Medium-chain specific acyl-CoA dehydrogenase	GI:8392833	41	47	8.6	13	39.9	3.75x10 <sup>6</sup>	75	2.0x10 <sup>-3</sup>
hh	Enoyl-CoA hydratase	GI:17530977	30	32	8.4	15	50.0	4.52x10 <sup>6</sup>	120	6.9x10 <sup>-8</sup>

ii	Enoyl-CoA hydratase	GI:17530977	30	32	8.4	12	44.1	$3.76 \times 10^4$	88	$1.1 \times 10^{-4}$
	Electron transfer flavoprotein subunit $\beta$	GI:51948412	30	28	7.6	6	25.5	$2.84 \times 10^4$	28	$1.1 \times 10^2$
jj	Hydroxyacyl-CoA dehydrogenase	GI:17105336	32	34	8.8	15	53.2	$3.07 \times 10^4$	88	$9.9 \times 10^{-5}$
	Hydroxymethylglutaryl-CoA lyase	GI:13242293	32	34	8.7	11	39.4	$1.60 \times 10^7$	58	$1.1 \times 10^{-1}$
kk	2,4-dienoyl-CoA reductase	GI:67476443	32	36	9.1	15	38.5	$2.47 \times 10^{10}$	104	$2.7 \times 10^{-6}$

**Table 3. Most alcohol-induced hyperacetylated proteins regulate liver metabolism**

<b>Protein</b>	<b>Spot</b>	<b>Fold increase</b>	<b>Subcellular Location</b>	<b>Function</b>	<b>Acetylated</b>
$\delta$ -Aminolevulinic acid dehydratase	k	14.1	Cyto.	Porphyrin metabolism	
Adenosine kinase	i	3.7	Cyto.	Nucleotide metabolism	
$\beta$ -Ureidopropionase	gg	15.2	Cyto.	Nucleotide metabolism	
4-trimethylamino-butylaldehyde dehydrogenase	f	23.1	Cyto.	AA metabolism (NAD <sup>+</sup> )	
Argininosuccinate synthase	dd	2.7	Cyto.	AA metabolism	
4-hydroxyphenyl pyruvate dioxygenase	aa	6.5	Cyto.	AA metabolism	
Glutamine synthetase	gg	15.2	Cyto.	AA metabolism	
1-pyrroline-5-carboxylate dehydrogenase	b	9.8	Cyto.	AA metabolism (NAD <sup>+</sup> )	
Dihydropicolinate synthase	n	8.8	Cyto.	AA metabolism	
Cystathionine $\gamma$ -lyase	ee	4.5	Cyto.	AA metabolism	
Glutathione peroxidase 1	q	8.1	Cyto.	Oxidative stress	+
Glutathione S-transferase $\mu$ 2	r	8.3	Cyto.	Oxidative stress	
Superoxide dismutase	s	2.9	Cyto.	Oxidative stress	+
Fructose-1,6-bisphosphatase 1	j	28.6	Cyto.	Gluconeogenesis	
Fructose-bisphosphate aldolase B	o	5.6	Cyto.	Glycolysis	+
Transaldolase	p	23.1			
	k	14.1	Cyto.	Pentose phosphate shunt	
	m	6.2			
Aconitate hydratase	d	99.6	Cyto.	TCA cycle	
$\beta$ -Actin	i	3.7	Cyto.	Cytoskeleton	+
26S protease regulatory Subunit S10 B	ff	22.6	Cyto.	Proteosomal degradation	( $\gamma$ actin)
60 kDa heat shock protein	t	1.4	Mito.	Chaperone	
	u	1.8			
Peroxisomal $\delta$ 3, $\delta$ 2-enoyl CoA isomerase	p	23.1	Mito.	Lipid metabolism	+
Trans-2-enoyl-CoA reductase	o	5.6	Mito.	Lipid metabolism	
Acyl-CoA thioesterase 2	aa	3.6	Mito.	Lipid metabolism	
	bb	4.5			
	cc	6.5			
Ethanolamine-phosphate cytidyltransferase	h	1.8	Mito.	Lipid metabolism	
Medium-chain specific acyl-CoA dehydrogenase	ee	4.5	Mito.	Lipid metabolism	
	gg	15.2			
Butyryl CoA synthetase 1	a	44.2	Mito.	Lipid metabolism	
3-oxo-5- $\beta$ -steroid-4-	m	6.2	Mito.	Lipid	

dehydrogenase				metabolism	
$\alpha$ -methylacyl-CoA racemase	l	18.1	Mito.	Lipid metabolism	
Enoyl-CoA hydratase	hh	4.5	Mito.	Lipid metabolism	
Hydroxyacyl-CoA dehydrogenase	ii	18.3		Lipid metabolism	
	jj	6.2	Mito.	(NAD <sup>+</sup> )	+
Hydroxymethylglutaryl-CoA lyase	jj	6.2	Mito.	Lipid metabolism	
				(NAD <sup>+</sup> )	
2,4-dienoyl-CoA reductase	kk	13.8	Mito.	Lipid metabolism	+
3-ketoacyl-CoA thiolase	cc	4.5	Mito.	Lipid metabolism	
	dd	2.7		Lipid metabolism	
Acetyl-CoA acetyltransferase	ee	4.5	Mito.	Lipid metabolism	+
				AA metabolism	
Ornithine transcarbamylase	m	6.2	Mito.	AA metabolism	+
Succinate-semialdehyde dehydrogenase	g	7.2	Mito.	AA metabolism	
				(NAD <sup>+</sup> )	
Isovaleryl-CoA dehydrogenase	v	2.2	Mito.	AA metabolism	+
Glutamate dehydrogenase 1	w	7.0	Mito.	AA metabolism	+
	x	27.0		(NAD <sup>+</sup> )	
	y	2.6			
	z	2.5			
Electron transfer flavoprotein subunit $\beta$	ii	18.3	Mito.	Electron transport chain	
ATP synthase $\beta$ subunit	e	4.6	Mito.	ATP synthesis	

The identified hyperacetylated proteins listed in Table 2 were grouped according to function. To determine the fold increase in acetylation, the density of the individual spots on both the gels and immunoblots were determined. The level of each immunoreactive spot was normalized to the relative protein level of its corresponding spot in the gel. Fold-increase in acetylation was calculated by comparing the control ratios to those from ethanol-treated samples. The subcellular location of each protein is indicated. Proteins that are known to be acetylated at steady state are indicated with a “+” sign. Cyto., cytosol; Mito., mitochondria

(SOD1) were all hyperacetylated in ethanol-treated samples (see Discussion). We also identified  $\beta$ -actin, whose highly related  $\gamma$ -actin isoform is known to be acetylated (Kim et al., 2006). Remarkably, almost all of the hyperacetylated proteins in the membrane

fraction were from mitochondria (Table 3). In general, these proteins fell into broad categories of lipid metabolism, amino acid metabolism and ATP synthesis indicating that these hyperacetylated proteins may be playing a role in the overall state of ethanol-induced mitochondrial dysfunction (see Discussion).

### ***GPx-1 and actin hyperacetylation is confirmed***

Considering that ethanol induces large changes in the redox state of the cell leading to oxidative stress and reactive oxygen species production, our identification of three hyperacetylated antioxidant proteins is intriguing. Since GPx-1 has previously been shown to be acetylated at steady state and the effects of ethanol on its activity are well characterized, we began our confirmation studies here. We first examined GPx-1 protein levels by immunoblotting control and ethanol liver fractions. A doublet at 23 kDa was observed for both the control and ethanol samples indicating that chronic ethanol consumption does not alter total or cytosolic GPx-1 levels, consistent with the literature (Bailey et al., 2001) (Fig. 20A). Importantly, the majority of GPx-1 was cytosolic further confirming the accuracy of our fractionation method. A small amount of GPx-1 was also detected in the total membrane population, which may reflect a population that is associated with the mitochondrial outer membrane (Bailey et al., 2001).

To confirm that GPx-1 was hyperacetylated, we immunoprecipitated it from control and liver cytosols. The unbound and bound fractions were immunoblotted for GPx-1 (Fig. 20B, top panels) or acetylated lysine residues (Fig. 20B, bottom panels). In both the

control and ethanol samples, we detected GPx-1 in the unbound and bound fractions indicating partial immunoprecipitation. The corresponding IgG light chain was only evident in the bound lanes indicating complete antibody recovery. In control immunoprecipitations, no immunoreactivity was detected in either the unbound or bound samples probed with anti-acetylated lysine antibodies. In contrast, a 23 kDa doublet was detected in both the unbound and bound ethanol-treated samples indicating that the enzyme was hyperacetylated.

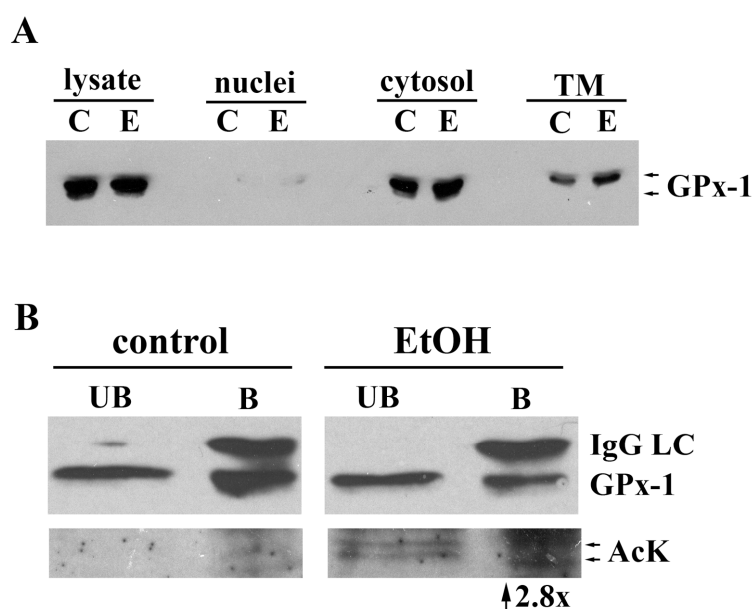


**Figure 20. Alcohol-induced hyperacetylation of glutathione peroxidase 1.** A, Nuclear, cytosolic and total membrane fractions were prepared from control (C) and ethanol-fed (E) rat livers. Fractions were immunoblotted for GPx-1. B, Cytosolic fractions were immunoprecipitated for GPx-1 and both the unbound (UB) and bound (B) samples were blotted for GPx-1 (top) or acetylated lysine (AcK) (bottom). The IgG light chain (IgG LC) is detected in the bound fractions. Immunoreactive acetylated bands are detected in both the UB and B fractions from the ethanol-treated samples, but not in control.

We also confirmed ethanol-induced acetylation of GPx-1 using a two-antibody sandwich ELISA. Anti-GPx-1 antibodies were adhered to the wells of ELISA strip plates and then incubated with either control or ethanol cytosolic fractions. After incubation and subsequent washes, only the captured GPx-1 remained in the wells. The captured GPx-1 was then incubated with anti-acetylated lysine antibodies. HRP-conjugated secondary antibodies were added and binding was detected colorimetrically. From these assays, we determined that GPx-1 from the ethanol-fed animals was hyperacetylated 2.8-fold more than from control samples (Fig. 20B).

Previous work from our lab and others has found that ethanol impairs clathrin-mediated endocytosis, secretion and delivery of newly synthesized membrane proteins to the basolateral membrane (McVicker and Casey, 1999; Tuma et al., 1990; Tuma et al., 1991a; Tuma and Sorrell, 1988). In addition, studies using TSA, have linked these impairments to increased protein acetylation (Joseph et al., 2008). Since both actin and its binding partner, cortactin, are likely required for clathrin-vesicle formation at the plasma membrane and TGN (Cao et al., 2003; Cao et al., 2005), an intriguing possibility is that actin hyperacetylation may contribute to the observed alcohol-induced defects in protein trafficking. Thus, we chose to confirm the acetylation of both actin and cortactin. We first immunoblotted liver whole homogenates for actin and cortactin protein expression levels. As observed for GPx-1, no changes were observed (Fig. 21A) indicating that hyperacetylation is not due to increased protein levels. To confirm hyperacetylation, we performed two-antibody sandwich ELISAs. Interestingly,

acetylation of both actin and cortactin was increased to a similar extent as GPx-1. Actin acetylation was increased by  $2.42 \pm 0.60$  whereas cortactin acetylation was enhanced  $2.53 \pm 0.43$ -fold in ethanol-treated samples (Fig. 21B).

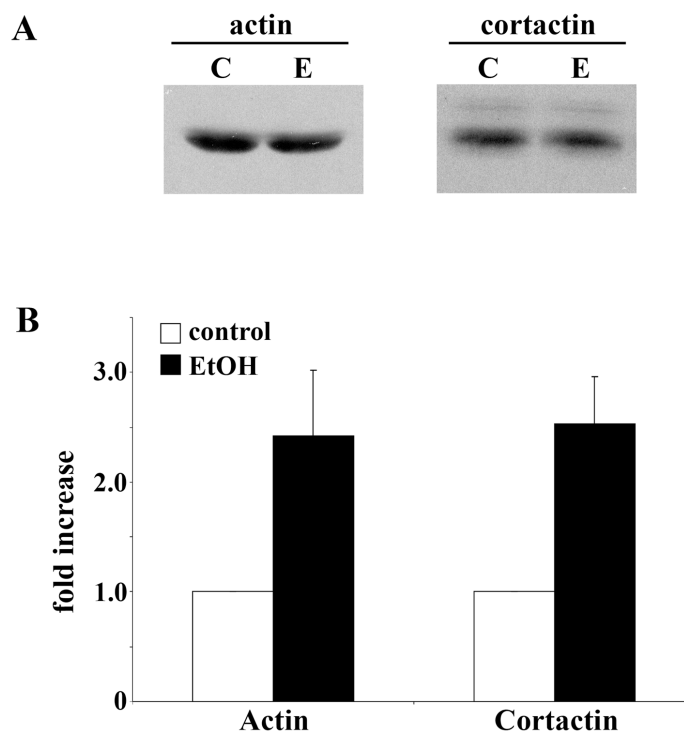


**Figure 21. Actin and cortactin are hyperacetylated in ethanol-treated liver cytosols.** A, Control (C) and Ethanol (E) liver homogenates were immunoblotted for cortactin or actin as indicated. B, Two-antibody sandwich ELISAs were performed to measure cortactin and actin acetylation in control or ethanol-treated samples. 20  $\mu$ g of each antibody was absorbed to wells, blocked, and lysates added. The captured antigen was further incubated with anti-acetylated lysine antibodies and detected with HRP-conjugated secondary antibodies. Absorbance was measured and hyperacetylation is plotted as a fold-increase over control. Values are expressed as the mean  $\pm$  SEM from 3-independent experiments performed in duplicate.

## CONCLUSIONS

A proteomics approach was used to identify cytosolic and membrane proteins that are hyperacetylated after chronic ethanol consumption. In all, we identified 40 non-nuclear proteins, half of which were from the cytosolic fraction and half from non-nuclear membranes. Remarkably, almost all of the hyperacetylated proteins in the latter fraction were from mitochondria and most were metabolic enzymes (Table 3). Similarly, cytosolic fractions were highly hyperacetylated after ethanol exposure and the proteins identified varied widely in function ranging from metabolic enzymes to proteins regulating oxidative stress to molecular chaperones. In order to confirm our proteomic results, we examined hyperacetylation of GPx-1 and actin directly. GPx-1 was found to be hyperacetylated by both immunoprecipitation and a two-antibody sandwich ELISA (2.8-fold). We also performed ELISAs to confirm actin hyperacetylation ( $2.42 \pm 0.6$ -fold increase) and to establish ethanol's impact on cortactin acetylation ( $2.53 \pm 0.43$ -fold increase).

While our results provide compelling evidence for ethanol's role in global hepatic acetylation, there are some limitations to the mass spectrometry method used. Because MALDI-MS is not optimized to detect post-translational modifications, acetylated residues could not be identified. However, 11 of these proteins were confirmed in a related study partially confirming our results (Kim et al., 2006). Clearly, the identification of the specific modified lysines will be required to not only confirm, but to determine the impact of such global hepatic protein acetylation.

### **Part III: Chronic ethanol administration impairs clathrin-mediated vesicle fission**

Previously, it has been shown that ethanol specifically impairs clathrin-mediated internalization. In order to determine the specific stage at which clathrin-mediated internalization is impaired and the possible mechanism(s), we took a morphological approach to examine the key components of clathrin-mediated internalization in the presence of both ethanol and TSA. In addition to the increased basolateral staining of clathrin heavy chain, we observed that both cortactin and  $\alpha$ -adaptin also accumulated at the surface in ethanol and TSA-treated cells suggesting a late stage of clathrin internalization is impaired. This was confirmed using TIRF microscopy and  $K^+$  depletion/repletion studies where ASGP-R internalization was delayed and blunted in the presence of ethanol and TSA. Consistent with a block in late stage internalization, we found that dynamin-2 surface labeling was lost in ethanol and TSA treated cells. Its membrane recruitment was significantly impaired when visualized by a  $K^+$  depletion/repletion assay and its association with members of the clathrin machinery was blunted. From this morphological data, we conclude that ethanol impairs the late stage clathrin-mediated vesicle scission by preventing proper dynamin-membrane association and this defect may be mediated by increased protein hyperacetylation.

## RESULTS

### *Components of the clathrin machinery accumulate at the plasma membrane in ethanol-treated cells*

Since the clathrin-mediated internalization of many unrelated proteins is impaired *in situ*, in isolated hepatocytes and in ethanol-treated WIF-B cells, it is likely that a universal regulator of clathrin-mediated internalization is impaired, not the receptors themselves. For that reason, we chose to examine the steady state distribution of some of the major players in clathrin-mediated internalization in ethanol-treated WIF-B cells. Previously, we found that ethanol leads to the accumulation of clathrin heavy chain in puncta at the plasma membrane suggesting proper clathrin coat assembly (Fernandez et al., 2009). To examine this more closely, we looked at  $\alpha$ -adaptin, one of the first proteins to be recruited to the plasma membrane during clathrin vesicle formation. As expected,  $\alpha$ -adaptin is localized to the plasma membrane in control cells (Fig. 22A). However, in the presence of ethanol,  $\alpha$ -adaptin staining becomes brighter and more discrete at the membrane (Fig. 22A). Measurement of the ratio of basolateral/intracellular staining revealed that there is a  $19 \pm 4\%$  increase in  $\alpha$ -adaptin at the plasma membrane in the presence of ethanol consistent with an increase in clathrin heavy chain.

Because clathrin,  $\alpha$ -adaptin and the receptors themselves appear to accumulate at the plasma membrane in discrete puncta, it is likely that the ethanol-induced defect in clathrin internalization may be at a later stage once the clathrin-coated pit has already formed. Cortactin, an actin binding protein known to induce actin polymerization, has

been implicated in clathrin-coated vesicle budding at both the Golgi and plasma membrane. As reported, cortactin is found primarily in intracellular structures in control cells (Fig. 22A). However, upon ethanol treatment, cortactin redistributes from these intracellular structures to the basolateral plasma membrane (Fig. 22A). However, there is no noticeable difference in rhodamine-labeled actin distribution after ethanol treatment (data not shown). Nonetheless, the observation that ethanol leads to the accumulation of clathrin machinery at the plasma membrane suggests that the clathrin internalization defect is occurring after vesicle invagination but prior to vesicle budding and scission.

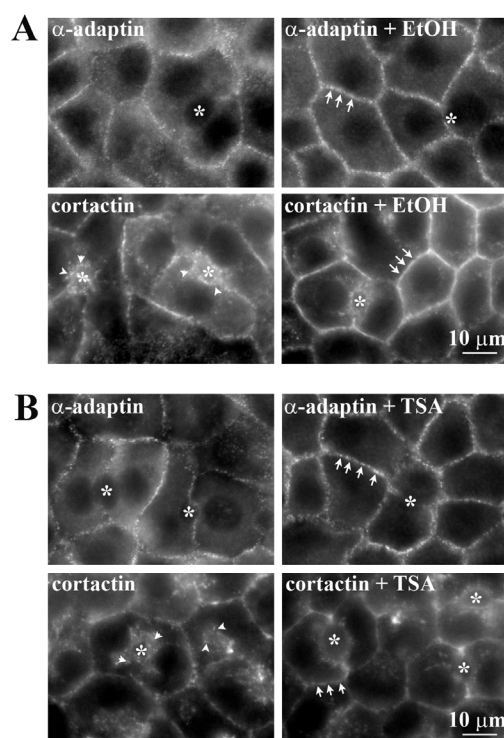


**Figure 22. Components of the clathrin machinery accumulate at the plasma membrane in ethanol and TSA-treated WIF-B cells.** Cells were incubated in the presence or absence of (A) 50 mM ethanol (EtOH) for 72 hours or (B) 50-250 nM TSA for 30 min and stained for  $\alpha$ -adaptin or cortactin as described. Asterisks are labeling bile canaliculi. Ethanol and TSA leads to increased plasma membrane staining. Arrows highlight areas of high membrane staining while arrowheads indicate the intracellular population of cortactin. Bar = 10  $\mu$ m.

***Protein hyperacetylation may contribute to the ethanol-induced defect in clathrin internalization***

Previously, we found that the clathrin-mediated internalization of ASGP-R and APN could be impaired in the absence of ethanol by the addition of TSA (Joseph et al., 2008). TSA is a broad inhibitor of HDACs that leads to protein hyperacetylation in the absence of ethanol. Since ethanol induces hyperacetylation of a large number of cytosolic proteins including microtubules, cortactin and actin (Shepard et al., 2009b; Shepard and Tuma, 2009), we chose to more closely examine the effects of TSA on clathrin-mediated internalization. As seen in Figure 22B, addition of 50-250 nM TSA for 30 min led to a similar accumulation of both  $\alpha$ -adaptin ( $38 \pm 17\%$  increase) and cortactin at the plasma membrane as in ethanol-treated cells. TSA also induced an accumulation of clathrin heavy chain at the plasma membrane suggesting that protein hyperacetylation plays a role in clathrin-mediated internalization (Fig. 26). The findings that TSA mimics the internalization defect observed with ethanol provides exciting evidence that ethanol-induced lysine hyperacetylation may be one of the underlying causes of this defect.

***Internalization is blocked at the cell surface***

Using traditional epifluorescence techniques, it is difficult to determine whether clathrin coated vesicles are at the cell surface or in newly internalized structures. In order to determine the stage at which ethanol impairs clathrin internalization, we used TIRF microscopy to visualize the bottommost 100 nm of the cell which is roughly the diameter of a clathrin-coated vesicle. We started by examining the distribution of two well-

characterized, clathrin-dependent receptors, ASGP-R and pIgA-R. In control cells, a few large, bright and discrete spots of ASGP-R were found at the cell surface (Fig. 23A). Additional spots were also detected, albeit smaller and dimmer, likely representing those vesicles that are undergoing vesicle fission or receptors not yet clustered into pits. In contrast, ethanol drastically increases the number of ASGP-R spots found at the cell surface (Fig. 23A). Compared to the control cells, ASGP-R puncta are more uniform in size and lack the diffuse background in the presence of ethanol which likely represents unclustered receptors (Compare Fig. 23A ASGP-R control and EtOH insets). pIgA-R, a transcytosing receptor, showed similar results. The increased number of uniform, larger spots with similar brightness indicates accumulation of the receptors at the cell surface.

In order to examine all clathrin-coated vesicles at the cell surface rather than a specific receptor population, we looked at clathrin heavy chain and  $\alpha$ -adaptin. In control cells, clathrin heavy chain is found in bright, discrete spots that are all uniform in size (Fig. 23B). These spots represent the coated pits at the cell surface that have yet to undergo vesicle fission and uncoating. As predicted, ethanol greatly increases the amount of clathrin heavy chain at the cell surface (Fig. 23B). Rather than a simple increase in the amount, ethanol also increases the overall size of these coated pits suggesting a defect in internalization (Compare Fig. 23B CHC control and EtOH insets). The clathrin heavy chain spots appear to merge together in the presence of ethanol, possibly forming large clathrin-coated “hot spots” that fail to pinch off in the presence of ethanol. Unlike clathrin heavy chain,  $\alpha$ -adaptin did not appear to change in the presence of ethanol (Fig.

23B). In control and ethanol-treated cells, the size, amount, and brightness of the  $\alpha$ -adaplin spots remain constant. At present, we cannot reconcile the disparate observations.

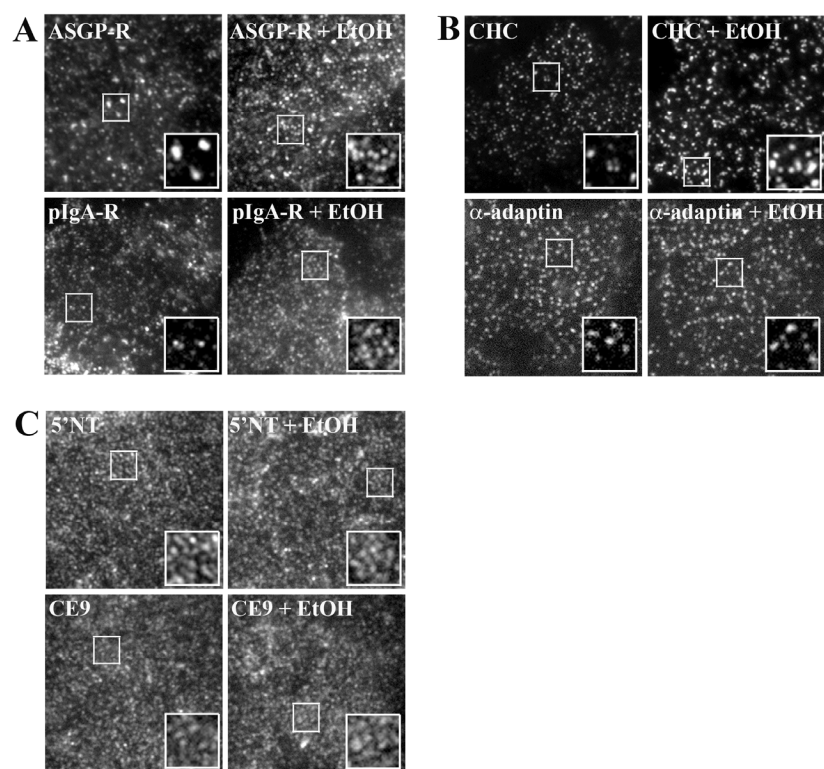


**Figure 23. Ethanol impairs clathrin-mediated internalization at the cell surface.** Cells were incubated in the presence or absence of 50 mM EtOH for 72 hours and stained for (A) clathrin-internalized receptors, ASGP-R and pIgA-R, (B) components of the clathrin machinery, clathrin heavy chain (CHC) and  $\alpha$ -adaplin, or (C) non-clathrin associated proteins, 5'NT and CE9. TIRF microscopy was performed as described in Materials and Methods to visualize the bottommost 100 nm of the coverslip. Boxed regions of interest are enlarged at the bottom right hand corner of each image. Ethanol treatment leads to an increase in the number and size of clathrin-coated pits at the plasma membrane.

In order to confirm our previous results that ethanol selectively impairs clathrin-mediated vesicle internalization, we examined two non-clathrin associated proteins: the GPI-anchored, raft internalized transcytosing protein, 5'NT, and a basolateral resident protein,

CE9 (Fig. 23C). In both control and ethanol-treated cells, 5'NT and CE9 are detected at the cell surface in high abundance. Neither of these proteins is present in large discrete spots unlike the clathrin vesicle components. Ethanol did not alter the distribution or amount of these two proteins confirming the specificity of the defect. From these results, and the increase in amount and size of clathrin-coated vesicles observed for ASGP-R, pIgA-R and clathrin heavy chain, we conclude that ethanol impairs clathrin-mediated endocytosis at a stage prior to vesicle budding and fission.

***Clathrin-mediated internalization is both delayed and impaired in ethanol-treated cells***

In order to examine the kinetics of clathrin coated vesicles in the presence of ethanol or TSA, we synchronized clathrin endocytosis by depleting WIF-B cells of  $K^+$  for 30 min to disrupt clathrin lattices.  $K^+$  depletion prevents the formation of new clathrin coated vesicles at the plasma membrane and by 30 min, all receptor internalization is blocked (Carpentier et al., 1989; Heuser and Anderson, 1989; Larkin et al., 1983; Larkin et al., 1985; Larkin et al., 1986). After the 30 min depletion, live cells were surface labeled on ice with ASGP-R antibodies specific to external epitopes and placed back in  $K^+$ -containing medium to allow for rapid coated pit assembly and internalization. We then followed the internalization and trafficking of ASGP-R up to 15 min after  $K^+$  repletion in both control and treated cells. Cells were fixed and labeled with secondary antibodies to detect the trafficked antigen-antibody complexes. Immediately following the 30 min  $K^+$  depletion (labeled 0 min), ASGP-R in control cells was found only at the basolateral plasma membrane, consistent with the surface labeling and a block in trafficking (Fig.

24A,B 0 min control). Interestingly, the receptor distribution along the membrane is much more uniform than under steady state conditions (compare Fig. 24A,B, 0 min and Fig. 26), suggesting that the receptors are not found in or around clathrin coated vesicles in the absence of  $K^+$ . After 5 min of  $K^+$  repletion, ASGP-R accumulates at or near the plasma membrane in punctate-like structures (Fig. 24A,B, 5 min control). These puncta are most likely highly invaginated pits or newly budded vesicles. This surface puncta is significantly reduced after 15 min corresponding to a reciprocal increase in the intracellular ASGP-R labeling indicating successful internalization (Fig. 24A,B, 15 min control). Since ASGP-R constitutively recycles in the absence of ligand, requiring ~10 min to complete one round from the basolateral plasma membrane, by 15 min we began to detect both internalized and recycled receptors. In the presence of ethanol or TSA, however, there is a clear delay and impairment in ASGP-R internalization. After 5 min, ASGP-R remains much more uniform along the membrane and there is a noticeable absence of any large puncta suggesting a delay in receptor clustering or clathrin vesicle formation (Fig. 24A,B, 5 min EtOH and TSA). ASGP-R only becomes punctate-like in appearance after 15 min of repletion, albeit to a lesser extent than control (Fig. 24A,B, 15 min EtOH and TSA) consistent with a block in the later steps of clathrin-mediated internalization. These data suggest that both ethanol and TSA delay receptor recruitment into clathrin coated pits and prevent complete internalization.

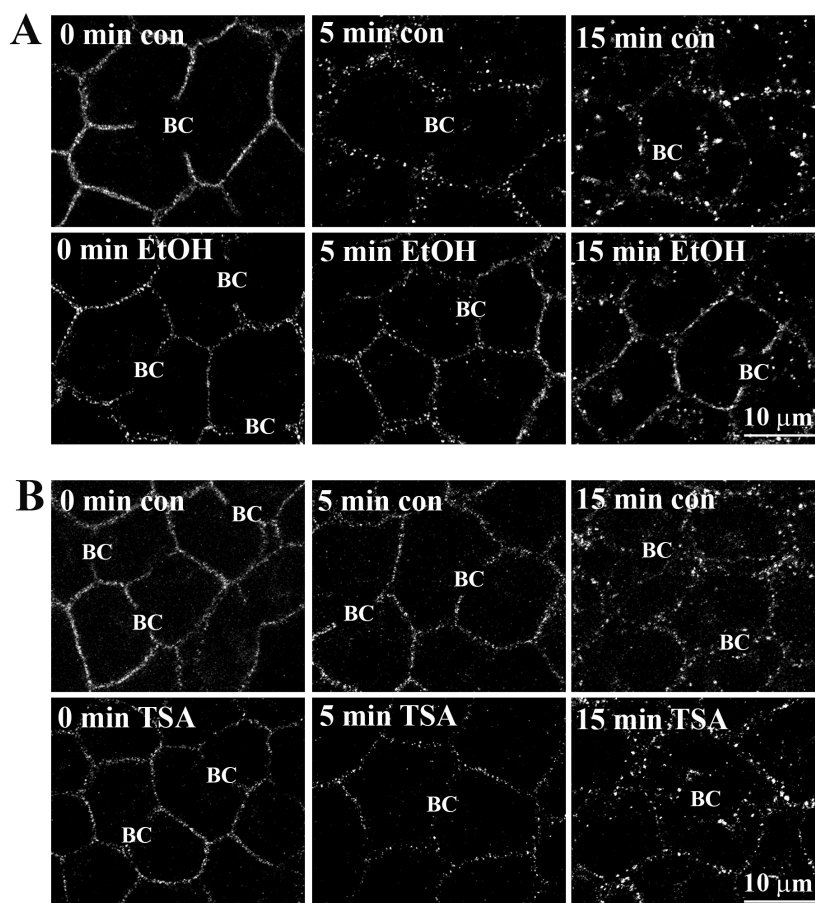


**Figure 24. Clathrin-mediated internalization is both delayed and impaired in ethanol and TSA-treated WIF-B cells.** Cells incubated in the presence or absence of (A) 50 mM EtOH for 72 hours or (B) 50 nM TSA for 30 min were rinsed and incubated in prewarmed  $K^+$ -depletion buffer for 30 min at  $37^\circ C$  to disrupt clathrin-coated pit formation. Depleted cells were surface labeled with the anti-ASGP-R antibody for 20 min on ice and then placed back into medium supplemented with 10 mM KCl. ASGP-R was allowed to traffic for 0, 5 or 15 min at  $37^\circ C$  and then fixed. Trafficked ASGP-R was visualized at indicated time points by confocal microscopy as described in the methods. BC = bile canaliculi. Bar = 10  $\mu m$ .

To better visualize the delay in clathrin internalization, we again turned to TIRF microscopy to examine the surface population of ASGP-R upon  $K^+$  depletion and repletion. Immediately after surface labeling in control cells, ASGP-R is found in discrete spots at the cell surface (Fig. 25, 0 min). Compared to the steady state control

(Fig. 23), the 0 min repletion control has more receptor on the surface and the spots are more uniform in size and shape (Compare Fig. 23 and Fig. 25, 0 min control). This is likely due to the lack of clathrin assembly and internalization which prevents receptor clustering. Interestingly, ethanol-treated cells had a significant increase in the amount of surface labeled ASGP-R immediately following  $K^+$  depletion (0 min) indicating an overall increase in the amount of cell surface receptor at the time of surface labeling. In control cells,  $K^+$  repletion resulted in a continual decrease in the amount of receptor at the cell surface as the clathrin coat formed and internalized the receptor. At 5 min repletion, there is a noticeable decrease in the number of receptors on the cell surface and those that remain are dimmer and smaller, likely within newly internalized vesicles (Fig. 25, 5 min control). After 15 min, most of the receptor is no longer at the surface, and what remains is likely the newly recycled population (Fig. 25, 15 min control). Consistent with our confocal data, ethanol significantly delayed the loss of the ASGP-R from the surface. After 5 min repletion, most of the spots remain and they are brighter and larger than control suggesting a lack of internalization (Fig. 25, 5 min EtOH). Although by 15 min there are decreased levels of receptor relative to 5 min repletion, there is significantly more receptor at the surface in ethanol-treated cells indicating impaired internalization. From these results, along with our confocal imaging, we conclude that ethanol both delays and impairs receptor internalization at a stage prior to vesicle fission.

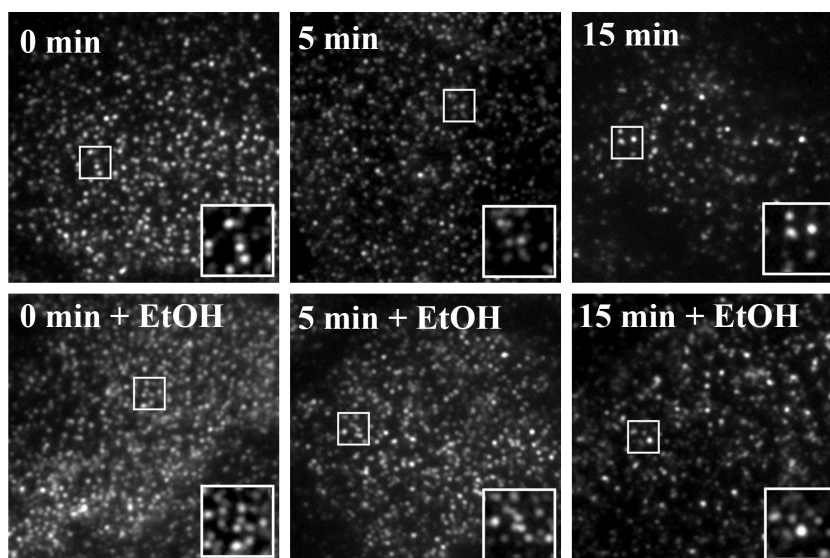


**Figure 25. Ethanol impairs receptor internalization prior to vesicle fission.** Cells were incubated in the presence or absence of 50 mM EtOH for 72 hours, depleted of  $K^+$  and surface labeled with anti-ASGP-R antibody as described in Figure 24. Trafficked ASGP-R was visualized at 0, 5 or 15 min as indicated using TIRF microscopy to detect receptor present on the bottommost 100 nm of the coverslip. Boxed regions of interest correspond to the enlarged images found in the bottom right hand corner.

To directly confirm a block in late-stage vesicle budding, we visualized control and treated cells by transmission electron microscopy (unpublished data, P.L. Tuma). Images of random clathrin coated vesicle profiles along the plasma membrane were acquired that captured clathrin coated vesicles in three stages of assembly: early, non-invaginated pits (stage 1), intermediate pits (stage 2) and highly invaginated pits (stage 3). In control cells, only ~25-35% of all clathrin-coated profiles observed were deeply invaginated (stage 3). In contrast, ~65 and 50% of profiles were deeply invaginated in ethanol and TSA treated cells, respectively (unpublished data, P.L. Tuma). This ultrastructural analysis confirms that ethanol blocks clathrin-mediated vesicle internalization at a late stage.

*Ethanol does not impair receptor recruitment into clathrin coated pits*

Since the receptors and clathrin machinery both accumulate in punctate structures at the plasma membrane, it is likely that the receptors are being properly recruited to sites of clathrin-coated pit formation and are then clustered inside these coated pits that fail to bud. To confirm this hypothesis, we examined the degree of colocalization between steady state labeled ASGP-R and clathrin heavy chain in control and treated cells. In control cells, ASGP-R is found in intracellular, perinuclear structures while clathrin heavy chain is primarily localized to intracellular structures (likely Golgi) with slight membrane staining (Fig. 26). To determine their degree of overlap, we analyzed the Pearson's coefficient which measures the degree of coincidence between fluorophore fluorescence. In control cells, the average Pearson's coefficient was 0.467 (Fig. 26A) and 0.449 (Fig. 26B) indicating a fraction of overlap between clathrin heavy chain and ASGP-R. Since we are interested in the degree of overlap at the cell surface, regions of interest along the basolateral cell surface were selected (Fig. 26 insets). In the case of control cells, the Pearson's coefficient dropped to  $0.279 \pm 0.02$  (Fig. 26A) and  $0.235 \pm 0.04$  (Fig. 26B) indicating little overlap between the receptor and clathrin on the cell surface.

Consistent with previous reports, both ethanol and TSA lead to a significant accumulation of ASGP-R and clathrin heavy chain at the basolateral plasma membrane suggesting impaired internalization (Fig. 26A,B). When these images are merged together, distinct green (ASGP-R) and red (CHC) puncta are observed at the plasma

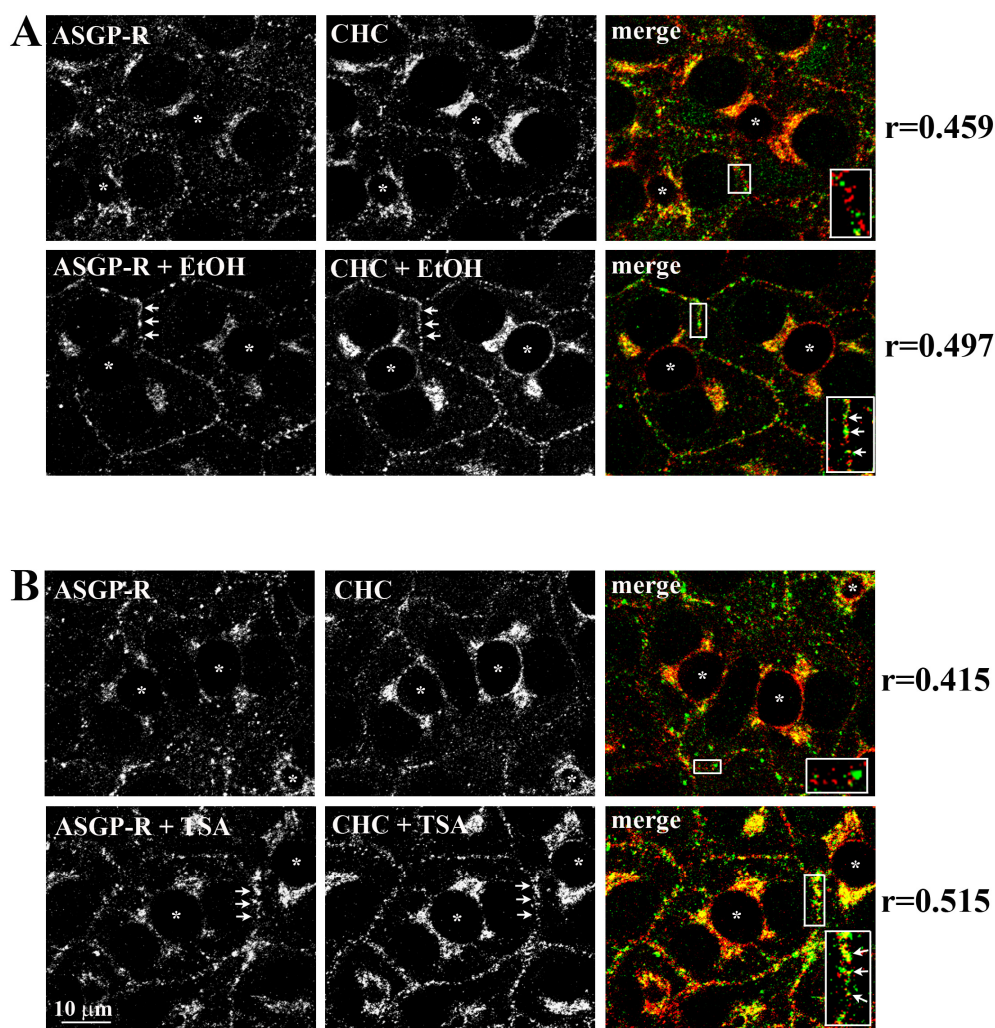


**Figure 26. Receptor recruitment is not impaired by ethanol or TSA.** Cells were incubated in the presence or absence of (A) 50 mM EtOH for 72 hours or (B) 50 nM TSA for 30 min and stained for both ASGP-R (green) and clathrin heavy chain (CHC) (red). Confocal images were merged and the degree of overlap (yellow) was assessed by the Pearson's coefficient and is indicated by the  $r$  value. To analyze colocalization at the plasma membrane, the Pearson's coefficient was calculated for membrane regions where discrete puncta were observed. These values are an average of 5 areas of discrete puncta/field. A, control  $r=0.279 \pm 0.02$ ; EtOH  $r=0.415 \pm 0.02$  B, control  $r=0.235 \pm 0.04$ ; TSA  $r=0.295 \pm 0.04$ . An example of one such region is boxed and enlarged in the lower right hand corner. Arrows indicate regions of significant overlap. Bar = 10  $\mu\text{m}$ .

membrane along with a degree of overlap (yellow). In ethanol-treated cells, the Pearson's correlation was 0.457, similar to that of control. When restricting the region of

interest to membrane regions where discrete receptor puncta are observed, the coefficient was  $0.415 \pm 0.02$ , a significant increase from control reflecting the increased surface labeling. For TSA cells, the overall Pearson's correlation was 0.500 with the membrane regions dropping to  $0.295 \pm 0.04$ . These correlations imply that some, but not all, of ASGP-R is properly recruited to sites of clathrin-vesicle formation. As clathrin coats are not specific for ASGP-R and there is more clathrin heavy chain found on the membrane as compared to receptor, complete overlap is not expected. From these images, we conclude that ethanol and TSA do not impair proper receptor clustering, suggesting that the impairment is in a later stage of clathrin-coated vesicle formation, once receptors are properly clustered and targeted to sites of pit formation.

### ***Ethanol impairs dynamin recruitment***

Our results suggest that ethanol impairs late stage clathrin vesicle budding, likely at the point of internalization. Because vesicle fission relies on the GTPase of dynamin 2, we examined dynamin 2 distribution in control and ethanol-treated cells. To better visualize membrane-associated dynamin, we first permeabilized cells with TX-100 to clear the largely soluble pool. In control cells, dynamin is found brightly labeling the plasma membrane, indicative of membrane binding (Fig. 27A). However, in ethanol and TSA-treated cells, dynamin staining at the plasma membrane is lost suggesting decreased membrane association and a defect in proper dynamin recruitment (Fig. 27A). This is consistent with our previous biochemical analysis where we found that the total membrane population of dynamin decreased from  $71.6 \pm 5.3\%$  in control cells to  $54.2 \pm$

2.9% in the presence of ethanol (Fernandez et al., 2009)

To directly test for a defect in dynamin recruitment, we utilized the  $K^+$  depletion/repletion assay as described for ASGP-R. After 30 min of  $K^+$  depletion, the cells were reincubated with medium containing  $K^+$  for up to 15 min to allow for clathrin vesicle formation and dynamin recruitment. In control cells, there is little dynamin detected at the plasma membrane immediately following the 30 min depletion (Fig. 27B, 0 min control). Since clathrin vesicle formation is inhibited upon  $K^+$  depletion, the lack of dynamin recruitment is expected. At 5 and 15 min post-depletion, dynamin membrane staining increases drastically consistent with proper internalization seen by the receptors (Fig. 27B, 5 and 15 min control). In contrast, both ethanol and TSA show a significant decrease in the amount of dynamin membrane staining after  $K^+$  repletion. With both treatments, no dynamin surface labeling is observed after 5 and 15 min of repletion suggesting impaired recruitment (Fig. 27B,C, 5 and 15 min). This data, along with our steady state and ultrastructural results suggest that ethanol impairs clathrin vesicle fission due to impaired dynamin recruitment and this defect may be mediated by ethanol-induced protein hyperacetylation (see discussion).

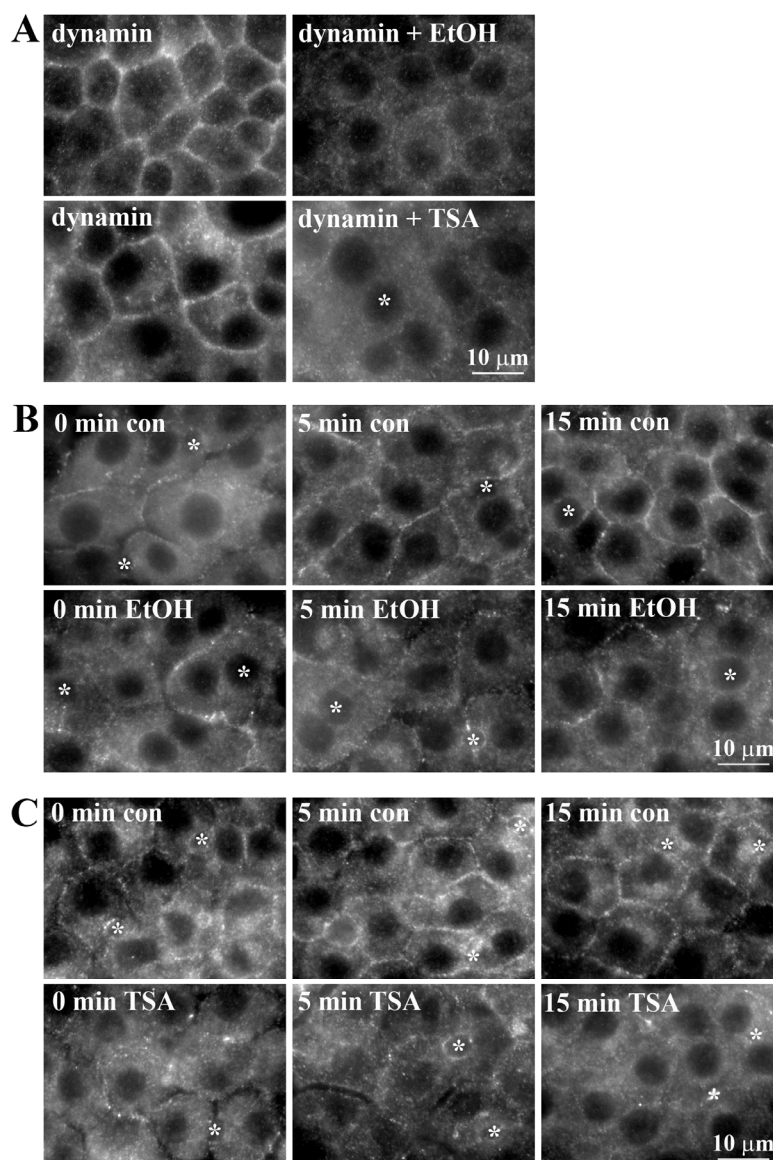


**Figure 27. Dynamin membrane recruitment is impaired in ethanol and TSA-treated cells.** A, Cells were incubated in the absence or presence of 50 mM EtOH for 72 hours or 50 mM TSA for 30 min and permeabilized with Triton X-100. Permeabilized cells were stained for dynamin-2 to assess membrane association. B, C, Cells were rinsed and incubated in prewarmed  $K^+$ -depletion buffer for 30 min at 37°C to disrupt clathrin-coated pit formation. Depleted cells were placed back in medium supplemented with 10 mM KCl for 0, 5 or 15 min to allow for the reformation of clathrin coated pits. To assess dynamin membrane recruitment, cells were permeabilized with triton-x and stained for dynamin-2. Asterisks mark bile canaliculi. Bar = 10 μm.

To biochemically confirm that ethanol impairs dynamin recruitment, we performed co-immunoprecipitations with dynamin, cortactin and clathrin heavy chain antibodies. As seen in Figure 28A, there is no difference in protein levels of any of the major proteins involved in clathrin internalization in control and ethanol-treated cells. However, in the presence of ethanol, there was an increased association between cortactin and clathrin heavy chain consistent with our steady state imaging indicating accumulated clathrin coated vesicles at the plasma membrane (Fig. 28B). Also consistent with our morphological results, co-immunoprecipitation between cortactin and dynamin was drastically reduced in the presence of ethanol (Fig. 28B, C). Additionally, immunoprecipitation of dynamin also revealed a decrease in its association with clathrin heavy chain (Fig. 28C). These results strongly suggest that ethanol impairs late stage clathrin-mediated internalization and this is most likely due to a defect in proper dynamin recruitment.

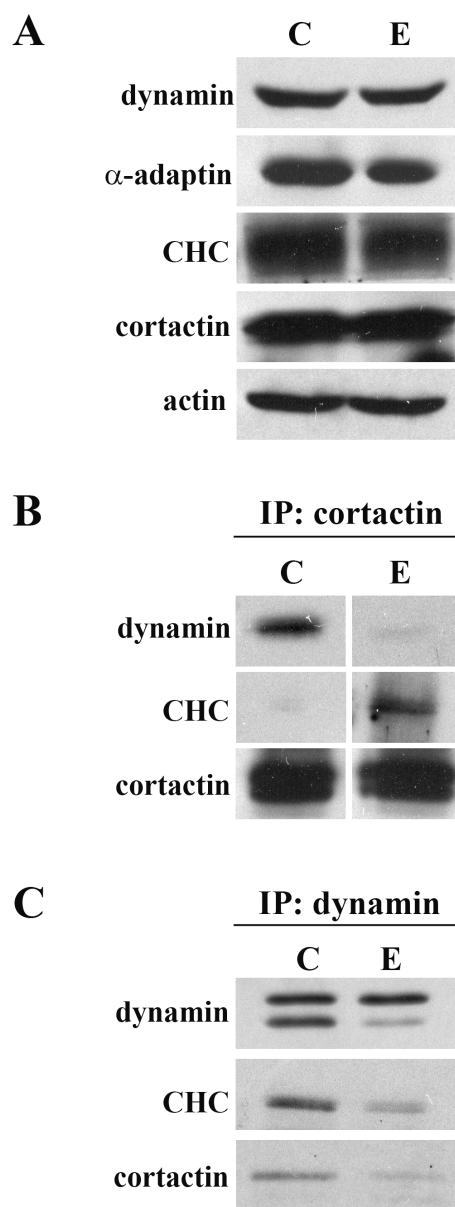


**Figure 28. Co-immunoprecipitation confirms decreased dynamin-2-clathrin pit association in the presence of ethanol.** A, Control (C) and EtOH (E) WIF-B homogenates were immunoblotted for components of the clathrin machinery as indicated. B, C, Control and EtOH WIF-B precleared detergent lysates were immunoprecipitated for cortactin (B) or dynamin (C) and the bound fractions were blotted for dynamin, cortactin and CHC as indicated.

## CONCLUSIONS

Previously, we determined that ethanol specifically impairs clathrin-mediated internalization. In this study, we sought to define the underlying mechanisms of this defect using a morphological approach. When observing members of the clathrin machinery, we found that ethanol led to their accumulation at the cell surface. In addition to clathrin heavy chain and clathrin-specific receptors,  $\alpha$ -adaptin and cortactin are found at the basolateral plasma membrane in discrete puncta, suggesting a block in late stage vesicle internalization. This was confirmed using TIRF microscopy and  $K^+$  depletion/repletion assays that established that ethanol causes a delay and impairment in vesicle budding at the cell surface. With a defect in vesicle scission, we turned to dynamin, whose GTPase activity is required for vesicle internalization. In the presence of ethanol, we found that dynamin membrane recruitment is impaired and its association with members of the clathrin machinery is decreased. Addition of TSA to induce protein hyperacetylation showed a similar impairment in vesicle internalization and dynamin recruitment. From this study, we conclude that ethanol impairs clathrin-mediated internalization by altering dynamin-membrane association and this defect may be caused by ethanol-induced protein hyperacetylation.

## DISCUSSION

For decades, ethanol has been linked to hepatotoxicity; chronic consumption leads to the progression of liver disease and general defects in hepatic function have been observed. These impairments range from alterations in the redox state of the cell to global clinical manifestations such as hepatomegaly and ascites accumulation in the peritoneal cavity. More recently, studies have begun to focus on the mechanisms by which alcohol exerts its physiological effects on the liver. In our lab, we found that ethanol leads to the hyperacetylation and stability of microtubules, one of the most important proteins involved in vesicular transport (Kannarkat et al., 2006). In Part I of this dissertation, it was determined that microtubule hyperacetylation correlates with impaired HDAC6-microtubule binding, most likely by a modification of the endogenous population of microtubules (see below) (Shepard et al., 2008). This microtubule hyperacetylation has also been correlated to alterations in hepatic protein trafficking including receptor internalization and protein secretion (Joseph et al., 2008). From Part II of this dissertation, it is evident that ethanol-induced lysine acetylation is not merely specific for microtubules, but chronic ethanol treatment also induces global lysine hyperacetylation (Shepard et al., 2009b). Of particular interest was the identification of both actin and cortactin as two of these modified proteins. Like microtubules, actin and cortactin play a prominent role in hepatic protein trafficking, mainly at the stage of vesicle budding and fission in clathrin-mediated endocytosis (Cao et al., 2003; Cao et al., 2005). In Part III of this dissertation, it was found that the clathrin-mediated internalization defect is impaired at the point of dynamin recruitment. Exciting evidence was also presented that allow us

to speculate that actin and cortactin hyperacetylation may be partially responsible for the defect in dynamin recruitment. Together, these three sections allow us to consider lysine acetylation as a general regulator of hepatic function and that the observed ethanol-induced hyperacetylation may exert deleterious effects on the liver.

**Lysine acetylation may be a regulator of hepatic protein function:**

The reversibility of lysine acetylation and its presence on numerous proteins have led some to postulate that it might rival phosphorylation in its ability to regulate cellular processes (Kouzarides, 2000). In general, the added acetyl group likely neutralizes the lysine positive charge while increasing the size and hydrophobicity of the side chain. Such changes may result in protein conformational changes that alter function. Also, lysine acetylation sites have been identified that overlap with nuclear localization signals (Kim et al., 2006) such that the modification may induce altered protein subcellular distributions. In general, lysine acetylation has been shown to regulate protein stability, protein-protein interactions, protein-DNA interactions, and protein localization. Not only can lysines be acetylated, they can also be methylated, sumoylated and ubiquitinated such that ethanol-induced hyperacetylation may displace other modifications further altering protein function. In fact, p300 acetylation has been shown to prevent its sumoylation thereby repressing its activity (Bouras et al., 2005). Clearly the understanding and appreciation for lysine acetylation is in its infancy.

**Mechanisms of ethanol-induced hyperacetylation – ethanol metabolism:**

In Part I, we found that HDAC6-microtubule binding was impaired in ethanol-treated WIF-B cells. However, its activity was not altered, nor was its ability to bind exogenous microtubules. Thus, it is exciting to speculate that tubulin from ethanol-treated cells is somehow modified, thereby preventing proper HDAC6 binding. What is the nature of the alcohol-induced tubulin modification? In this study, we determined that impaired HDAC6 binding to microtubules was partially mediated by acetaldehyde, and from our previous work, we determined that alcohol-induced tubulin hyperacetylation was also mediated by acetaldehyde (Kannarkat et al., 2006; Shepard et al., 2008). Because this highly reactive ethanol metabolite can readily, covalently modify a highly reactive lysine in  $\alpha$ -tubulin *in vitro* (Tuma et al., 1991b), one provocative possibility is that tubulin-acetaldehyde adducts impede HDAC6 binding. Because decreased HDAC6 binding to microtubules was only partially prevented by 4-MP, we cannot rule out the possibility that some of the other reactive ethanol metabolites (shown in Figure 2) also formed detrimental tubulin adducts.

The idea that protein adduction leads to microtubule hyperacetylation can be expanded for all of the newly identified nonnuclear hyperacetylated proteins. Currently, little is known about the modifying enzymes that control this global non-nuclear acetylation. However, as for tubulin, it is possible that the proteins themselves or their modifying enzymes are altered in the presence of ethanol. In the case of ethanol-induced histone H3 hyperacetylation, it was found that ethanol increased both p300 protein levels and overall nuclear HAT activity. It is likely that the change in enzyme activity is also

linked to ethanol metabolism. Addition of acetate, the end product of ethanol metabolism, also increased nuclear HAT activity (Bardag-Gorce et al., 2007; Choudhury and Shukla, 2008; Park et al., 2005). Although acetate itself is nonreactive, it is clear that ethanol metabolism plays an important role in controlling enzyme activity and may contribute to the observed global hyperacetylation.

Since not much is known about the global non-nuclear hyperacetylation described in part II, attention is being turned to those modifying enzymes that are exclusively cytosolic (HDAC6 and SirT2) and mitochondrial (SirT3-5) or shuttle between the nucleus and cytoplasm (PCAF, TIP60 and HDACs 5, 7, 9 and 10) (Shepard and Tuma, 2009) (Figure 4). For mitochondrial proteins, only protein levels of SirT3 and 5 have been examined. Although SirT3 is considered the predominant mitochondrial deacetylase, its expression levels were not changed in rat livers from ethanol-fed rats (Picklo, 2008). In contrast, SirT5 protein levels were significantly decreased, but the specific sirtuin activity has not yet been addressed (Picklo, 2008). In a recent study examining the effects of a fatty liver induced by a high fat diet, the authors found a decrease in SirT3 activity correlating with mitochondrial hyperacetylation. Given the overlap between the identified hyperacetylated proteins in their study and those in Part II, it is possible that ethanol also impairs SirT3 activity (Kendrick et al.). Given the prominence of mitochondrial hyperacetylation, more work is clearly needed to understand the role that ethanol and ethanol metabolism plays within the mitochondria (see below).

While not identified during the proteomics screen, we found that ethanol induces

cortactin hyperacetylation  $2.53 \pm 0.43$  fold in our sandwich ELISA confirmation assay (Shepard et al., 2009b). As for tubulin, cortactin is also a substrate of HDAC6 (Zhang et al., 2007) and the interaction between these two which occurs within its actin binding region, leads to deacetylation of cortactin. Cortactin acetylation generates two charged patches that control its association with F actin. When acetylated, these positive charged acetyl groups prevent proper actin binding and polymerization and have been implicated in impaired translocation to the cell periphery in migrating cells (Zhang et al., 2007). In addition to HDAC6, cortactin acetylation has also been shown to be regulated by SirT1 and SirT2 as well as acetyltransferases p300 and PCAF (Zhang et al., 2007; Zhang et al., 2009). SirT2, the other microtubule deacetylase, has not been detected in WIF-B cells (Shepard et al., 2008). Furthermore, SirT1, a nuclear HDAC, apparently shuttles into the cytoplasm in cancer cell lines to contribute to cell migration (Zhang et al., 2009). In our studies, it is likely that HDAC6 is the predominant deacetylase. Because of this, it is tempting to speculate that a similar mechanism for tubulin hyperacetylation may be extended to cortactin. Clearly the role of ethanol metabolism on cortactin and actin, as well as the global non-nuclear acetylation, should be examined.

### **Consequences of ethanol-induced hyperacetylation – gene expression:**

We determined that ethanol treatment decreased nuclear HDAC activity to  $67.8 \pm 5.5\%$  of control implicating increased histone acetylation (Shepard et al., 2008).

Although traditionally it has been thought that histone acetylation promotes DNA relaxation which better allows for transcription factor binding and increased transcription

(Eberharter and Becker, 2002), an emerging hypothesis is that the dynamic turnover of histone modifications, rather than continued acetylation, leads to increased transcription (Clayton et al., 2006; Mellor, 2006). In fact, histone hyperacetylation has been shown to lead to nucleosome instability that allows transcription at cryptic promoters resulting in aberrant transcription (Clayton et al., 2006; Mellor, 2006). Thus, altered histone acetylation may not only explain the decreased levels of HDAC6 in ethanol treated cells due to changes in transcriptional regulation, but may also have profound effects on general hepatic gene expression.

While histone modifications are appreciated as a primary means of controlling gene expression, acetylation of transcription factors also plays an important role. One such example is alcohol-induced acetylation of two opposing transcriptional regulators of fatty acid expression, SREBP-1c and PGC-1 $\alpha$ . From studies performed in H4IIEC3 cells, overexpressing SirT1 and p300 were found to deacetylate or acetylate SREBP-1c, respectively, confirming that SREBP-1c is a substrate for both enzymes (You et al., 2008). Increasing ethanol concentrations enhanced p300-mediated SREBP acetylation in these cells while a concomitant decrease in SirT1 protein levels was observed (Lieber et al., 2008; You et al., 2008). Thus, SREBP-1c hyperacetylation was the result of changes in both types of modifying enzymes. As for SREBP-1c, PGC-1 $\alpha$  hyperacetylation was also correlated with decreased SirT1 protein expression (Lieber et al., 2008; You et al., 2008).

SREBP-1c, a transcription factor that regulates lipid and cholesterol synthesis, promotes the expression of many genes involved in lipogenesis that are up-regulated after

alcohol consumption (Donohue, 2007). SREBP-1c is known to be acetylated in its DNA binding domain, and when acetylated, DNA binding is enhanced. In addition, it is also known to be ubiquitinated on the same lysine residues leading to its proteosomal degradation (Giandomenico et al., 2003). Thus, in alcohol-treated hepatocytes, the prediction is that hyperacetylation prevents SREBP-1c proteosomal degradation by displacing the ubiquitin while enhancing its DNA binding leading to increased transcription of lipogenic enzymes (Shepard and Tuma, 2009). A similar scenario is emerging for the transcriptional activator, PGC-1 $\alpha$ . In this case, the deacetylation of PGC-1 $\alpha$  leads to the upregulation of genes regulating fatty acid  $\beta$ -oxidation (Rodgers et al., 2008). Therefore, in ethanol-treated hepatocytes, the prediction is that the hyperacetylated PGC-1 $\alpha$  will be inactive leading to decreased  $\beta$ -oxidation and increased fatty acid levels (Shepard and Tuma, 2009). The altered transcriptional activation in either case leads to hepatic fatty acid accumulation that likely contributes to the development of steatosis. Because many other components of the transcriptional machinery are known to be acetylated (Table ) (Shepard et al., 2009b), it is likely that alcohol-induced hyperacetylation will have far-reaching effects on hepatic gene expression that will lead to altered hepatocellular function.

### **Consequences of ethanol-induced hyperacetylation – mitochondrial dysfunction:**

The results presented in Part II and results from others have shown that numerous mitochondrial proteins are hyperacetylated in the presence of ethanol (Picklo, 2008; Shepard et al., 2009b). However, little is known about the functional consequences of

this global mitochondrial protein acetylation. To date, the effects of acetylation on mitochondrial activity have been examined only on glutamate dehydrogenase and AceCS2. In both cases, increased acetylation correlated with decreased activity (Schwer et al., 2006). Thus, the simple prediction is that acetylation functions as an on/off switch for these and other mitochondrial metabolic enzymes such that alcohol-induced changes in this modification alter hepatic metabolism.

Alternatively, it has been recently hypothesized that mitochondrial protein acetylation functions as a sensor for the overall energy status of the cell (Kim et al., 2006). According to this hypothesis, acetyl-CoA and  $\text{NAD}^+$  levels are the key indicators of energy status. This hypothesis stems from two observations. First, is that over 44% of mitochondrial dehydrogenases that require  $\text{NAD}^+$  for activity are known to be acetylated (Kim et al., 2006). Second, is that acetyl-CoA and  $\text{NAD}^+$  are cofactors for HATs and a subset of HDACs, respectively. Thus, one possibility is that lysine acetylation serves as a feedback mechanism for the regulation of dehydrogenases. For example, when cellular energy status is high (reflected in low  $\text{NAD}^+$  levels), the subset of HDACs are less active resulting in higher protein acetylation and dehydrogenase activities. In contrast, when acetyl-CoA levels are limiting (the energy status is low), HATs are inactivated leading to decreased protein acetylation and increased dehydrogenase activities. Thus, the simple prediction in the alcoholic liver where  $\text{NAD}^+$  is depleting is that increased acetylation leads to impaired dehydrogenase activity and by extension, impaired mitochondrial function. Interestingly, our proteomics survey identified 4 mitochondrial enzymes that require  $\text{NAD}^+$  as a cofactor (Table 3). Although

NAD<sup>+</sup> levels may recover after prolonged ethanol exposure, the finding that hyperacetylation remains long after chronic ethanol withdrawal (Picklo, 2008) suggests that this mechanism may have physiologic relevance.

### **Consequences of ethanol-induced hyperacetylation – oxidative stress:**

It is well-established that chronic alcohol consumption leads to increased hepatic oxidative stress (reviewed in Wu and Cederbaum, 2003). Not only are reactive oxygen species produced by CYP2E1-mediated ethanol metabolism, they are also produced as a result of alcohol-induced mitochondrial dysfunction. Many of these and other reactive species can form covalent modifications with cellular proteins, lipids and DNA that can in turn, lead to hepatic dysfunction and disease (Tuma and Casey, 2003; Wu and Cederbaum, 2003). Alcohol consumption also induces overexpression of CYP2E1 while inhibiting the expression or activities of protective, antioxidant enzymes thereby reinforcing the vicious cycle. Thus, our findings that three key antioxidant enzymes (GPx-1, GST $\mu$ 2 and SOD1) are hyperacetylated in livers from ethanol-fed rats are particularly interesting.

The activities of many antioxidant enzymes are known to be impaired in ethanol-treated cells, including GPx-1 and superoxide dismutase (Bailey et al., 2001; Farbiszewski et al., 1991; Mari and Cederbaum, 2000; Oh et al., 1998). Overexpression of CYP2E1 has also been shown to impair GPx-1 activity suggesting ethanol metabolism may be required for this impairment (Mari and Cederbaum, 2000). Another intriguing possibility is that the alcohol-induced hyperacetylation of GPx-1 and other antioxidant

enzymes may also be regulating enzymatic activity. If acetylation/deacetylation is functioning as a simple on/off switch as described above for the mitochondrial enzymes, the simple prediction is that alcohol-induced hyperacetylation leads to impaired antioxidant activities of GPx-1, GST $\mu$ 2, SOD1 and other antioxidant proteins thereby enhancing oxidative stress.

**Consequences of ethanol-induced hyperacetylation – proteasome inhibition and aggresome formation:**

The proteasome, located mainly in the cytosol and nucleus, serves as one of the main proteolytic centers in the cell. Upon ubiquitinylation, misfolded and damaged proteins are targeted to the 26S proteasome for an ATP-dependent degradation (Kopito, 2000; Osna and Donohue, 2007). During periods of low oxidative stress, proteasome activity is increased to promptly clear damaged proteins. However, if the cell is in a state of high oxidative stress, the proteasome activity is repressed due to damage to the enzyme itself (Osna and Donohue, 2007). Induction of CYP2E1 activity by ethanol metabolism is one example of a period of high oxidative stress within the liver. The CYP2E1 enzyme is typically degraded by the 26S proteasome to avoid prolonged exposure to its toxic metabolic byproducts. However, in the presence of ethanol, CYP2E1 is stabilized and protected against proteolysis which leads to the increased production of ethanol metabolites (Bardag-Gorce et al., 2006; Osna and Donohue, 2007; Perez and Cederbaum, 2003). As with so many proteins within the cell, components of the proteasome are also subject to modification by ethanol-induced adduct formation.

The adduction of these proteins and the production of reactive oxygen species (ROS) within the liver shut down proteasome activity, leading to the accumulation of damaged proteins (Bardag-Gorce et al., 2006; Osna and Donohue, 2007; Perez and Cederbaum, 2003). Upon proteasome inhibition, damaged proteins accumulate in aggresomes located throughout the cell (Kopito, 2000). In the liver, these aggresomes take the form of Mallory Denk Bodies, which are dense inclusion bodies comprised of modified keratins and other damaged proteins and chaperones (see introduction for more details) (Bardag-Gorce et al., 2006). Ultimately, aggresome formation and proteasome inhibition overwhelm the cell leading to apoptosis.

Interestingly, recent studies have found that HDAC6 plays a role in both aggresome formation and clearance via quality control autophagy during periods of proteasome inhibition (Kawaguchi et al., 2003; Lee et al., 2010; Lee and Yao, 2010). HDAC6 interacts with both ubiquitinated proteins via its BUZ domain and with dynein, a microtubule minus-end directed motor by its second catalytic domain (Kawaguchi et al., 2003). In this model, HDAC6 serves as a bridge between polyubiquitinated misfolded proteins and the dynein motor. Therefore, during periods of proteasome inhibition (i.e. ethanol metabolism), misfolded and damaged proteins are recognized by HDAC6 where they are carried to the aggresome (Kawaguchi et al., 2003). For proper clearance, HDAC6 recruits and deacetylates cortactin allowing for actin polymerization (Lee et al., 2010; Lee and Yao, 2010). Polymerized actin allows for autophagosome-lysosome fusion and aggresome clearance by quality-control autophagy (Lee et al., 2010; Lee and Yao, 2010). From this dissertation and work from other labs, we have seen that ethanol

exposure results in proteasome inhibition, impaired HDAC6 binding, increased cortactin acetylation and decreased autophagy in a CYP2E1-dependent manner (Osna and Donohue, 2007; Shepard et al., 2008; Shepard et al., 2009b; Wu et al., 2010). From these observations, it is tempting to suggest that ethanol impairs aggresome formation and clearance by way of HDAC6. Besides HDAC6-microtubule binding, it is possible that dynein may be similarly modified by ethanol metabolites, thereby preventing proper HDAC6 binding. Furthermore, the observed cortactin hyperacetylation may result in impaired actin polymerization around the autophagosome preventing proper fusion. Clearly the link between ethanol and aggresome formation and clearance should be investigated further.

Additionally, one of the many 26S protease regulatory subunits, S10B or p42, was found to be hyperacetylated in our proteomics screen in Part II (Shepard et al., 2009b). While not much is known about this particular subunit, these regulatory proteins play an important role in promoting ATP-dependent degradation of ubiquitinated proteins. It is possible that the lysine acetylation may contribute to the deregulation of the proteasome, participating in its inhibition during periods of ethanol metabolism. The exact role that acetylation play on the proteasome should be further examined.

### **Ethanol impairs late-stage clathrin-vesicle internalization – our working model:**

During late stage clathrin-mediated internalization, ligand bound receptors accumulate in highly invaginated clathrin-coated pits. In control cells (Fig. 29A), vesicle scission is preceded by actin polymerization and dynamin-2 membrane association.

Actin polymerization, induced by actin-binding proteins (i.e. cortactin), enhances membrane constriction at the necks of coated vesicles. Dynamin-2 oligomerization and GTPase activity provides the conformational change necessary to promote vesicle fission and internalization. In the presence of ethanol, however, internalization is blocked immediately prior to vesicle fission (Fig. 29B). We propose that the ethanol-induced cortactin acetylation prevents proper actin polymerization and dynamin interaction. As a result, dynamin-2 membrane recruitment is impaired preventing proper vesicle internalization. (see below)

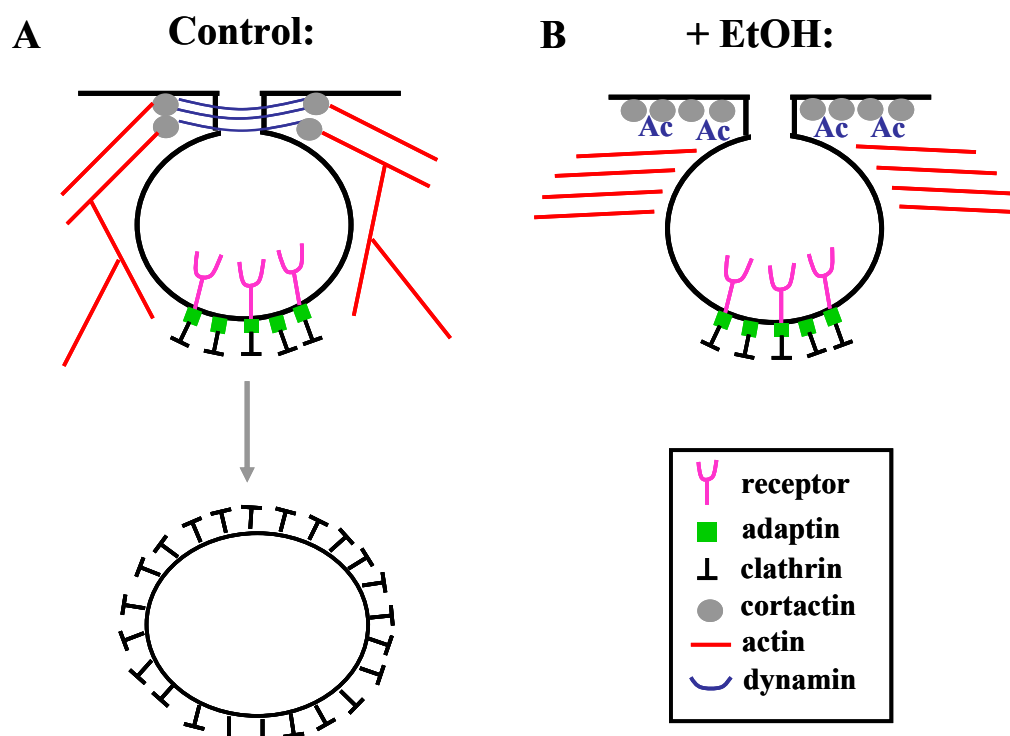


**Figure 29. Ethanol impairs late stage clathrin-vesicle internalization.** A., In control cells, receptors associate with adaptin molecules in a highly invaginated clathrin-coated vesicle. Actin polymerization is induced at the necks of clathrin-coated vesicles by actin binding proteins (i.e. cortactin). Dynamin is recruited to the membrane, oligomerizes and hydrolyzes GTP leading to vesicle internalization. B., Ethanol-induced cortactin and actin acetylation (Ac) impairs actin polymerization and dynamin-membrane recruitment. The lack of dynamin-2 to promote scission prevents vesicle internalization resulting in the accumulation of highly invaginated pits at the cell surface in ethanol-treated cells.

**Consequences of ethanol-induced hyperacetylation – protein trafficking:**

From the work presented in Part III of this dissertation, it is clear that ethanol impairs late stage clathrin vesicle fission, likely due to impaired dynamin recruitment. As a result, deeply invaginated coated pits are found in high abundance along the hepatocyte plasma membrane poised for scission. These coated pits are characteristic of the latest stage of internalization, occurring immediately prior to membrane fission. Although a comprehensive list of the molecular players involved in vesicle scission is still lacking, it is characterized primarily by dynamin-membrane association and GTPase activity as well as actin polymerization. Dynamin, a 100 kDa GTPase, acts as the molecular machine required for membrane scission (Chappie et al., 2010; Hinshaw, 2000; Marks et al., 2001; Mettlen et al., 2009; Ramachandran, 2010). While it has a low affinity for GTP, its hydrolysis rate is high, especially when stimulated. Dynamin has two important traits that are required for stimulated GTPase activity. It assembles into higher order oligomers (it naturally exists as a dimer or tetramer) and can bind membrane lipids (PIP<sub>2</sub>) via its pleckstrin homology (PH) domain (Chappie et al., 2010; Hinshaw, 2000; Marks et al., 2001; Mettlen et al., 2009; Ramachandran, 2010; Tuma and Collins, 1994; Tuma and Collins, 1995). When dynamin self assembles into a collar at the necks of coated vesicles, its GTPase activity is stimulated by both its GTPase and GTPase effector (GED) domains. This activity results in a conformational change promoting either membrane constriction or stretching leading to destabilization and ultimately membrane fission (Chappie et al., 2010; Hinshaw, 2000; Marks et al., 2001; Mettlen et al., 2009; Ramachandran, 2010). As dynamin-membrane association is required for

vesicle scission, the lack of dynamin recruitment in the presence of ethanol prevents the completion of clathrin-mediated internalization.

What causes the ethanol-induced defect in clathrin-mediated internalization and dynamin recruitment? Previously, we found that microtubule hyperacetylation induced by ethanol or by addition of a deacetylase inhibitor correlated with impaired clathrin-mediated endocytosis and secretion (Joseph et al., 2008). In addition, Part II of this dissertation established that ethanol also leads to the hyperacetylation of actin and cortactin. In Part III, we found that the ethanol-induced defect in clathrin internalization is mediated, in part, by altered dynamin function. From our morphological data, dynamin appears to be less tightly associated with the membrane. Since both cortactin and actin associate with dynamin and are thought to participate in late-stage vesicle fission, an exciting possibility is that the hyperacetylation of actin and cortactin prevent proper dynamin recruitment, thereby preventing vesicle internalization. To test this, we used TSA to induce hyperacetylation in the absence of ethanol. As for ethanol, TSA led to the redistribution of clathrin machinery, *but not dynamin*, and a similar block in late stage vesicle internalization. While TSA is a broad inhibitor of histone deacetylases and these results are not conclusive for actin and cortactin, it is clear that ethanol-induced protein hyperacetylation contributes to the observed defect in clathrin internalization. Further knowledge of the individual acetylated lysines in both actin and cortactin will allow for a more complete analysis and determination of the exact role that these two proteins play in the defect.

While the link between cortactin, actin and dynamin provide an exciting scenario

by which its recruitment is altered by ethanol, there are some other possibilities as well. Dynamin has the ability to bind to a multitude of other SRC homology 3 (SH3)-containing proteins via its proline-rich domain (PRD) and like cortactin, many of these interactors play a direct or indirect role in actin polymerization at sites of vesicle internalization. In fact, deletion of the PRD led to the mislocalization of dynamin, suggesting that its membrane binding domain (PH domain) is not sufficient and that these interactions with SH3-containing proteins are crucial to proper membrane localization (Klein et al., 1998; Lemmon and Ferguson, 2000). With this expanding list of dynamin interactors, the alteration of any one of these could also contribute to the ethanol-induced defect in dynamin recruitment (Kim and Chang, 2006). Of particular relevance to these studies, dynamin has recently been found to interact with several BAR- and F-BAR-containing proteins. Through the BAR domain, these proteins bind and tubulate membranes at sites of internalization. One of these proteins, sorting nexin 9 (SNX9) has been found in a complex with dynamin in the cytosol. Phosphorylation of SNX9 led to membrane recruitment of SNX9 and dynamin and increased actin polymerization. When SNX9 was knocked down, a decrease in dynamin recruitment and transferrin internalization was observed (Lundmark and Carlsson, 2002; Lundmark and Carlsson, 2003; Lundmark and Carlsson, 2004; Soulet et al., 2005). Like SNX9, members of the F-BAR proteins have also been linked to dynamin and actin polymerization at sites of membrane curvature (Itoh et al., 2005). In addition to the membrane curvature BAR domain, these proteins contain an FCH domain which is linked to actin nucleation through actin regulator proteins such as N-WASP. Actin polymerization appears to lie at

the heart of all of these dynamin interactors and determining the exact order and location of these interactions will help to elucidate the exact mechanism by which dynamin leads to membrane scission and may be altered by ethanol consumption.

Besides dynamin-protein interactions, membrane composition plays an important role in regulating dynamin function. Dynamin has been shown to interact with acidic phospholipids which promote its GTPase activity and any alteration of plasma membrane composition would likely alter dynamin recruitment (Burger et al., 2000; Tuma et al., 1993). Coincidentally, ethanol has been found to impair lipid synthesis and delivery as well as overall membrane composition (Carrasco et al., 1996; French, 1967; Kharbanda et al., 2007; Miceli and Ferrell, 1973; Polokoff et al., 1985; Seenaiiah et al., 1998). Specifically, studies have found that ethanol decreases the concentration of both phosphatidylcholine and phosphatidylserine on the plasma membrane (Kharbanda et al., 2007; Polokoff et al., 1985). As an acidic phospholipid, phosphatidylserine contributes to dynamin binding and function at the membrane and decreased amounts may help explain impaired dynamin recruitment. Phosphatidylcholine, a neutral phospholipid, can be converted to phosphatidic acid by phospholipase D. The presence of phosphatidic acid promotes membrane fission due to its small polar head which is stable in curved membranes (Roth, 2008). Both phospholipase D and phosphatidic acid have been shown to regulate clathrin endocytosis (Antonescu et al., 2010) and alterations in either (due to decreased phosphatidylcholine) may contribute to the observed ethanol-induced defect in clathrin internalization.

Impaired internalization may also be mediated by ethanol metabolism. Addition

of 4MP prevented the internalization of both ASGP-R and Tf-R in both HepG2 and WIF-B cells and in isolated rat hepatocytes (Beloqui et al., 1986; Clemens et al., 1996; Joseph et al., 2008). Furthermore, addition of acetaldehyde in the absence of ethanol caused similar impairments in hepatic protein trafficking (Volentine et al., 1987). These findings suggest that the generation of acetaldehyde and its adduction of proteins and lipids could be an underlying cause of the ethanol-induced defect in clathrin internalization. As for tubulin, it is possible that acetaldehyde production leads to the adduction of dynamin or one of its binding partners thereby preventing recruitment. Also possible is that the adduction and peroxidation of membrane lipids is preventing dynamin interaction. Acetaldehyde has been found to covalently modify phosphatidylethanolamine and phosphatidylserine (Kenney, 1982). Moreover, ethanol-induced reactive oxygen species induces membrane lipid peroxidation damaging the cell membrane (Wu and Cederbaum, 2003). Clearly the analysis of the role of ethanol metabolites on dynamin-membrane binding and clathrin internalization is needed to fully elucidate the mechanism by which dynamin is impaired.

### **Defects from the Golgi: is there is similar mechanism?**

In addition to the ethanol-induced defects in protein trafficking from the plasma membrane, ethanol also exerts its deleterious effects at the Golgi. Both the delivery of newly synthesized membrane glycoproteins and the secretion of albumin and other proteins are impaired in the presence of ethanol. Furthermore, studies using radiolabeling determined that these processes are blocked at the TGN leading to an accumulation of

proteins within this organelle. As for the defect in clathrin-mediated internalization from the plasma membrane, addition of acetaldehyde also impaired secretion and delivery from the Golgi suggesting a role for ethanol metabolism in this defect.

In general, proteins destined for either the secretory pathway or delivery and insertion into the basolateral plasma membrane encode a signal sequence that directs their docking and cotranslational entry into the ER. During transit through the ER, secretory proteins are step-wise glycosylated, properly folded and eventually packaged into coatamer II-coated vesicles for delivery to the *cis*-Golgi. Throughout the Golgi, the proteins are further modified (e.g., sulfation or phosphorylation) and their carbohydrates further trimmed and modified. In the TGN, the newly synthesized proteins are terminally glycosylated by the addition of N-acetylglucosamine, galactose, sialic acid and/or fucose moieties. While the mechanistic details regulating sorting at the TGN are not fully understood, these proteins are packaged into discrete vesicles, delivered to the basolateral surface and released (Saucan and Palade, 1994). In general, surface delivery is a microtubule-dependent process that is mediated by a host of other molecules (De Matteis and Luini, 2008; McNiven and Thompson, 2006; Ponnambalam and Baldwin, 2003; Rodriguez-Boulan and Musch, 2005).

As for the clathrin defect at the plasma membrane, a similar scenario may also evolve for proteins involved in vesicle budding and fission from the TGN. Basolateral resident proteins contain targeting information that likely promotes their recruitment into clathrin-coated vesicles at the TGN (Rodriguez-Boulan and Musch, 2005). These basolateral targeting signals are similar to the signals required for clathrin-internalization

and the majority are either tyrosine-based or contain a di-leucine motif (Rodriguez-Boulan and Musch, 2005). Thus, one exciting possibility is that a similar mechanism exists as described in Part III for the defect in vesicle budding and fission from the TGN. Although constitutive secretory proteins are thought to bud from the TGN in different vesicle populations than transmembrane proteins (Saucan and Palade, 1992), it is not yet clear what factors are required for their formation. Because constitutive secretion is also impaired in ethanol-treated hepatic cells, one possibility is that at least some components of the clathrin machinery are shared, and that these components are readily modified by reactive alcohol metabolites. Clearly, this is a fertile area of investigation for future research.

### **Ethanol-induced hyperacetylation – a new therapeutic approach:**

The work presented in this dissertation highlights the importance of protein acetylation as a regulator of cellular processes. Clearly protein hyperacetylation greatly changes cell dynamics leading to altered gene expression, protein trafficking and metabolic reactions. These observations are supported by work done with either HDAC knockdowns or small molecular HDAC inhibitors. As expected, HDAC inhibition leads to altered transcriptional activity of numerous transcription factors including p53 and p21, two important cell cycle regulators (Lane and Chabner, 2009). In general, HDAC inhibition leads to apoptosis likely through the stabilization of p53 that promotes cell cycle arrest and the expression of proapoptotic genes and death receptor ligands (Fas, tumor necrosis factor  $\alpha$  (TNF- $\alpha$ ) and TNF-related apoptosis-inducing ligand (TRAIL)

(Lane and Chabner, 2009). Studies have also found that HDAC inhibition blocked the intracellular stress response pathway and decreased chaperone-mediated protein folding due to heat shock protein 90 (HSP90) hyperacetylation (Lane and Chabner, 2009). Coincidentally, many of these physiological impairments have been observed in studies examining ethanol-mediated toxicity. Ethanol consumption leads to increased apoptosis in a Fas- and p53-dependent manner and induces ER stress strongly implicating lysine hyperacetylation as a contributor to alcoholic liver disease (Derdak et al., 2011; Esfandiari et al., 2010; McVicker et al., 2006).

HDAC inhibition is currently being investigated as a potential cancer therapeutic. Research has shown that cancer cells are more sensitive to HDAC inhibitors than healthy cells providing a possible targeted therapy (Lane and Chabner, 2009; Tan et al., 2010). Currently there are more than 80 class I and II HDAC inhibitors in clinical trials and almost all of them mediate their effects by promoting apoptosis and preventing angiogenesis (Lane and Chabner, 2009; Tan et al., 2010). In 2006, Vorinostat became the first (and only) HDAC inhibitor to be approved to treat human lymphoid cancers. This class I, II and IV inhibitor leads to significant histone hyperacetylation and increased expression of p21 and p53 and decreased STAT5 ultimately leading to cell cycle arrest and apoptosis (Lane and Chabner, 2009; Siegel et al., 2009).

While protein hyperacetylation may be a promising cancer therapeutic, patients with chronic liver diseases may benefit from reducing acetylation. The class III deacetylase, SirT1, has been implicated in multiple metabolic pathways ranging from insulin secretion to  $\beta$ -oxidation providing strong evidence that agonists may be useful in

treating various metabolic diseases (Jiang, 2008; Lomb et al., 2010; Milne and Denu, 2008; Milne et al., 2007). One such agonist is resveratrol (*trans*-3,5,4'-trihydroxystilbene), a naturally occurring polyphenol found in a variety of plants and red wine. Recent studies have found that resveratrol and more potent synthetic sirtuin activators such as SRT-501, SRT1460, SRT1720 and SRT2183 are well-tolerated in humans and are currently in clinical trials for treatment of type 2 diabetes and other metabolic diseases (Jiang, 2008; Lomb et al., 2010; Milne and Denu, 2008; Milne et al., 2007; Wood et al., 2004).

Of great interest to the study of alcohol-induced toxicity, preliminary evidence suggests that resveratrol is hepatoprotective against alcohol (Ajmo et al., 2008; Bujanda et al., 2006; Kasdallah-Grissa et al., 2007; Kasdallah-Grissa et al., 2006). When mice and rats are fed resveratrol with alcohol both oxidative damage and fatty liver are prevented. Livers from mice fed a chronic ethanol diet supplemented with resveratrol for the last 2 weeks did not exhibit any lipid droplet accumulation and were protected against oxidative stress (Ajmo et al., 2008). These physiological findings correlated with increased SirT1 protein levels and reduced PGC-1 $\alpha$  acetylation. Examination of the specific lipid metabolism pathways revealed that resveratrol suppressed the expression of SREBP-1c-regulated lipogenic enzymes and increased expression of those involved in  $\beta$ -oxidation thereby leading to decreased fatty acid accumulation (Ajmo et al., 2008). From this study, we can conclude that ethanol-induced protein hyperacetylation correlates with the clinically observed progression of alcoholic liver disease and the manipulation of the modifying enzymes provides a promising therapy.

## REFERENCES

- Ajmo, J.M., X. Liang, C.Q. Rogers, B. Pennock, and M. You. 2008. Resveratrol Alleviates Alcoholic Fatty Liver in Mice. *Am J Physiol Gastrointest Liver Physiol*.
- Alberts, B., A. Johnson, J. Lewis, M. Raff, K. Roberts, and P. Walter. 2002. *Molecular Biology of the Cell*. Garland Science, New York, NY.
- Antonescu, C.N., G. Danuser, and S.L. Schmid. 2010. Phosphatidic acid plays a regulatory role in clathrin-mediated endocytosis. *Mol Biol Cell*. 21:2944-52.
- Apodaca, G. 2001. Endocytic traffic in polarized epithelial cells: role of the actin and microtubule cytoskeleton. *Traffic*. 2:149-59.
- Bailey, S.M., V.B. Patel, T.A. Young, K. Asayama, and C.C. Cunningham. 2001. Chronic ethanol consumption alters the glutathione/glutathione peroxidase-1 system and protein oxidation status in rat liver. *Alcohol Clin Exp Res*. 25:726-33.
- Bardag-Gorce, F., B.A. French, M. Joyce, M. Baires, R.O. Montgomery, J. Li, and S. French. 2007. Histone acetyltransferase p300 modulates gene expression in an epigenetic manner at high blood alcohol levels. *Exp Mol Pathol*. 82:197-202.
- Bardag-Gorce, F., B.A. French, L. Nan, H. Song, S.K. Nguyen, H. Yong, J. Dede, and S.W. French. 2006. CYP2E1 induced by ethanol causes oxidative stress, proteasome inhibition and cytokeratin aggresome (Mallory body-like) formation. *Exp Mol Pathol*. 81:191-201.
- Bastaki, M., L.T. Braiterman, D.C. Johns, Y.H. Chen, and A.L. Hubbard. 2002. Absence of direct delivery for single transmembrane apical proteins or their "Secretory" forms in polarized hepatic cells. *Mol Biol Cell*. 13:225-37.
- Bataller, R., and D.A. Brenner. 2005. Liver fibrosis. *J Clin Invest*. 115:209-18.
- Beloqui, O., R.M. Nunes, B. Blades, P.D. Berk, and B.J. Potter. 1986. Depression of iron uptake from transferrin by isolated hepatocytes in the presence of ethanol is a pH-dependent consequence of ethanol metabolism. *Alcohol Clin Exp Res*. 10:463-70.
- Bertos, N.R., A.H. Wang, and X.J. Yang. 2001. Class II histone deacetylases: structure, function, and regulation. *Biochem Cell Biol*. 79:243-52.
- Bouras, T., M. Fu, A.A. Sauve, F. Wang, A.A. Quong, N.D. Perkins, R.T. Hay, W. Gu, and R.G. Pestell. 2005. SIRT1 deacetylation and repression of p300 involves lysine residues 1020/1024 within the cell cycle regulatory domain 1. *J Biol Chem*. 280:10264-76.

- Braet, F., D. Luo, I. Spector, D. Vermijlen, and E. Wisse. 2001. Endothelial and Pit Cells. *In The Liver: biology and pathobiology*. I.M. Arias, J.L. Boyer, F.V. Chisari, N. Fausto, D. Schachter, and D.A. Shafritz, editors. Lippincott Williams & Wilkins, Philadelphia.
- Bretscher, A. 1991. Microfilament structure and function in the cortical cytoskeleton. *Annu Rev Cell Biol*. 7:337-74.
- Brooks, P.J. 1997. DNA damage, DNA repair, and alcohol toxicity--a review. *Alcohol Clin Exp Res*. 21:1073-82.
- Bujanda, L., M. Garcia-Barcina, V. Gutierrez-de Juan, J. Bidaurrazaga, M.F. de Luco, M. Gutierrez-Stampa, M. Larzabal, E. Hijona, C. Sarasqueta, M. Echenique-Elizondo, and J.I. Arenas. 2006. Effect of resveratrol on alcohol-induced mortality and liver lesions in mice. *BMC Gastroenterol*. 6:35.
- Burger, K.N., R.A. Demel, S.L. Schmid, and B. de Kruijff. 2000. Dynamin is membrane-active: lipid insertion is induced by phosphoinositides and phosphatidic acid. *Biochemistry*. 39:12485-93.
- Cao, H., J.D. Orth, J. Chen, S.G. Weller, J.E. Heuser, and M.A. McNiven. 2003. Cortactin is a component of clathrin-coated pits and participates in receptor-mediated endocytosis. *Mol Cell Biol*. 23:2162-70.
- Cao, H., S. Weller, J.D. Orth, J. Chen, B. Huang, J.L. Chen, M. Starnes, and M.A. McNiven. 2005. Actin and Arp1-dependent recruitment of a cortactin-dynamin complex to the Golgi regulates post-Golgi transport. *Nat Cell Biol*. 7:483-92.
- Carpentier, J.L., F. Sawano, D. Geiger, P. Gorden, A. Perrelet, and L. Orci. 1989. Potassium depletion and hypertonic medium reduce "non-coated" and clathrin-coated pit formation, as well as endocytosis through these two gates. *J Cell Physiol*. 138:519-26.
- Carrasco, M.P., M.C. Sanchez-Amate, C. Marco, and J.L. Segovia. 1996. Evidence of differential effects produced by ethanol on specific phospholipid biosynthetic pathways in rat hepatocytes. *Br J Pharmacol*. 119:233-8.
- Chappie, J.S., S. Acharya, M. Leonard, S.L. Schmid, and F. Dyda. 2010. G domain dimerization controls dynamin's assembly-stimulated GTPase activity. *Nature*. 465:435-40.
- Choudhury, M., and S.D. Shukla. 2008. Surrogate alcohols and their metabolites modify histone H3 acetylation: involvement of histone acetyl transferase and histone deacetylase. *Alcohol Clin Exp Res*. 32:829-39.

- Clayton, A.L., C.A. Hazzalin, and L.C. Mahadevan. 2006. Enhanced histone acetylation and transcription: a dynamic perspective. *Mol Cell*. 23:289-96.
- Clemens, D.L., C.M. Halgard, J.R. Cole, R.M. Miles, M.F. Sorrell, and D.J. Tuma. 1996. Impairment of the asialoglycoprotein receptor by ethanol oxidation. *Biochem Pharmacol*. 52:1499-505.
- Clemens, D.L., C.M. Halgard, R.R. Miles, M.F. Sorrell, and D.J. Tuma. 1995. Establishment of a recombinant hepatic cell line stably expressing alcohol dehydrogenase. *Arch Biochem Biophys*. 321:311-8.
- Conner, S.D., and S.L. Schmid. 2003. Regulated portals of entry into the cell. *Nature*. 422:37-44.
- De Matteis, M.A., and A. Luini. 2008. Exiting the Golgi complex. *Nat Rev Mol Cell Biol*. 9:273-84.
- Derdak, Z., C.H. Lang, K.A. Villegas, M. Tong, N.M. Mark, S.M. de la Monte, and J.R. Wands. 2011. Activation of p53 enhances apoptosis and insulin resistance in a rat model of alcoholic liver disease. *J Hepatol*. 54:164-72.
- Desmet, L.J. 2001. Organizational principles. In *The Liver: biology and pathobiology*. I.M. Arias, J.L. Boyer, F.V. Chisari, N. Fausto, D. Schachter, and D.A. Shafritz, editors. Lippincott Williams & Wilkins, Philadelphia.
- Doherty, G.J., and H.T. McMahon. 2009. Mechanisms of Endocytosis. *Annu Rev Biochem*.
- Donohue, T.M., Jr. 2007. Alcohol-induced steatosis in liver cells. *World J Gastroenterol*. 13:4974-8.
- Eberharter, A., and P.B. Becker. 2002. Histone acetylation: a switch between repressive and permissive chromatin. Second in review series on chromatin dynamics. *EMBO Rep*. 3:224-9.
- Esfandiari, F., V. Medici, D.H. Wong, S. Jose, M. Dolatshahi, E. Quinlivan, S. Dayal, S.R. Lentz, H. Tsukamoto, Y.H. Zhang, S.W. French, and C.H. Halsted. 2010. Epigenetic regulation of hepatic endoplasmic reticulum stress pathways in the ethanol-fed cystathionine beta synthase-deficient mouse. *Hepatology*. 51:932-41.
- Farbiszewski, R., M. Chwiecko, A. Holownia, and D. Pawlowska. 1991. The decrease of superoxide dismutase activity and depletion of sulfhydryl compounds in ethanol-induced liver injury. *Drug Alcohol Depend*. 28:291-4.

- Fath, K.R., S.N. Mamajiwalla, and D.R. Burgess. 1993. The cytoskeleton in development of epithelial cell polarity. *J Cell Sci Suppl.* 17:65-73.
- Fernandez, D.J., B.L. McVicker, D.J. Tuma, and P.L. Tuma. 2009. Ethanol selectively impairs clathrin-mediated internalization in polarized hepatic cells. *Biochem Pharmacol.* 78:648-55.
- French, S.W. 1967. Effect of chronic ethanol feeding on rat liver phospholipid. *J Nutr.* 91:292-8.
- Giandomenico, V., M. Simonsson, E. Gronroos, and J. Ericsson. 2003. Coactivator-dependent acetylation stabilizes members of the SREBP family of transcription factors. *Mol Cell Biol.* 23:2587-99.
- Glozak, M.A., N. Sengupta, X. Zhang, and E. Seto. 2005. Acetylation and deacetylation of non-histone proteins. *Gene.* 363:15-23.
- Grozinger, C.M., C.A. Hassig, and S.L. Schreiber. 1999. Three proteins define a class of human histone deacetylases related to yeast Hda1p. *Proc Natl Acad Sci U S A.* 96:4868-73.
- Heuser, J.E., and R.G. Anderson. 1989. Hypertonic media inhibit receptor-mediated endocytosis by blocking clathrin-coated pit formation. *J Cell Biol.* 108:389-400.
- Hildmann, C., D. Riester, and A. Schwienhorst. 2007. Histone deacetylases--an important class of cellular regulators with a variety of functions. *Appl Microbiol Biotechnol.* 75:487-97.
- Hinshaw, J.E. 2000. Dynamin and its role in membrane fission. *Annu Rev Cell Dev Biol.* 16:483-519.
- Hubbert, C., A. Guardiola, R. Shao, Y. Kawaguchi, A. Ito, A. Nixon, M. Yoshida, X.F. Wang, and T.P. Yao. 2002. HDAC6 is a microtubule-associated deacetylase. *Nature.* 417:455-8.
- Ihrke, G., G.V. Martin, M.R. Shanks, M. Schrader, T.A. Schroer, and A.L. Hubbard. 1998. Apical plasma membrane proteins and endolyn-78 travel through a subapical compartment in polarized WIF-B hepatocytes. *J Cell Biol.* 141:115-33.
- Ihrke, G., E.B. Neufeld, T. Meads, M.R. Shanks, D. Cassio, M. Laurent, T.A. Schroer, R.E. Pagano, and A.L. Hubbard. 1993. WIF-B cells: an in vitro model for studies of hepatocyte polarity. *J Cell Biol.* 123:1761-75.

- Itoh, T., K.S. Erdmann, A. Roux, B. Habermann, H. Werner, and P. De Camilli. 2005. Dynamin and the actin cytoskeleton cooperatively regulate plasma membrane invagination by BAR and F-BAR proteins. *Dev Cell*. 9:791-804.
- Jennett, R.B., M.F. Sorrell, E.L. Johnson, and D.J. Tuma. 1987. Covalent binding of acetaldehyde to tubulin: evidence for preferential binding to the alpha-chain. *Arch Biochem Biophys*. 256:10-8.
- Jennett, R.B., M.F. Sorrell, A. Saffari-Fard, J.L. Ockner, and D.J. Tuma. 1989. Preferential covalent binding of acetaldehyde to the alpha-chain of purified rat liver tubulin. *Hepatology*. 9:57-62.
- Jennett, R.B., D.J. Tuma, and M.F. Sorrell. 1980. Effect of ethanol and its metabolites on microtubule formation. *Pharmacology*. 21:363-8.
- Jiang, W.J. 2008. Sirtuins: novel targets for metabolic disease in drug development. *Biochem Biophys Res Commun*. 373:341-4.
- Joseph, R.A., B.D. Shepard, G.T. Kannarkat, T.M. Rutledge, D.J. Tuma, and P.L. Tuma. 2008. Microtubule acetylation and stability may explain alcohol-induced alterations in hepatic protein trafficking. *Hepatology*. 47:1745-53.
- Kannarkat, G.T., D.J. Tuma, and P.L. Tuma. 2006. Microtubules are more stable and more highly acetylated in ethanol-treated hepatic cells. *J Hepatol*. 44:963-70.
- Kasdallah-Grissa, A., B. Mornagui, E. Aouani, M. Hammami, M. El May, N. Gharbi, A. Kamoun, and S. El-Fazaa. 2007. Resveratrol, a red wine polyphenol, attenuates ethanol-induced oxidative stress in rat liver. *Life Sci*. 80:1033-9.
- Kasdallah-Grissa, A., B. Mornagui, E. Aouani, M. Hammami, N. Gharbi, A. Kamoun, and S. El-Fazaa. 2006. Protective effect of resveratrol on ethanol-induced lipid peroxidation in rats. *Alcohol Alcohol*. 41:236-9.
- Kawaguchi, Y., J.J. Kovacs, A. McLaurin, J.M. Vance, A. Ito, and T.P. Yao. 2003. The deacetylase HDAC6 regulates aggresome formation and cell viability in response to misfolded protein stress. *Cell*. 115:727-38.
- Kendrick, A.A., M. Choudhury, S.M. Rahman, C.E. McCurdy, M. Friederich, J.L. Vanhove, P.A. Watson, N. Birdsey, J. Bao, D. Gius, M.N. Sack, E. Jing, C.R. Kahn, J.E. Friedman, and K.R. Jonscher. Fatty liver is associated with reduced SIRT3 activity and mitochondrial protein hyperacetylation. *Biochem J*.
- Kenney, W.C. 1982. Acetaldehyde adducts of phospholipids. *Alcohol Clin Exp Res*. 6:412-6.

- Kharbanda, K.K., M.E. Mailliard, C.R. Baldwin, H.C. Beckenhauer, M.F. Sorrell, and D.J. Tuma. 2007. Betaine attenuates alcoholic steatosis by restoring phosphatidylcholine generation via the phosphatidylethanolamine methyltransferase pathway. *J Hepatol.* 46:314-21.
- Kim, J.S., and S.D. Shukla. 2005. Histone h3 modifications in rat hepatic stellate cells by ethanol. *Alcohol Alcohol.* 40:367-72.
- Kim, J.S., and S.D. Shukla. 2006. Acute in vivo effect of ethanol (binge drinking) on histone H3 modifications in rat tissues. *Alcohol Alcohol.* 41:126-32.
- Kim, S.C., R. Sprung, Y. Chen, Y. Xu, H. Ball, J. Pei, T. Cheng, Y. Kho, H. Xiao, L. Xiao, N.V. Grishin, M. White, X.J. Yang, and Y. Zhao. 2006. Substrate and functional diversity of lysine acetylation revealed by a proteomics survey. *Mol Cell.* 23:607-18.
- Kim, Y., and S. Chang. 2006. Ever-expanding network of dynamin-interacting proteins. *Mol Neurobiol.* 34:129-36.
- Klassen, L.W., G.M. Thiele, M.J. Duryee, C.S. Schaffert, A.L. DeVeney, C.D. Hunter, P. Olinga, and D.J. Tuma. 2008. An in vitro method of alcoholic liver injury using precision-cut liver slices from rats. *Biochem Pharmacol.* 76:426-36.
- Klein, D.E., A. Lee, D.W. Frank, M.S. Marks, and M.A. Lemmon. 1998. The pleckstrin homology domains of dynamin isoforms require oligomerization for high affinity phosphoinositide binding. *J Biol Chem.* 273:27725-33.
- Kopito, R.R. 2000. Aggresomes, inclusion bodies and protein aggregation. *Trends Cell Biol.* 10:524-30.
- Kouzarides, T. 2000. Acetylation: a regulatory modification to rival phosphorylation? *Embo J.* 19:1176-9.
- Ku, N.O., P. Strnad, B.H. Zhong, G.Z. Tao, and M.B. Omary. 2007. Keratins let liver live: Mutations predispose to liver disease and crosslinking generates Mallory-Denk bodies. *Hepatology.* 46:1639-49.
- Laemmli, U.K. 1970. Cleavage of structural proteins during the assembly of the head of bacteriophage T4. *Nature.* 227:680-5.
- Lane, A.A., and B.A. Chabner. 2009. Histone deacetylase inhibitors in cancer therapy. *J Clin Oncol.* 27:5459-68.

- Larkin, J.M., M.S. Brown, J.L. Goldstein, and R.G. Anderson. 1983. Depletion of intracellular potassium arrests coated pit formation and receptor-mediated endocytosis in fibroblasts. *Cell*. 33:273-85.
- Larkin, J.M., W.C. Donzell, and R.G. Anderson. 1985. Modulation of intracellular potassium and ATP: effects on coated pit function in fibroblasts and hepatocytes. *J Cell Physiol*. 124:372-8.
- Larkin, J.M., W.C. Donzell, and R.G. Anderson. 1986. Potassium-dependent assembly of coated pits: new coated pits form as planar clathrin lattices. *J Cell Biol*. 103:2619-27.
- Lee, J.Y., H. Koga, Y. Kawaguchi, W. Tang, E. Wong, Y.S. Gao, U.B. Pandey, S. Kaushik, E. Tresse, J. Lu, J.P. Taylor, A.M. Cuervo, and T.P. Yao. 2010. HDAC6 controls autophagosome maturation essential for ubiquitin-selective quality-control autophagy. *EMBO J*. 29:969-80.
- Lee, J.Y., and T.P. Yao. 2010. Quality control autophagy: A joint effort of ubiquitin, protein deacetylase and actin cytoskeleton. *Autophagy*. 6.
- Lee, Y.J., and S.D. Shukla. 2007. Histone H3 phosphorylation at serine 10 and serine 28 is mediated by p38 MAPK in rat hepatocytes exposed to ethanol and acetaldehyde. *Eur J Pharmacol*. 573:29-38.
- Lemmon, M.A., and K.M. Ferguson. 2000. Signal-dependent membrane targeting by pleckstrin homology (PH) domains. *Biochem J*. 350 Pt 1:1-18.
- Li, D., and S.L. Friedman. 2001. Hepatic stellate cells: morphology, function, and regulation. *In The Liver: biology and pathobiology*. I.M. Arias, J.L. Boyer, F.V. Chisari, N. Fausto, D. Schachter, and D.A. Shafritz, editors. Lippincott Williams & Wilkins, Philadelphia.
- Li, W., B. Zhang, J. Tang, Q. Cao, Y. Wu, C. Wu, J. Guo, E.A. Ling, and F. Liang. 2007. Sirtuin 2, a mammalian homolog of yeast silent information regulator-2 longevity regulator, is an oligodendroglial protein that decelerates cell differentiation through deacetylating alpha-tubulin. *J Neurosci*. 27:2606-16.
- Lieber, C.S., and L.M. DeCarli. 1989. Liquid diet technique of ethanol administration: 1989 update. *Alcohol Alcohol*. 24:197-211.
- Lieber, C.S., M.A. Leo, X. Wang, and L.M. Decarli. 2008. Effect of chronic alcohol consumption on Hepatic SIRT1 and PGC-1alpha in rats. *Biochem Biophys Res Commun*. 370:44-8.

- Lomb, D.J., G. Laurent, and M.C. Haigis. 2010. Sirtuins regulate key aspects of lipid metabolism. *Biochim Biophys Acta*. 1804:1652-7.
- Lundmark, R., and S.R. Carlsson. 2002. The beta-appendages of the four adaptor-protein (AP) complexes: structure and binding properties, and identification of sorting nexin 9 as an accessory protein to AP-2. *Biochem J*. 362:597-607.
- Lundmark, R., and S.R. Carlsson. 2003. Sorting nexin 9 participates in clathrin-mediated endocytosis through interactions with the core components. *J Biol Chem*. 278:46772-81.
- Lundmark, R., and S.R. Carlsson. 2004. Regulated membrane recruitment of dynamin-2 mediated by sorting nexin 9. *J Biol Chem*. 279:42694-702.
- Mari, M., and A.I. Cederbaum. 2000. CYP2E1 overexpression in HepG2 cells induces glutathione synthesis by transcriptional activation of gamma-glutamylcysteine synthetase. *J Biol Chem*. 275:15563-71.
- Marks, B., M.H. Stowell, Y. Vallis, I.G. Mills, A. Gibson, C.R. Hopkins, and H.T. McMahon. 2001. GTPase activity of dynamin and resulting conformation change are essential for endocytosis. *Nature*. 410:231-5.
- Matsuyama, A., T. Shimazu, Y. Sumida, A. Saito, Y. Yoshimatsu, D. Seigneurin-Berny, H. Osada, Y. Komatsu, N. Nishino, S. Khochbin, S. Horinouchi, and M. Yoshida. 2002. In vivo destabilization of dynamic microtubules by HDAC6-mediated deacetylation. *Embo J*. 21:6820-31.
- Mayor, S., and R.E. Pagano. 2007. Pathways of clathrin-independent endocytosis. *Nat Rev Mol Cell Biol*. 8:603-12.
- Mays, R.W., K.A. Beck, and W.J. Nelson. 1994. Organization and function of the cytoskeleton in polarized epithelial cells: a component of the protein sorting machinery. *Curr Opin Cell Biol*. 6:16-24.
- McNiven, M.A., and H.M. Thompson. 2006. Vesicle formation at the plasma membrane and trans-Golgi network: the same but different. *Science*. 313:1591-4.
- McVicker, B.L., and C.A. Casey. 1999. Effects of ethanol on receptor-mediated endocytosis in the liver. *Alcohol*. 19:255-60.
- McVicker, B.L., D.J. Tuma, J.L. Kubik, P.L. Tuma, and C.A. Casey. 2006. Ethanol-induced apoptosis in polarized hepatic cells possibly through regulation of the Fas pathway. *Alcohol Clin Exp Res*. 30:1906-15.

- McVicker, B.L., P.L. Tuma, K.K. Kharbanda, S.M.L. Lee, D.J. Tuma. 2009. Relationship between oxidative stress and hepatic glutathione levels in ethanol-mediated apoptosis of polarized hepatic cells. *World J Gastroenterol.* 15:2609-2616.
- Meads, T., and T.A. Schroer. 1995. Polarity and nucleation of microtubules in polarized epithelial cells. *Cell Motil Cytoskeleton.* 32:273-88.
- Mellor, J. 2006. Dynamic nucleosomes and gene transcription. *Trends Genet.* 22:320-9.
- Mettlen, M., T. Pucadyil, R. Ramachandran, and S.L. Schmid. 2009. Dissecting dynamin's role in clathrin-mediated endocytosis. *Biochem Soc Trans.* 37:1022-6.
- Miceli, J.N., and W.J. Ferrell. 1973. Effects of ethanol on membrane lipids 3. Quantitative changes in lipid and fatty acid composition of nonpolar and polar lipids of mouse total liver, mitochondria and microsomes following ethanol feeding. *Lipids.* 8:722-7.
- Milne, J.C., and J.M. Denu. 2008. The Sirtuin family: therapeutic targets to treat diseases of aging. *Curr Opin Chem Biol.* 12:11-7.
- Milne, J.C., P.D. Lambert, S. Schenk, D.P. Carney, J.J. Smith, D.J. Gagne, L. Jin, O. Boss, R.B. Perni, C.B. Vu, J.E. Bemis, R. Xie, J.S. Disch, P.Y. Ng, J.J. Nunes, A.V. Lynch, H. Yang, H. Galonek, K. Israelian, W. Choy, A. Iffland, S. Lavu, O. Medvedik, D.A. Sinclair, J.M. Olefsky, M.R. Jirousek, P.J. Elliott, and C.H. Westphal. 2007. Small molecule activators of SIRT1 as therapeutics for the treatment of type 2 diabetes. *Nature.* 450:712-6.
- Naito, M., G. Hasegawa, Y. Ebe, and T. Yamamoto. 2004. Differentiation and function of Kupffer cells. *Med Electron Microsc.* 37:16-28.
- North, B.J., B.L. Marshall, M.T. Borra, J.M. Denu, and E. Verdin. 2003. The human Sir2 ortholog, SIRT2, is an NAD<sup>+</sup>-dependent tubulin deacetylase. *Mol Cell.* 11:437-44.
- O'Farrell, P.H. 1975. High resolution two-dimensional electrophoresis of proteins. *J Biol Chem.* 250:4007-21.
- O'Shea, R.S., S. Dasarathy, and A.J. McCullough. Alcoholic liver disease. *Hepatology.* 51:307-28.
- Oh, S.I., C.I. Kim, H.J. Chun, and S.C. Park. 1998. Chronic ethanol consumption affects glutathione status in rat liver. *J Nutr.* 128:758-63.

- Omary, M.B., N.O. Ku, P. Strnad, and S. Hanada. 2009. Toward unraveling the complexity of simple epithelial keratins in human disease. *J Clin Invest.* 119:1794-805.
- Oriolo, A.S., F.A. Wald, V.P. Ramsauer, and P.J. Salas. 2007. Intermediate filaments: a role in epithelial polarity. *Exp Cell Res.* 313:2255-64.
- Osna, N.A., and T.M. Donohue, Jr. 2007. Implication of altered proteasome function in alcoholic liver injury. *World J Gastroenterol.* 13:4931-7.
- Pal-Bhadra, M., U. Bhadra, D.E. Jackson, L. Mamatha, P.H. Park, and S.D. Shukla. 2007. Distinct methylation patterns in histone H3 at Lys-4 and Lys-9 correlate with up- & down-regulation of genes by ethanol in hepatocytes. *Life Sci.* 81:979-87.
- Park, P.H., R.W. Lim, and S.D. Shukla. 2005. Involvement of histone acetyltransferase (HAT) in ethanol-induced acetylation of histone H3 in hepatocytes: potential mechanism for gene expression. *Am J Physiol Gastrointest Liver Physiol.* 289:G1124-36.
- Park, P.H., R. Miller, and S.D. Shukla. 2003. Acetylation of histone H3 at lysine 9 by ethanol in rat hepatocytes. *Biochem Biophys Res Commun.* 306:501-4.
- Perez, M.J., and A.I. Cederbaum. 2003. Proteasome inhibition potentiates CYP2E1-mediated toxicity in HepG2 cells. *Hepatology.* 37:1395-404.
- Picklo, M.J., Sr. 2008. Ethanol intoxication increases hepatic N-lysyl protein acetylation. *Biochem Biophys Res Commun.*
- Polevoda, B., and F. Sherman. 2002. The diversity of acetylated proteins. *Genome Biol.* 3:reviews0006.
- Polokoff, M.A., T.J. Simon, R.A. Harris, F.R. Simon, and M. Iwahashi. 1985. Chronic ethanol increases liver plasma membrane fluidity. *Biochemistry.* 24:3114-20.
- Ponnambalam, S., and S.A. Baldwin. 2003. Constitutive protein secretion from the trans-Golgi network to the plasma membrane. *Mol Membr Biol.* 20:129-39.
- Ramachandran, R. 2010. Vesicle scission: Dynamin. *Semin Cell Dev Biol.*
- Rodgers, J.T., C. Lerin, Z. Gerhart-Hines, and P. Puigserver. 2008. Metabolic adaptations through the PGC-1 alpha and SIRT1 pathways. *FEBS Lett.* 582:46-53.
- Rodriguez-Boulan, E., and A. Musch. 2005. Protein sorting in the Golgi complex: shifting paradigms. *Biochim Biophys Acta.* 1744:455-64.

- Roth, M.G. 2008. Molecular mechanisms of PLD function in membrane traffic. *Traffic*. 9:1233-9.
- Saucan, L., and G.E. Palade. 1992. Differential colchicine effects on the transport of membrane and secretory proteins in rat hepatocytes in vivo: bipolar secretion of albumin. *Hepatology*. 15:714-21.
- Saucan, L., and G.E. Palade. 1994. Membrane and secretory proteins are transported from the Golgi complex to the sinusoidal plasmalemma of hepatocytes by distinct vesicular carriers. *J Cell Biol*. 125:733-41.
- Schachter, D. 2001. The hepatocyte plasma membrane: organization, differentiation, biogenesis, and turnover. *In The Liver: biology and pathobiology*. I.M. Arias, J.L. Boyer, F.V. Chisari, N. Fausto, D. Schachter, and D.A. Shafritz, editors. Lippincott Williams & Wilkins, Philadelphia.
- Schaffert, C.S., S.L. Toderò, B.L. McVicker, P.L. Tuma, M.F. Sorrell, and D.J. Tuma. 2004. WIF-B cells as a model for alcohol-induced hepatocyte injury. *Biochem Pharmacol*. 67:2167-74.
- Schwer, B., J. Bunkenborg, R.O. Verdin, J.S. Andersen, and E. Verdin. 2006. Reversible lysine acetylation controls the activity of the mitochondrial enzyme acetyl-CoA synthetase 2. *Proc Natl Acad Sci U S A*. 103:10224-9.
- Seenaiah, B., E. Bichenkov, and J.S. Ellingson. 1998. The effects of chronic ethanol consumption on the formation of phosphatidylethanolamine molecular species and their appearance at the plasma membrane. *Alcohol Clin Exp Res*. 22:1245-54.
- Shanks, M.R., D. Cassio, O. Lecoq, and A.L. Hubbard. 1994. An improved polarized rat hepatoma hybrid cell line. Generation and comparison with its hepatoma relatives and hepatocytes in vivo. *J Cell Sci*. 107 ( Pt 4):813-25.
- Shepard, B.D., D.J. Fernandez, and P.L. Tuma. 2009a. Alcohol consumption impairs hepatic protein trafficking: mechanisms and consequences. *Genes Nutr*.
- Shepard, B.D., R.A. Joseph, G.T. Kannarkat, T.M. Rutledge, D.J. Tuma, and P.L. Tuma. 2008. Alcohol-induced alterations in hepatic microtubule dynamics can be explained by impaired histone deacetylase 6 function. *Hepatology*.
- Shepard, B.D., D.J. Tuma, and P.L. Tuma. 2009b. Chronic Ethanol Consumption Induces Global Hepatic Protein Hyperacetylation. *Alcohol Clin Exp Res*.
- Shepard, B.D., and P.L. Tuma. 2009. Alcohol-induced protein hyperacetylation: mechanisms and consequences. *World J Gastroenterol*. 15:1219-30.

- Siegel, D., M. Hussein, C. Belani, F. Robert, E. Galanis, V.M. Richon, J. Garcia-Vargas, C. Sanz-Rodriguez, and S. Rizvi. 2009. Vorinostat in solid and hematologic malignancies. *J Hematol Oncol.* 2:31.
- Smith, S.L., R.B. Jennett, M.F. Sorrell, and D.J. Tuma. 1992. Substoichiometric inhibition of microtubule formation by acetaldehyde-tubulin adducts. *Biochem Pharmacol.* 44:65-72.
- Sorrell, M.F., D.J. Tuma, E.C. Schafer, and A.J. Barak. 1977. Role of acetaldehyde in the ethanol-induced impairment of glycoprotein metabolism in rat liver slices. *Gastroenterology.* 73:137-44.
- Soulet, F., D. Yarar, M. Leonard, and S.L. Schmid. 2005. SNX9 regulates dynamin assembly and is required for efficient clathrin-mediated endocytosis. *Mol Biol Cell.* 16:2058-67.
- Strnad, P., C. Stumptner, K. Zatloukal, and H. Denk. 2008a. Intermediate filament cytoskeleton of the liver in health and disease. *Histochem Cell Biol.* 129:735-49.
- Strnad, P., K. Zatloukal, C. Stumptner, H. Kulaksiz, and H. Denk. 2008b. Mallory-Denk-bodies: lessons from keratin-containing hepatic inclusion bodies. *Biochim Biophys Acta.* 1782:764-74.
- Tan, J., S. Cang, Y. Ma, R.L. Petrillo, and D. Liu. 2010. Novel histone deacetylase inhibitors in clinical trials as anti-cancer agents. *J Hematol Oncol.* 3:5.
- Tang, B.L., and C.E. Chua. 2008. SIRT2, tubulin deacetylation, and oligodendroglia differentiation. *Cell Motil Cytoskeleton.* 65:179-82.
- Tuma, D.J., and C.A. Casey. 2003. Dangerous byproducts of alcohol breakdown--focus on adducts. *Alcohol Res Health.* 27:285-90.
- Tuma, D.J., C.A. Casey, and M.F. Sorrell. 1990. Effects of ethanol on hepatic protein trafficking: impairment of receptor-mediated endocytosis. *Alcohol Alcohol.* 25:117-25.
- Tuma, D.J., C.A. Casey, and M.F. Sorrell. 1991a. Effects of alcohol on hepatic protein metabolism and trafficking. *Alcohol Alcohol Suppl.* 1:297-303.
- Tuma, D.J., M.R. Newman, T.M. Donohue, Jr., and M.F. Sorrell. 1987. Covalent binding of acetaldehyde to proteins: participation of lysine residues. *Alcohol Clin Exp Res.* 11:579-84.
- Tuma, D.J., S.L. Smith, and M.F. Sorrell. 1991b. Acetaldehyde and microtubules. *Ann N Y Acad Sci.* 625:786-92.

- Tuma, D.J., and M.F. Sorrell. 1988. Effects of ethanol on protein trafficking in the liver. *Semin Liver Dis.* 8:69-80.
- Tuma, P.L., and C.A. Collins. 1994. Activation of dynamin GTPase is a result of positive cooperativity. *J Biol Chem.* 269:30842-7.
- Tuma, P.L., and C.A. Collins. 1995. Dynamin forms polymeric complexes in the presence of lipid vesicles. Characterization of chemically cross-linked dynamin molecules. *J Biol Chem.* 270:26707-14.
- Tuma, P.L., and A.L. Hubbard. 2001. The hepatocyte surface: dynamic polarity. *In The Liver: biology and pathobiology.* I.M. Arias, J.L. Boyer, F.V. Chisari, N. Fausto, D. Schachter, and D.A. Shafritz, editors. Lippincott Williams & Wilkins, Philadelphia.
- Tuma, P.L., M.C. Stachniak, and C.A. Collins. 1993. Activation of dynamin GTPase by acidic phospholipids and endogenous rat brain vesicles. *J Biol Chem.* 268:17240-6.
- Ujhazy, P., H. Kipp, S. Misra, Y. Wakabayashi, and I.M. Arias. 2001. The biology of the bile canaliculus. *In The Liver: biology and pathobiology.* I.M. Arias, J.L. Boyer, F.V. Chisari, N. Fausto, D. Schachter, and D.A. Shafritz, editors. Lippincott Williams & Wilkins, Philadelphia.
- Verdel, A., S. Curtet, M.P. Brocard, S. Rousseaux, C. Lemerrier, M. Yoshida, and S. Khochbin. 2000. Active maintenance of mHDA2/mHDAC6 histone-deacetylase in the cytoplasm. *Curr Biol.* 10:747-9.
- Volentine, G.D., K.A. Ogden, D.K. Kortje, D.J. Tuma, and M.F. Sorrell. 1987. Role of acetaldehyde in the ethanol-induced impairment of hepatic glycoprotein secretion in the rat in vivo. *Hepatology.* 7:490-5.
- Volentine, G.D., D.J. Tuma, and M.F. Sorrell. 1984. Acute effects of ethanol on hepatic glycoprotein secretion in the rat in vivo. *Gastroenterology.* 86:225-9.
- Westermann, S., and K. Weber. 2003. Post-translational modifications regulate microtubule function. *Nat Rev Mol Cell Biol.* 4:938-47.
- Wood, J.G., B. Rogina, S. Lavu, K. Howitz, S.L. Helfand, M. Tatar, and D. Sinclair. 2004. Sirtuin activators mimic caloric restriction and delay ageing in metazoans. *Nature.* 430:686-9.
- Wu, D., and A.I. Cederbaum. 2003. Alcohol, oxidative stress, and free radical damage. *Alcohol Res Health.* 27:277-84.

- Wu, D., X. Wang, R. Zhou, and A.I. Cederbaum. 2010. CYP2E1 enhances ethanol-induced lipid accumulation but impairs autophagy in HepG2 E47 cells. *Biochem Biophys Res Commun.*
- Xu, D.S., R.B. Jennett, S.L. Smith, M.F. Sorrell, and D.J. Tuma. 1989. Covalent interactions of acetaldehyde with the actin/microfilament system. *Alcohol Alcohol.* 24:281-9.
- Yang, X.J., and S. Gregoire. 2005. Class II histone deacetylases: from sequence to function, regulation, and clinical implication. *Mol Cell Biol.* 25:2873-84.
- Yoon, Y., N. Torok, E. Krueger, B. Oswald, and M.A. McNiven. 1998. Ethanol-induced alterations of the microtubule cytoskeleton in hepatocytes. *Am J Physiol.* 274:G757-66.
- You, M., X. Liang, J.M. Ajmo, and G.C. Ness. 2008. Involvement of mammalian sirtuin 1 in the action of ethanol in the liver. *Am J Physiol Gastrointest Liver Physiol.* 294:G892-8.
- Zatloukal, K., S.W. French, C. Stumptner, P. Strnad, M. Harada, D.M. Toivola, M. Cadrin, and M.B. Omary. 2007. From Mallory to Mallory-Denk bodies: what, how and why? *Exp Cell Res.* 313:2033-49.
- Zhang, J., R. Sprung, J. Pei, X. Tan, S. Kim, H. Zhu, C.F. Liu, N.V. Grishin, and Y. Zhao. 2008. Lysine acetylation is a highly abundant and evolutionarily conserved modification in *E. coli*. *Mol Cell Proteomics.*
- Zhang, X., Z. Yuan, Y. Zhang, S. Yong, A. Salas-Burgos, J. Koomen, N. Olashaw, J.T. Parsons, X.J. Yang, S.R. Dent, T.P. Yao, W.S. Lane, and E. Seto. 2007. HDAC6 modulates cell motility by altering the acetylation level of cortactin. *Mol Cell.* 27:197-213.
- Zhang, Y., N. Li, C. Caron, G. Matthias, D. Hess, S. Khochbin, and P. Matthias. 2003. HDAC-6 interacts with and deacetylates tubulin and microtubules in vivo. *Embo J.* 22:1168-79.
- Zhang, Y., M. Zhang, H. Dong, S. Yong, X. Li, N. Olashaw, P.A. Kruk, J.Q. Cheng, W. Bai, J. Chen, S.V. Nicosia, and X. Zhang. 2009. Deacetylation of cortactin by SIRT1 promotes cell migration. *Oncogene.* 28:445-60.